THE MECHANISM OF DUMPING IN SIEVE TRAYS IN DISTILLATION COLUMNS

A Thesis submitted for the Degree of Doctor of Philosophy in the Faculty of Engineering of the University of London

by

Arie Kupferberg, B.Sc., M.Sc.

Department of Chemical Engineering
and Chemical Technology
City and Guilds College
Imperial College
London S.W.7

July, 1968

ABSTRACT

As a first step in the study of dumping or weeping, a theoretical model for the mechanism of bubble formation has been set up. Equations have been derived for pressures involved in a single orifice bubbling system and for radial expansion of a spherical bubble. The theory has known limitations; nevertheless a fair agreement with the experiments has been found over a certain range in the 'dumping region'.

A simplified model for behaviour of a sieve tray, based on the single orifice theory, has been suggested.

A simplified criterion for dumping in a single orifice or a sieve tray is described. It is shown that the mean pressure in the gas chamber under a plate and the liquid pressure behind a bubble rising above a plate has considerable effects in the dumping studies. A fair qualitative analysis of the behaviour of a system for predicting different degrees in dumping rate has been made possible using the present theory.

Experiments have been carried out for measuring bubble frequency, pressure fluctuations in gas chamber and dumping rates. High speed cine photographs have been taken both from a three dimensional apparatus and from a two dimensional apparatus, the latter mainly for distinct observations of the dumping phenomenon.

ACKNOWLEDGEMENTS

The author wishes to express his deepest gratitude to Dr. G. J. Jameson, his personal supervisor, for his invaluable stimulation and helpful advice throughout the course of this work.

The author would like to thank Mr. J. S. Oakley and his staff, Mr. D. P. Roch and Mr. M. Topp for their technical advice and assistance.

Finally, the author wishes to thank the B'nai B'rith Leo Baeck London Lodge Scholarship Fund and particularly Mr. M. M. Kasriel and Mr. H. S. Garfield for the scholarship awarded during the three years of the work.

CONTENTS

CHAPTER 1

INTRODUCTION

Sieve trays (perforated plates) have been used for many years for liquid vapour contacting in distillation or absorption columns. These trays have many distinct advantages over conventional bubble cap trays, being easier to fabricate and more economical.

However, their usage was limited until a few years ago, because of their poor performance, resulting from poor design. It is a fact that almost any bubble cap plate design, no matter how poor, will operate fairly well over a reasonably wide range of vapour rates; whereas perforated plates must be designed carefully to give good operation.

A turning point in the conventional attitude towards sieve trays began about 15 years ago when more fundamental design procedures started to be published. Studies by Mayfield et al. (1) and Arnold et al. (2) showed that the possible range of vapour and liquid flow for stable operating condition of a sieve tray is sufficiently wide for many applications in the chemical industry. Several years later more studies dealing with the performance of such sieve trays were published, some of them being of considerable importance for present design (3, 4, 5, 6).

For the last few years it has been known that sieve tray efficiencies are greater than those for bubble cap trays under similar conditions, they have greater capacities, and their hydraulic gradient, entrainment and pressure drop characteristics are superior to those of bubble cap trays. So the use of perforated plates must be seriously considered in any particular case, and there are signs that they are becoming the standard plates for most normal duties.

There are several books (7, 8, 9) in which considerable data on sieve trays design has been published.

Stability of a sieve tray requires intimate contact between vapour and liquid, with no liquid passing through the holes and vapour passing through all the holes in as uniform manner as possible. Harris (10) shows the typical shape of a sieve tray stability region, and points out the limits for a stableoperation of such a plate, as a function of liquid and vapour rates.

It is quite obvious that the limitations for a stable operation are much more dependent on the vapour flow rate, especially in the lower range of flow rates. A convenient way of describing the action of a perforated plate is by a plot of pressure drop against vapour velocity through the holes, for constant liquid load, as shown by Prince (11).

He defines the "seal point" as the vapour rate required to just maintain the liquid level on a plate at the weir height, i. e. all liquid

fed to the plate weeps through the perforations. Similarly, the "weep point" is defined as the vapour rate required to prevent any liquid from weeping through the plate perforations. The region between these two points may be referred to as the "weeping range" (dumping range). The cverall pressure drop shows little or no increase over this range.

Workers on sieve tray stability (1, 3, 11, 12) have tried to predict the weep point, either visually or graphically (beyond the weep point, the pressure drop will increase more rapidly).

Lockhart and Legget (13) have produced a purely empirical correlation for weeping, based upon observations of Leibson et al. (12) and Mayfield et al. (1). The graphical correlation relates the dry pressure drop to the calculated head of liquid on the plate at the outlet weir.

Davidson and Schüler (17) have calculated a critical value of flow rate, for the prediction of the weep point.

The different weep points reported by various workers, differ a great deal, not only in the magnitudes and ranges of the values found, but even qualitatively in the trends observed with changes in conditions. There is no doubt that these results can reflect on the complex behaviour of a tray in the weeping range, and the difficulties in predicting the true mechanism of dumping for such a tray.

Prince and Chan (14, 15) have suggested, and it is a fact, that a plate can be operated also in the "weeping range", provided that the proportion of liquid which weeps through a plate is low enough to allow reasonable overall mass transfer efficiency. Therefore they have tried to predict the seal point, which seems to be the lower limit of operation of a perforated distillation plate.

In the paper referred to (14) a model has been set up for fluid flow in the weeping range, by postulating that the variation of liquid to vapour flow through a particular hole is caused by periodic pressure fluctuations. By further postulating that the amplitude of these fluctuations is the minimum required to obtain the overall fluid flow through the plate, the seal point corresponding to any set of external conditions, could be predicted. In their second paper (15) they have shown that for a multiplate column operating at low loads, periodic and stable pressure fluctuation will always be set up between the plates.

Their work might be regarded as an attempt for a qualitative explanation of the "dumping" phenomenon, but nevertheless it is far from explaining the true mechanism of this process.

Considering a plate working in the "weeping range", at a particular instant we could have liquid flow through some of the holes (dumping), vapour flow through some others (bubbling) and no flow

through the rest of the holes (bridging). The number of holes showing each of the mentioned types of flow will depend on the relative flow rates between the phases. At every instant the behaviour of the holes can be different.

These visual observations have led to the idea that the periodic behaviour of each hole, consists of bubbling and either dumping or bridging. The size of the bubbles and their frequency are some of the most important factors in studying the dynamics of a particular system, which can determine whether dumping will occur, or not.

It is quite obvious that any attempt at describing the mechanism of dumping must be followed by an accurate prediction of bubbles properties.

Despite the intensive research which has been carried out for determining the diameter of bubbles formed on perforated trays, there is not even a single pure theoretical equation, but empirical correlations only. Even among the empirical equations there is hardly any general agreement between different workers, which can emphasise the complexity of this problem.

Many workers have tried to examine the bubbling process in its simplest form, i. e. the formation of single bubbles at submerged orifices. Accordingly, they have pointed out that in many cases conditions on sieve trays are not radically different from those

at single orifices; so much of the knowledge gained with the latter can be applied in modified form to a plate.

Nevertheless, even in this field of research, and despite the relative simplicity of the experimental arrangements involved, the conclusions of different workers do not always agree.

Valentin (9) pointed out 18 different principal factors which might be expected to affect the diameter of a bubble formed at an orifice, and some are necessarily dependent on each other. So it is quite obvious that most of the published work contains empirical correlations only.

In addition to the simplest mechanism of bubble formation at a capillary tube, there have been several attempts at setting up theoretical models for the formation of bubbles such as that of Davidson and Schüler (16, 17) which is limited to low flow rates through comparatively small orifices.

The present investigation is of a somewhat more basic nature. It is an attempt at deriving a general theoretical model for the formation of bubbles, mainly in the "dumping region", for conditions much more applicable in industry.

A model is set up for bubbling through a single orifice, and an attempt is made at describing the mechanism of bubbling through a sieve plate. The simplicityof the model, in spite of its limitations, is necessary in order to arrive at a fair qualitative explanation of the

mechanism of dumping through an orifice, and with further assumptions, through a sieve tray.

CHAPTER 2

FORMATION OF BUBBLES-LITERATURE SURVEY

2.1. Bubbling at a Single Orifice

Because of the large number of factors which are responsible for the formation of bubbles at an orifice, and because none of the workers so far were able to take into account all of them, it is quite clear that discrepancies exist in the conclusions concerning this problem.

Nevertheless there are some general trends in the behaviour of bubbles, and a brief summary of the effect of some main parameters is given below.

2.1.1. Effect of gas flow rate

Many workers (12, 17, 18, 20, 21, 22, 30) have tried to explain the mechanism of bubble formation for various gas flow rates, distinguishing among various regimes. Others (9, 23) have tried to summarize the work in this field and to reach some general conclusions.

It seems that there exist 4 different regimes, for the formation of the bubbles.

a. Constant volume region: For very low gas flow rates. The region extends up to an orifice Reynolds number of 200 (9). Bubble diameter is a function of orifice diameter and surface tension. Gas

flow rate and liquid viscosity have negligible effects. The bubbles are formed individually and regularly in shape.

The diameter of the bubble is calculated by balancing the buoyancy against the surface tension force. Nevertheless a correction factor might be included, depending on viscosity of liquid, volume of gas chamber, etc. (19, 29):

$$D_B = \text{const} \left[\frac{6 D_o \sigma}{(\rho_L - \rho_G) g} \right]^{1/3} \qquad (2.1)$$

b. Slowly increasing volume region: Still for comparatively low gas flow rates. Reynolds number up to 1000(9). Bubble diameter is a stronger function of gas flow rate, but also a weak function of diameter of the orifice. There seems to be some effect of viscosity and inertia of the liquid. The bubbles are still formed mainly individually, but there are some possibilities of formation in pairs, this mainly to the effect of volume of gas chamber underneath the orifice (19).

The weak effect of the viscosity on bubble diameter has been shown by Quigley et al. (30) who have suggested the correlation:

$$D_B = \text{const}\, D_o^{0.33}\, G^{0.125 \cdot 002} + \text{const}\, G^{1.09} \qquad (2.2)$$

The second term is only a correction for large orifice diameters and high gas flow rates.

The main contribution to the studies of this region is the work of Davidson and Schüler (16, 17), who distinguish between the two extreme cases; that is, constant gas flow rate and constant pressure of gas.

They have found out that for constant gas flow rate, the volume of the bubble is a function of gas flow rate and kinematic viscosity only, whereas for constant gas pressure, the orifice diameter and the surface tension become also important in determining the bubble volume.

The suggested equation for constant gas flow rate:

$$V = \text{const} \left(\frac{15\,\nu G}{2g}\right)^{3/4} \tag{2.3}$$

The suggested equations for constant gas pressure:

$$\frac{dV}{dt} = k\left(p_V - \rho g h - \frac{2\sigma}{a} + \rho g s\right)^{1/2}$$

$$\nu g = 6\pi\nu \left(\frac{3V}{4\pi}\right)^{1/3} \frac{ds}{dt} + \frac{11}{16}\nu \frac{d^2 s}{dt^2} + \frac{11}{16}\frac{ds}{dt}\frac{dV}{dt} \tag{2.4}$$

The detachment of the bubble from the orifice will occur when the distance between the centre of the bubble and the point of gas supply is equal to the radius of the bubble ($s = a$); or $s = a + a_o$, if the radius of the orifice (a_o) is large enough.

Behaviour of any particular system used for formation of bubbles will therefore be in between these two extreme regions.

c. "Laminar" region: For moderate gas flow rates. Reynolds number below 2100 (9, 12). In this region the bubble frequency is constant, depending on the orifice diameter (24). Surface tension becomes less important, and inertia of the liquid appears as a main factor in determining bubble diameter.

Davidson and Harrison (25) have suggested an equation similar to that derived by Davidson and Schüler (16), for the volume of bubble, which balance the buoyancy force against the rate of change of upward momentum of the liquid surrounding the bubble:

$$V = \text{const} \frac{G^{6/5}}{g^{3/5}} \tag{2.5}$$

Leibson et al. (12) have suggested the following correlation, which is in agreement with Davidson and Amick (19) results:

$$D_B = \text{const}\, D_o^{1/2}\, Re^{1/3} \tag{2.6}$$

Van Krevelen and Hoftijzer (22), from their work with capillary tubes, have calculated a critical value of gas velocity through the orifice:

$$u_o = \text{const} \left[\frac{\sigma^5 D_o^5}{\rho_L^3 g^2 (\rho_L - \rho_G)^2} \right]^{1/6} \tag{2.7}$$

Below that critical value there is a moderate dependence of the diameter of the bubble on the gas flow rate and viscosity of the liquid:

$$D_B = \text{const}\left[\frac{G\mu}{g(\rho_L-\rho_G)}\right]^{1/4} \qquad (2.8)$$

Above the critical value, the dependency on the gas flow rate is stronger, but practically no more dependence on viscosity:

$$D_B = \text{const}\left[\frac{\rho_L}{g(\rho_L-\rho_G)}\right]^{1/5} G^{2/5} \qquad (2.9)$$

When the bubbles are formed at a comparatively high frequency, the spacing between them decreases, and each forming bubble can be affected by the presence of the preceeding one.

This is the region in which coalescence may start to occur. (Observations were mainly for air bubbles in water.) Bubbles can be formed either individually or in groups of two.

d. "Turbulent" region: For high gas flow rates. Reynolds number up to 10000(9,12). The orifice diameter and gas flow rate have a weak decreasing effect on bubble diameter, till about Reynolds number of 5000. Above this range, the ultimate bubble size depends primarily on the turbulence in the continuous phase. There are no correlations for the bubble diameter in this region.

Coalescence may occur very close to the orifice, and it is possible to form groups of two, three or even four bubbles, which are quite irregular in shape (12, 18, 19, 21). The predominant shapes of bubbles in this region are spherical cap and toroidal bubbles.

Leibson et al. (12) describe another region of higher turbulence for Reynolds numbers above 10000. The gas turbulence becomes fully developed, and what appears to be a continuous jet of gas is actually a series of closely spaced, irregular bubbles, rising with a very rapid counterclockwise swirling motion.

The average diameter of the bubbles, for this high turbulent region, is given by: $D_B = \text{const } (Re)^{-0.05}$ (2.10)

2.1.2. Effect of physical properties of the system

Because the main work carried out for investigating the formation of bubbles at submerged orifices is forthe system air-water only, there is limited information on the effect of different physical parameters on other types of systems. Nevertheless, some of the conclusions gathered so far are described below.

a. Effect of surface tension: Surface tension has the predominant effect in determining the diameter of the bubble, for the very low gas flow rates. By increasing the flow rate, surface tension effects become less important.

Hayes et al. (18) have distinguished between two regions of flow rates for which surface tension force is greater or smaller compared to rate of change of the momentum of the gas entering the bubble.

According to Davidson and Schuler (16), for a constant gas flow,

the surface tension has no effect other than that due to small forces arising from contact round the edge of the orifice, whereas, for constant gas pressure, the surface tension has an appreciable effect on the pressure in the bubble, and so to some extent, governs the flow into the bubble.

Surface tension may have also effect on the coalescence of bubbles (28).

b. Effect of viscosity of the liquid: There is very limited published information concerning the effect of viscosity of liquid. For comparatively low gas flow rate, where Stoke's law is a fair approximation, since the velocity of a rising bubble is inversely proportional to the viscosity, an increase in viscosity will therefore increase the size of the bubble before detachment, as proved by Davidson and Schüler (16).

Although the pressure within a viscous moving liquid is not the same in all directions, the nett effect on the mean pressure in the bubble can be neglected for this range of flows.

Comparatively high gas flow rates into a viscous liquid would give rise to foaming and jetting.

c. Effect of density of the liquid: An increase in density of liquid has the effect of increasing the velocity of rise of a bubble, therefore, for a constant gas flow rate, the ultimate size of a bubble tends to decrease.

The pressure into a growing bubble is related to hydrostatic head, which is proportional to the density of the liquid. Therefore, for a rising bubble under constant gas pressure conditions, increase of density will decrease the hydrostatic head, resulting in a decrease in the pressure of the bubble, that is, an increase of the gas flow rate into the bubble.

These conclusions were verified by Davidson and Schüler (16).

2.1.3. Effect of gas chamber volume

Many workers (14, 17, 18, 19, 20) have acknowledged the strong effect of the volume of gas chamber underneath the orifice, on the formation of bubbles under various conditions.

Hughes et al. (20) have defined a "capacitance number" N_c which relates the acoustical properties of the gas-orifice system to the chamber volume:

$$N_c = \frac{g(\rho_L - \rho_G)V_c}{A_o \rho_G c_o^2} \qquad (2.11)$$

Their visual observations have shown that for small chamber volumes ($N_c < 0.85$), delayed release occurs; that is, the bubble grows slowly, separating when its buoyance becomes too large. Bubbles are steady and independent on chamber volume.

For larger chamber volumes ($N_c > 0.85$), immediate release occurs; that is, the flow is large just prior to break off and the

conditions are similar to constant chamber pressure. There is a continuous rise in bubble volume, for increasing chamber volumes, however, there is simultaneously also a tendency towards formation of bubbles in pairs, rather than individually.

Further increase in the chamber volume, has no more effect on the diameter of the bubbles, as stated also by Hayes et al. (18).

Davidson and Amick (19) have observed the same type of behaviour, but have suggested that the critical value of N_c is also a function of gas flow rate and it may decrease till 0.2 for high flow rates.

In the light of these observations it is possible to estimate the importance of Davidson and Schüler's work (16, 17), who distinguish between the two extreme cases, i.e. constant gas flow rate (no effect of gas chamber) and constant gas pressure (infinite volume of gas chamber). Most of their conclusions are reported in sections 2.1.1 and 2.1.2.

2.1.4. Coalescence of bubbles

Coalescence of bubbles occurs when the flow rate of the gas is high enough to cause a second bubble, from a "double bubble" formation, to penetrate into the first one. Coalescence may take place closer and closer to the orifice, depending on the gas flow rate.

Some workers (19, 21) have tried to explain the mechanism of

coalescence. It seems that there are two possibilities for coalescence:

a. The liquid film separating the two bubbles will break, resulting in a larger bubble with shape of the first one;

b. The liquid film will remain unruptured and the second bubble will either be partially or completely swallowed by the first bubble, or will shoot completely through the first bubble, rising through the inner column of liquid in the bubble and emerging on top.

Walters and Davidson (27) have derived a simple criterion for the coalescence to occur, by postulating that the velocity of the front of the second bubble must be equal to, or exceed the velocity of the rear surface of the previous bubble, just when it has left the orifice:

$$G \geq \text{const } g^{1/2} a_o^{5/2} \qquad (2.12)$$

In fact there are limited industrially practicable systems in which fully coalescing conditions can occur, as has been described by most of the workers for air-water systems.

Although there is no precise mechanism by which coalescence is actually hindered, it is evident that forces which accelerate the thinning or drainage of the liquid film separating the bubbles, will promote coalescence, while forces opposing thinning will reduce this tendency, as stated also by Danckwerts et al. (28). Main effects in reducing this tendency might be the "surface elasticity", due to a

resistance to the formation of fresh high surface tension surface, and the "surface viscosity", due to a concentration of polar-nonpolar molecules at the surface.

2.2. Bubbling on a Sieve Tray

In addition to most of the factors which can affect the formation of bubbles at a submerged orifice, the plate geometry is one more main factor which is responsible for the formation of bubbles on a sieve tray.

Under specific conditions of flow rate, the perforations diameter, the arrangement of the perforations and the distance between two consecutive perforations, can determine the extent by which interaction between neighbouring bubbles can occur, resulting in a specific bubble size distribution along the plate. Some photographs which correspond to such a complex behaviour have been shown by Helsby (21).

Most of the workers on bubbling at a single orifice have suggested that their correlations might be useful, to a certain degree of accuracy, also for the bubbling on sieve trays.

Some workers (24, 29, 31, 32) have investigated actual perforated plates, and have tried to relate the results to single orifice behaviour. Most of the work in this field has been summarized by others (9, 23, 33).

Because of the size distribution of the bubbles formed on a plate, the most useful method for determining the average diameter is by calculating the Sauter mean bubble size, which is given by:

$$\bar{D}_B = \frac{\sum n D_B^3}{\sum n D_B^2} \qquad (2.13)$$

Unfortunately most of the published work on bubble size refers to the ultimate size of the bubbles, that is, to the bubble size distribution at a certain level of the column, which do not always agree with the actual size distribution on the plate itself, because of coalescence or collapse of the bubbles, as they ascend through the column.

Nevertheless, the general trends of the effect of gas flow rate is as follows:

a. Low gas flow rate. Reynolds number below 1000. Practically no bubbles size distribution. They ascend independently through the liquid, essentially in the same manner as a single bubble. Therefore, most of the correlations for diameter of bubbles formed at a single orifice hold also for bubbling on a plate.

b. Moderate gas flow rate. Reynolds number up to about 2500. Bubbles are randomly distributed in size, due to collapse or coalescence. The mean diameter of the bubbles increases with increase of the flow rate. Some of the correlations for a single orifice are still used for calculation of the mean diameter of the bubble, especially for small

perforations.

This is the region in which foam formation is observed (34).

c. High gas flow rate. Reynolds number above 2500. Smaller and stable bubbles are produced, having approximately the same size. The mean diameter of the bubble is no more dependent on gas flow rate. There are no correlations for bubble size in this region.

Calderbank (31) and Yoshitome (29) have observed a constant value of about 3 - 4 mm., for the mean diameter of air bubbles in water.

This is the region in which froth formation is observed. The Leibson correlation (2.10), has been confirmed also by Calderbank (24) to hold for the mean diameter of bubbles on a plate, for the highly turbulent region.

CHAPTER 3

APPARATUS AND EXPERIMENTAL TECHNIQUES

Two types of bubbling apparatus were used for investigating the mechanisms of bubble formation and dumping through a single orifice plate.

An apparatus for formation of two dimensional bubbles, through a gap between two plates, has been used, primarily for the purpose of photographing the sequence of events for the bubble formation and leakage through the gap. Studies of these photographs have led to the ideas used for the investigation of the mechanism of dumping through a sieve plate.

An apparatus for formation of three dimensional bubbles, through a single orifice in a plate, has been used primarily for investigating the behaviour of the type of bubbles which are formed in practice, under various conditions.

The schematic diagram for the experimental apparatus, is given in figure 3. 1.

3. 1 "Two dimensional bubble" Apparatus

The constructional details can be seen in figure 3. 2.

The two dimensional (cylindrical) bubbles were formed by blowing air into a water layer, through the gap between two pieces of brass,

SCHEMATIC DIAGRAM OF EXPERIMENTAL APPARATUS.

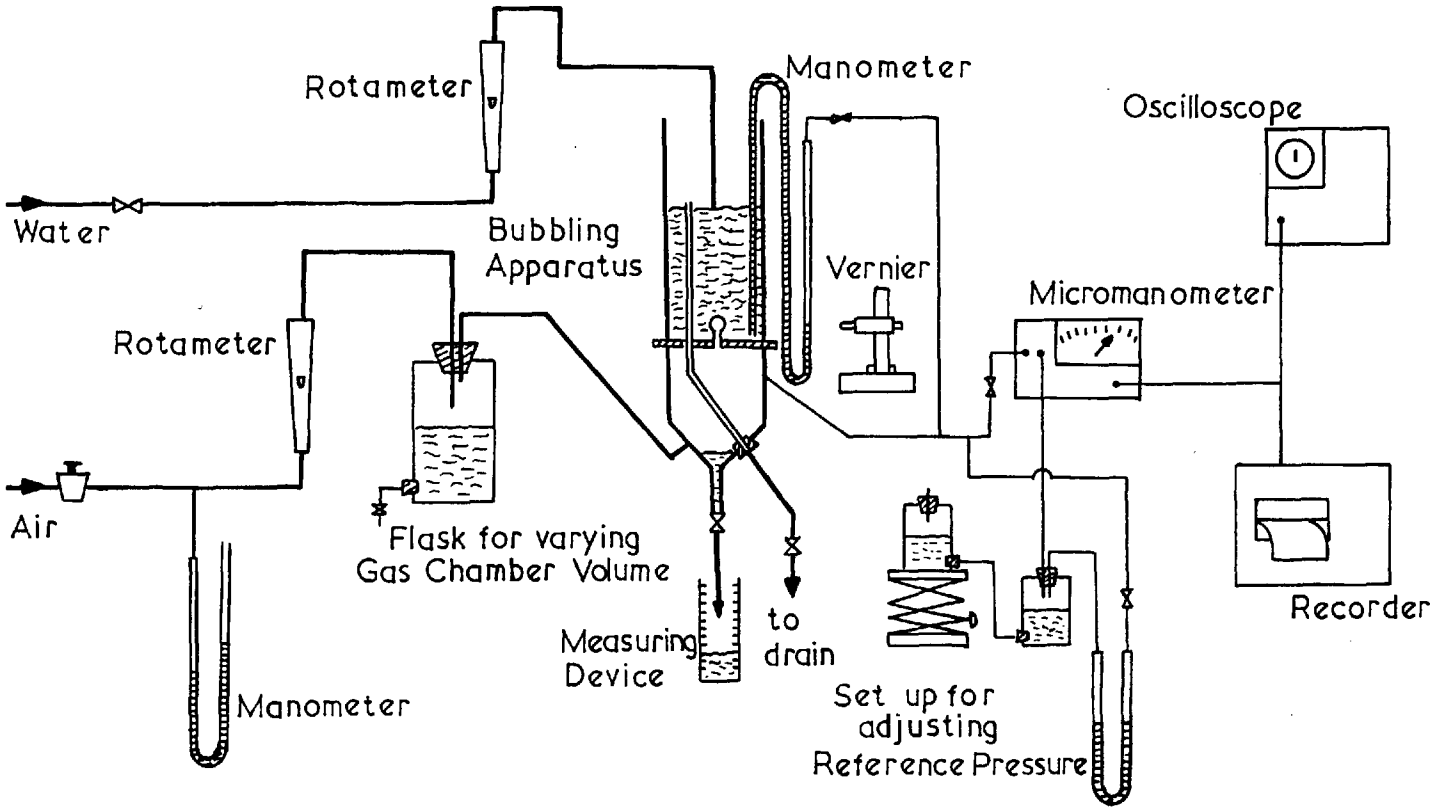

FIG. 3.1.

FIG. 3.2.

"TWO DIMENSIONAL BUBBLES" APPARATUS.

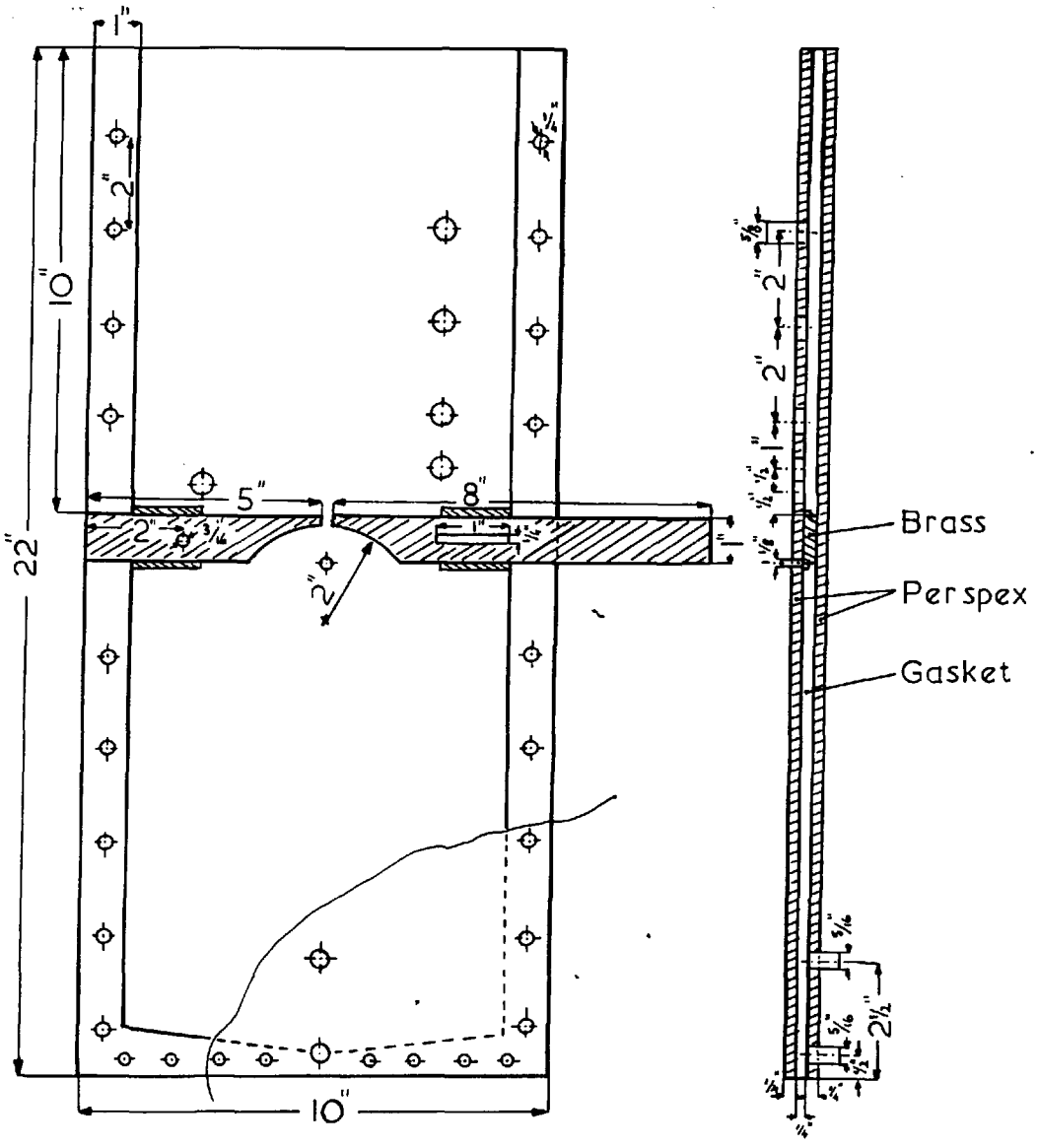

SCALE 1:4

FIG. 3.3.

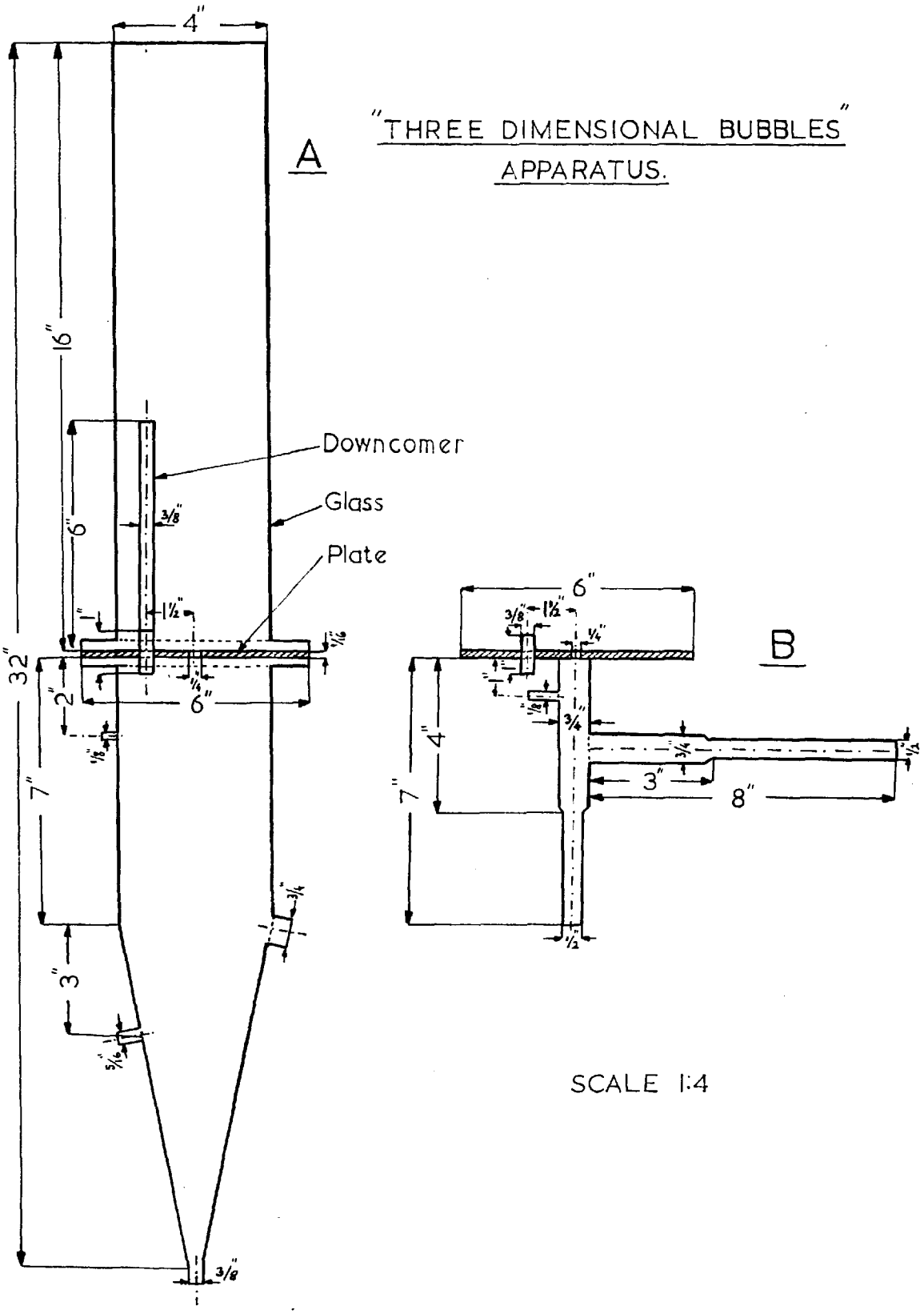

SCALE 1:4

held between two flat perspex sheets 18 x 10 x 0.25 in., which were 0.25 in. apart.

The gap between the brass plates was variable up to 1 in., so that the orifice dimensions could be varied up to 1 x 0.25 in.

The thickness of the brass plate near the orifice was changed by using 3 different plates. Thickness investigated 1/32, 1/4, 1/2, in.

The rear perspex sheet had 5 openings for changing the position of the tube for the overflow liquid. Thus the liquid layer depth could be varied to 0.5, 1, 2, 4, 6 in.

Air was supplied through a 1/4 in. rubber tube, connected near the bottom of the perspex sheet. Water was supplied in the open gap between the upper parts of the perspex sheets.

The pressure into the vessel was measured through a 3/16 in. rubber tube, connected below the gap between the brass plates.

The rate of liquid dumping was measured by collecting the liquid which flew through a 1/4 in. rubber tube, connected at the bottom of the perspex sheet.

3.2. "Three dimensional bubble" Apparatus

The constructional details can be seen in figure 3.3.

The three dimensional bubbles were formed by blowing air into

a water layer, through an orifice drilled in a plate, held between 2 glass flange joints, type FG100. (Supplied by Quickfit - I. D. approximately 10 cm.), which were modified as shown in figure 3. 3. A.

The connection between the flanges was made with a fitted clip, type JC 100F.

The two orifices investigated - diameters 1/8 and 1/4 in. - were made by drilling single holes in the centre of 1/16 in. brass plates (6 in. diameter of the plate).

About 1. 5 in. apart from the centre of the orifice, another hole was drilled, through which a 3/8 in. copper tube, 1 in. long, was soldered. Other four copper tubes of different lengths were used, to get various liquid depths (0. 5, 1, 2, 4, 6 in.), by screwing each of them respectively, to the soldered tube.

Air was supplied through a 1/4 in. rubber tube, connected to the chamber below the plate. Water was supplied in the open vessel above the plate.

The pressure in the chamber was measured through a 3/16 in. rubber tube, connected about 2 in. below the plate.

The rate of liquid dumping was measured by collecting the liquid which flowed through a 1/4 in. rubber tube, connected at the bottom of the chamber.

The overflow liquid was drained through a 1/4 in. rubber tube,

connected to the downcomer, which passed across the chamber and extended through a 3/4 in. opening in the chamber wall, towards a drain.

A few runs were made under constant gas flow rate conditions. These conditions were obtained by welding a piece of 1/8 in. sintered brass (Porosint Sinter Metal Filters - grade C, produced by Sintered Products Ltd.), to the lower side of the orifices investigated.

Runs were made with ethanol (methylated spirit) as well as water. In these experiments, the overflow liquid was recycled with a centrifugal pump, supplied by Stuart Tanner Ltd. , which had a capacitance of 40 gallon/hour, for a head of 20 ft.

The same apparatus was used also for investigating a sieve plate behaviour. Two different plates were used, in which the number of holes was varied by closing some of the perforations.

a. 7 holes maximum, 1/4 in. diameter each, arranged in a triangular pitch of 3/4 in.

b. 19 holes maximum, 1/8 in. diameter each, arranged in a triangular pitch of 3/4 in.

The volume of the chamber underneath the orifice was 2250 cc. To investigate the effect of smaller volumes, the chamber was replaced by a 3/4 in. copper tube, as shown in figure 3. 3. B. Minimum volume obtained under these conditions was 200 c. c.

A glass flask, filled partially with water, and connected in series to this tube, was used for varying the volume of the gas chamber.

In most of the runs in which cine photographs were taken, for improving their quality, the upper glass vessel was replaced by a square vessel, made of 4 perspex flat sheets 9 x 4 x 1/8 in.

3.3. Experimental Techniques

3.3.1. Photographic Techniques

The formation of bubbles was photographed either by a Milliken cine camera - Model DBM-5, at 200 frames/sec. (max. speed obtainable with such a camera - 400 frames/sec.), or by a Bolex-Paillard cine camera, at 64 frames/sec. The Milliken camera was run by an internal motor connected to an external D. C. power source of 28 Volt. It had a timing light which provided light mark on the edge of the running film, each 1/100 sec.

Rear illumination was found to provide the best quality of lighting at the image plane. The necessary intensity of light was provided by a 500 watt "photo pearl" lamp. Kodak trace paper was used as a diffusing screen to ensure a fair distribution of the illumination intensity across the image plane.

Films used were 16 mm Kodak Tri-X or 4-X, which possess very fine grain size and fast emulsion speeds.

In several runs it was necessary to take simultaneously photographs of the sequence of formation of bubbles and the relative pressure fluctuations in the chamber underneath the plate, which were shown by a trace on the oscilloscope, connected to the system. For this purpose, a mirror was set up in front of the bubbling apparatus, in a plane inclined 45^{o} in respect to the bubbles plane. The oscilloscope was located in a plane perpendicular to the bubbles plane, at a distance from the mirror, equal to the distance of the bubbling plane from the mirror. Thus, it was ensured that the rear image of the trace will be in the same plane as the bubbles.

3. 3. 2. Pressure Measurements

Measurements were made for pressure fluctuations and mean pressure in the gas chamber underneath the plate.

The pressure fluctuations were measured by an I. R. D. Micromanometer - type M. D. C., supplied by Furness Controls Ltd. It is a capacitance manometer supplied with various measuring heads, according to the range of differential pressures required. The micromanometer has a range switch which can reduce the sensitivity of the measuring circuit, by a factor of 10. The head used was for a full scale range of $\pm$ 12. 5 mm. H_2O, so it was possible to record fluctuations up to $\pm$ 125 mm. H_2O, by operating the range switch.

Being a differential instrument, one side of the micromanometer should be connected to a reference pressure, which is in the limits of the mean chamber pressure. The set up of the reference pressure, as shown in figure 3. 1, included two flasks, partially filled with water and connected in series with the instrument. One of the flasks, which was left open to the ambient atmosphere, was lifted with a laboratory jack, with respect to the other closed flask. The pressure in the closed flask, which was connected to the micromanometer, had increased gradually, till a pressure equal to the mean pressure in the gas chamber was obtained, shown by a balance between the two limbs of the U type water manometer.

The connection of the other side of the micromanometer to the measuring source was by a contraction to a 1/16 in. polythene tube. It was decided on experimental grounds to use such a tube, it having the minimum diameter which had ensured against any damping of the pressure fluctuations through the entire length of the tube.

The pressure fluctuations were recorded by connecting the micromanometer output, either to a recorder or to an oscilloscope.

The recorder used was an U. V. Recorder, type S. E. 2005, supplied by S. E. Laboratories Ltd. This is a direct writing oscillograph which utilises different recording galvanometers according to the range of frequencies required. It was found adequate to use a

galvanometer of type A. 35 which gives a flat response up to 20 cycles/ sec. The speed of the recording paper could be varied between 1. 25 - 2000 mm/sec., depending on the frequency of the fluctuations.

Full details of the resistances circuit to adjust the actual micro-manometer output to the galvanometer sensitivity, and the method for calibration of the recorder, are given in the Instruction Manual for this type of recorder.

The oscilloscope used was of type 515 A, supplied by Tektronix Guernsey Ltd. The pressure fluctuations were recorded by a trace, moving vertically only (the horizontal display switch was set in external position). The position of the trace was photographed simultaneously with the related position of the bubble, by the method described in (3. 3. 1).

The mean pressure was measured by an S-type water manometer, with one limb submerged in the water layer above the plate and the other limb connected to the chamber underneath the plate, as shown in figure 3. 1. The measurements were taken by a Vernier Microscope, with an accuracy of 0. 1 mm.

3. 3. 3. Bubbles Frequency Measurements

Three different methods for bubbles frequency measurements were applied, under different experimental conditions.

a. Photographic method: The frequency was calculated by counting the number offrames per bubble, for a given speed of photographing of the bubble formation.

b. Stroboscopic method: A stroboflash, type No.1200 D, supplied by Dawe Instruments Ltd. was used for direct measurements of bubbles frequency. Range of frequencies of the stroboflash was 250 - 18000 sec so for very low frequencies, the number of bubbles per unit time were visually counted.

c. Recorded pressure fluctuations method: The frequency of the bubbles was calculated from the number of cycles of pressure fluctuations recorded for a given speed of the recording paper.

CHAPTER 4

MECHANISM OF THE DYNAMIC BEHAVIOUR OF A BUBBLING SYSTEM

4.1. Basic Assumptions on the Behaviour of the System

From experimental observations for the air-water system it has become quite clear that in the region where dumping has occurred, large discrete bubbles were formed in the liquid. The gas flow rates used were low to moderate. Under certain conditions, the formation of bubbles was in pairs; the secondary bubble being much smaller often coalesced with the first one, right above the orifice.

Following these observations, several assumptions are necessary for the developing of a theoretical model for the bubble formation.

a. Irrotational Fluid Motion: Since the motion of the forming bubble starts practically from rest, it is assumed that the motion is initially irrotational. Studies of solid spheres accelerating from rest in a fluid have shown that the 'wake' behind the sphere is not fully established until the sphere has moved an appreciable distance. It seems likely to expect the similar behaviour for flow around an accelerating bubble.

This assumption enables the use of potential flow theory, which

includes more powerful mathematical methods for solution of fluid dynamics problems, rather than solution of the dynamic equations by direct integration.

Further postulating incompressible fluid motion, the mass-conservation equation becomes the well known Laplace' s Equation

$$\nabla^2 \phi = 0 \qquad (4.1)$$

This equation is used for determining the velocity distribution of the liquid around the bubble

b. Inviscid Liquid Flow: The effect of the viscosity on the motion of the bubble is assumed negligible, thus the inviscid fluid theory can be applicable in this case.

For the flow of a real fluid past a body at rest or in motion, no matter how small the viscosity is, its effect is significant in the neighbourhood of rigid boundaries, in the form of a boundary layer. Thus the no-slip condition at a rigid surface can be satisfied, resulting in a relative fluid velocity which increases from zero at the surface to some value characteristic of an inviscid fluid at the other end.

Boundary layers occur also at free surfaces and at interfaces between fluids, such as an air-water interface. In such cases the layer is characterised by rapid changes in velocity gradient determined by stress conditions at the interface, and not only by velocity conditions. Moore (36) has used this assumption of stress continuity at the interface

to calculate the thickness of the boundary layer on a spherical gas bubblerising steadily through liquid of small viscosity and has found that it is small.

Provided that separation of the boundary layer does not occur, it is possible to apply inviscid fluid theory. Even in cases in which separation does occur, there are large parts of the flow which locally are not affected significantly by the viscosity of the fluid, and the inviscid fluid theory may still be applied. The obvious case of separation of the boundary layer is the formation of a 'wake' behind a bubble, resulting from the vorticity created by the action of the viscous stresses in the boundary layer.

The drag coefficient for a spherical gas bubble was calculated by Moore (36) from the dissipation of energy in the boundary layer at the bubble surface and in the wake:

$$c_D = \frac{48}{Re_L}\left[1 - \frac{2.2}{Re_L^{1/2}} + 0(Re_L^{-5/6})\right] \qquad (4.2)$$

Using this equation it is obvious that the drag force of a steadily rising air bubble in water is negligible compared to other forces which affect the bubble motion, for the type of bubbles of interest in the present investigation.

Thus, adding the assumption of inviscid liquid flow to the former

assumptions of irrotational and incompressible flow, the general equation of motion (Navier-Stokes equation) is reduced to the well known Bernoulli's Equation, for unsteady flow (Batchelor (38), p. 383):

$$\frac{\partial \phi}{\partial t} + \frac{p}{\rho_L} + \frac{1}{2} q^2 - F(t) = \text{const.} \qquad (4.3)$$

This equation is used for determining the pressure around the bubble. F(t) in the present investigation is the gravity force.

c. Spherical Bubble Formation: It is assumed that the bubble is spherical throughout formation. Nevertheless, while the bubble rises through the liquid, there is an increasing tendency of distortion, which can be caused by different dynamic forces.

The criterion for distortion of a bubble rising in a comparatively inviscid liquid is given by the relative magnitude of the dynamic pressure $\rho_L u^2$ causing distortion, and the surface tension pressure $\frac{2\sigma}{a}$ available to resist it:

$$We = \frac{2a\rho_L u^2}{\sigma} \qquad (4.4)$$

For We << 1 the bubble will remain spherical, and for We >> 1 there is a great distortion. Moore (35) has shown that moderate distortion will cause the initially spherical bubble to become oblate spheroid, for which the ratio of the cross stream axis to the parallel axis is given by:

$$\chi = 1 + \frac{9}{64} \, We + 0(We^2) \tag{4.5}$$

It has been observed that for very viscous liquid, the bubble tends to remain spherical, even when its radius is so large that the effect of surface tension could not be dominant. Because the bubble size is not important, the distortion will depend mainly on liquid properties, so the criterion is in the form of the dimensionless group M, defined as:

$$M = \frac{g\mu_L^4}{\rho_L \sigma^3} \tag{4.6}$$

For example, Moore (37) has shown that 5°/o distortion occurs when the Reynolds number is:

$$Re_L = 1.1 \, M^{-1/5} \tag{4.7}$$

Despite these limitations, since the field of interest in the present investigation is mainly for bubble formation and behaviour in the vicinity of the orifice, the above assumption of sphericity of the bubble is partially justified. Even if the bubble is found to be spheroidal, the calculations will be for an equi-volume sphere.

Further, it is assumed that the motion of the bubble is not affected by the presence of another bubble immediately above it. It is obvious that this assumption is invalid for a secondary bubble, in a group of two bubbles, which formation is mainly affected by the

pressure field behind the primary bubble. (Usually it is an elongated bubble having a much smaller volume and which coalesces with the first one.)

The theoretical prediction for the volume of a bubble which is derived in the present investigation assumes that bubbles form individually, throughout all range of flows studied.

4.2. Mechanism of the Behaviour of a Single Orifice Bubbling System

4.2.1. The Idealised Stages for the Bubbling System

Hayes et al. (18) have applied Newton's Second Law for the motion of a bubble, postulating that the velocity of the centre of the bubble is equal to the rate of growth of the radius of the bubble throughout the entire period of growth of the bubble, whereas Davidson and Schuler (17) have distinguished, right from the very beginning of the motion, between these two velocities, postulating that the rate of growth of the radius of the bubble is determined by the pressure difference across the orifice (for the case of constant pressure flow).

It seems that the true mechanism is of a more complex nature, as has been also acknowledged by Krishnamurthi et al. (39).

The proposed mechanism in the present investigation is a three stage mechanism (Figure 4. 1).

a. 'Growing Stage': The bubble grows above the orifice, laying

IDEALISED STAGES FOR THE BUBBLE FORMATION.

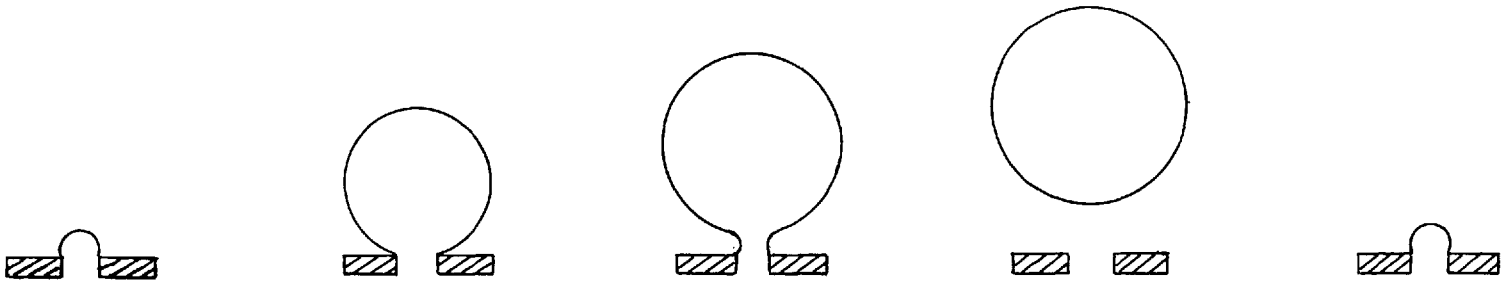

FIG. 4.1.

on the plate. Throughout this stage, the sum of the downward forces (inertia forces and reaction forces due to presence of the plate) exceed the upward forces (buoyancy forces), though the difference between them reduces gradually as the bubble expands. This stage terminates at the moment in which the buoyancy force just equals the inertia force.

b. 'Elongating Stage': The bubble continues growing while moving away from the plate but being still connected to the orifice by a small tail. Throughout this stage there is a balance between the upward and downward forces. This stage terminates at the moment in which the bubble has lifted to such an extent that the tail breaks off and the bubble accelerates away from the plate. It has been observed experimentally that the break off occurs when the bubble has moved a distance approximately equal to the radius of the orifice for an 1/4 in. orifice diameter, and nearly twice the radius of the orifice for an 1/8 in. orifice diameter.

c. 'Waiting Stage': The pressure in the gas chamber increases gradually to such an extent that another bubble starts forming above the orifice.

4.2.2. Equation of Motion for a Growing Bubble

The motion of a growing bubble is governed by two simultaneous effects: a) Translation, that is, the upward movement of the

centre of the bubble, b) Pulsation, that is, the radial expansion of the bubble. The method of describing this motion is by the velocity potential function, derived from Laplace's Equation (4.1). The velocity potential for the flow around a translating sphere in an infinite inviscid liquid, which satisfies the boundary conditions:

(1) $-\frac{\partial \phi}{\partial r} = 0$ at a plane in infinity

(2) $-\frac{\partial \phi}{\partial r} = u \cos \theta$ at the surface of the sphere

is given by (Lamb [40], p. 123): $\phi_T = \frac{ua^3}{2r^2} \cos \theta$ (4.8)

where (r, θ) are polar coordinates fixed at the centre of the moving sphere.

Similarly, the velocity potential for the flow around a pulsating sphere in an infinite inviscid liquid, which satisfies the boundary contions:

(1) $-\frac{\partial \phi}{\partial r} = 0$ at a plane in infinity

(2) $-\frac{\partial \phi}{\partial r} = \frac{da}{dt}$ at the surface of the sphere

is given by (Lamb [40], p. 122): $\phi_p = \frac{a^2 \frac{da}{dt}}{r}$ (4.9)

Since both equations (4.8) and (4.9) are linear solutions of Laplace's Equation, the overall velocity potential which describes the motion around the bubble is given by their summation:

$$\phi = \phi_T + \phi_p \tag{4.10}$$

Since the growth of the bubble is affected by the presence of the plate, the well known ' Method of Images' is applied for the correction of the values of the velocity potential. Full details of the method applied is given in Appendix A.

Provided the depth of the liquid is more than a few bubble diameters, the assumption of infinite depth of liquid is accurate. Hayes et al. (18) have assumed that minimum depth necessary is about two bubble diameters.

Shiffman and Friedman (45) have derived an approximate theory for the velocity potential for the flow around a sphere pulsating between a rigid and a free surface, assuming a flat free surface, which might have been taken in account for the present investigation. Preliminary calculations of this effect have shown negligible contribution to overall value of the velocity potential.

Such an approximation is invalid when the bubble diameter is nearly as large as the liquid depth, mainly because the free surface ceases to remain flat. A further approximation has to include the effect of the surface waves on the velocity potential, in a similar way to that shown by Kirkwood (45). Nevertheless, the forthcoming theory neglects any effect of the free surface, assuming infinite depth of liquid.

Thus the values of the velocity potential obtained as a result of

the plate effect only:

$$\phi_T = \frac{ds}{dt}\left[\frac{a^3}{2r^2} + \frac{a^3 r}{c^3} + \frac{a^6}{2c^3 r^2} + \frac{a^6 r}{c^6} + \frac{a^9}{2r^2 c^6}\right]\cos\theta \qquad (4.11.a)$$

$$\phi_p = \frac{da}{dt}\left[\frac{a^2}{r} + \left(\frac{a^2 r}{c^2} + \frac{a^5}{2c^2 r^2} + \frac{a^5 r}{c^5} + \frac{a^8}{2c^5 r^2}\right)\cos\theta\right] \qquad (4.11.b)$$

Substituting (4.11) in (4.10) and noticing that $c = 2s$ (by definition):

$$\phi = \frac{ds}{dt}\left[\frac{a^3}{2r^2} + \frac{a^3 r}{8s^3} + \frac{a^6}{16s^3 r^2} + \frac{a^6 r}{64s^6} + \frac{a^9}{128 r^2 s^6}\right]\cos\theta + \frac{da}{dt}\left[\frac{a^2}{r} + \left(\frac{a^2 r}{4s^2} + \frac{a^5}{8s^2 r^2} + \frac{a^5 r}{32s^5} + \frac{a^8}{64 s^5 r^2}\right)\cos\theta\right] \qquad (4.12)$$

Applying equation (4.3) for determination of the pressure in the liquid around the bubble:

$$\frac{p}{\rho_L} = \frac{\partial\phi}{\partial t} - \frac{1}{2}q^2 - g(s + r\cos\theta) + \frac{p_\infty}{\rho_L} \qquad (4.13)$$

Since a, s, r and θ are functions of t, the value of $\frac{\partial\phi}{\partial t}$ is calculated by:

$$\frac{\partial\phi}{\partial t} = \frac{\partial\phi}{\partial a}\frac{da}{dt} + \frac{\partial\phi}{\partial s}\frac{ds}{dt} + \frac{\partial\phi}{\partial r}\frac{dr}{dt} + \frac{\partial\phi}{\partial\theta}\frac{d\theta}{dt} \qquad (4.14)$$

where the rate of change of r and θ for a fixed point in space (Lamb [40], p. 124):

$$\frac{dr}{dt} = -\frac{ds}{dt}\cos\theta \qquad \frac{d\theta}{dt} = \frac{\frac{ds}{dt}\sin\theta}{r} \qquad (4.15)$$

The absolute velocity in space, in polar coordinates

$$q^2 = \left(\frac{\partial \phi}{\partial r}\right)^2 + \left(\frac{1}{r}\,\frac{\partial \phi}{\partial \theta}\right)^2 \tag{4.16}$$

Substituting (4.14) and (4.16) in (4.13), the pressure change due to the liquid motion around the surface of the bubble (that is for r = a), and neglecting powers of $(\frac{a}{s})$ higher than the seventh:

$$\begin{aligned}\frac{p-p_\infty}{\rho_L} = {} & \left[a\frac{d^2a}{dt^2} + \frac{3}{2}\left(\frac{da}{dt}\right)^2 - gs \right] + \cos\theta \left[a\frac{d^2a}{dt^2}\left(\frac{3a^2}{8s^2} + \frac{3a^5}{64s^5}\right)\right. \\ & + a\frac{d^2s}{dt^2}\left(\frac{1}{2} + \frac{3a^3}{16s^3} + \frac{3a^6}{128s^6}\right) + \left(\frac{da}{dt}\right)^2\left(\frac{9a^2}{8s^2} + \frac{9a^5}{32s^5}\right) \\ & \left. + \left(\frac{ds}{dt}\right)^2\left(-\frac{9a^4}{16s^4} - \frac{9a^7}{64s^7}\right) + \frac{da}{dt}\frac{ds}{dt}\left(\frac{3}{2} - \frac{9a^6}{128s^6}\right) - ga \right] \\ & + \cos^2\theta \left[\frac{1}{2}\left(\frac{ds}{dt}\right)^2 \right] - \sin^2\theta \left[\left(\frac{ds}{dt}\right)^2\left(\frac{5}{8} + \frac{9a^3}{32s^3} + \frac{6.7a^6}{128s^6}\right)\right. \\ & \left. + \left(\frac{da}{dt}\right)^2\left(\frac{9a^4}{128s^4} + \frac{2.25a^7}{128s^7}\right) + \frac{da}{dt}\frac{ds}{dt}\left(\frac{9a^2}{16s^2} + \frac{9a^5}{64s^5}\right) \right]\end{aligned} \tag{4.17}$$

The nett upward force on the bubble is found by integrating the vertical component of the pressure over its surface:

$$F = \int_0^\pi (2\pi r^2\, p \sin\theta \cos\theta)_{r=a}\, d\theta \tag{4.18}$$

As stated previously, the 'Growing Stage' terminates when the nett upward force becomes zero, that is the buoyancy force F_B just

equals the inertia force F_I.

For this stage s is identical to a. Substituting (4.17) in (4.18) and putting F = 0:

$$F_B = ga$$

$$F_I = 1.13\, a\frac{d^2a}{dt^2} + 2.13\,(\frac{da}{dt})^2 \qquad (4.19)$$

For the initial stages of the growth of the bubble, when its radius is slightly larger than the radius of the orifice, and because the bubble is connected to the orifice, there is an error in integrating the vertical component of the pressure from 0 to π. The error decreases quite rapidly with the increase of the radius of the bubble. An attempt has been made to derive a modified equation, compared to equation (4.19), while the integration has been carried out over the part of the surface of the bubble which is in contact with the liquid. Since equation (4.19) is valid only for the termination of the 'growing stage' where the radius of the bubble is larger compared to the radius of the orifice, the results which have been obtained have shown a negligible difference for the total time of growth of the bubble and its ultimate volume, using either of the two equations.

For the 'Elongating Stage' the nett upward force is consistently zero, while the bubble accelerates away from the plate, that is s is no longer identical to a. The equation of motion is found again by

substituting (4. 17) in (4. 18) and putting F = 0:

$$\frac{d^2s}{dt^2} = \frac{1}{0.5+0.188\frac{a^3}{s^3}+0.023\frac{a^6}{s^6}}\left[g - (0.375\frac{a^2}{s^2}+0.047\frac{a^5}{s^5})\frac{d^2a}{dt^2}\right.$$

$$- (1.125\frac{a^2}{s^2}+0.282\frac{a^5}{s^5})\frac{1}{a}(\frac{da}{dt})^2 + (0.563\frac{a^4}{s^4}+0.141\frac{a^7}{s^7})\frac{1}{a}(\frac{ds}{dt})^2$$

$$\left. - (1.5 - 0.070\frac{a^6}{s^6})\frac{1}{a}\frac{da}{dt}\frac{ds}{dt}\right] \qquad (4.20)$$

4.2.3. Equations for the Radical Expansion of the Bubble and Pressures in the System

The growth rate of a bubble depends on the gas flow rate and pressure change in the bubble, which are related to the pressure change in the gas chamber. Thus, an equation for the radial expansion of a bubble might be obtained from the corresponding dynamic pressure equations which are derived below.

I. It is assumed that the initial conditions for the growing of a bubble, that is for t = 0, are:

(1) The radius of the bubble is equal to the radius of the orifice:

$$(a)_o = a_o.$$

(2) The growth rate is zero: $(\frac{da}{dt})_o = 0.$

(3) The pressure in the gas chamber is equal to the sum of pressure at the orifice and the surface tension pressure, which is

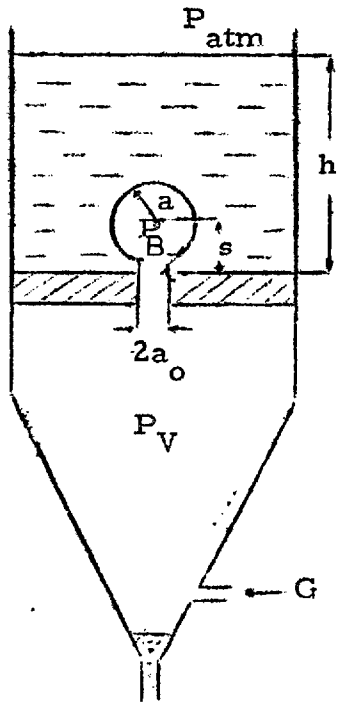

Fig. 4.2

Schematic Model of the

Bubbling System

the minimum pressure required for starting the growth of the bubble:

$$(P_V)_o = P_{atm} + \rho_L gh + \frac{2\sigma}{a_o}$$

It is most convenient to describe the relation between the pressure in the gas chamber (P_V) and the pressure in the bubble (P_B), for the bubbling period (figure 4.2), by a set of three equations, as follows:

a. Pressure drop across the orifice

If u_o is the gas velocity through the orifice, the pressure drop is given by

$$\frac{P_V - P_B}{\rho_G} = Ku_o^2 \qquad (4.21)$$

where K is an experimental constant.

Putting $$u_o = \frac{\frac{dV}{dt}}{A_o} = \frac{4\pi a^2 \frac{da}{dt}}{A_o}$$

equation (4.21) becomes:

$$\frac{P_V - P_B}{\rho_G} = \frac{16\pi^2 K a^4}{A^2_o} \left(\frac{da}{dt}\right)^2 \qquad (4.22)$$

b. Pressure in the Gas Chamber

Adiabatic conditions are assumed for the flow of gas through the chamber. Thus:

$$P_V V_c^{\gamma} = \text{const} \qquad (4.23)$$

The relation between velocity of sound and pressure in the gas chamber is given by: $$c_o = \left(\frac{\gamma P_V}{\rho_G}\right)^{1/2} \qquad (4.23a)$$

Differentiating equation (4.23) and substituting the value of γ from (4.23a) the change in pressure in the chamber is given by:

$$\frac{dP}{dV} = \frac{-c_o^2 \rho_G}{V_c} \qquad (4.24)$$

While the bubble grows the pressure in the gas chamber changes from its initial value $(P_V)_o$ to a value P_V, whereas the volume changes from $(V_c + V_o)$ to $(V_c + V)$ [i.e. the change in volume is $(V - V_o)$] . Thus, by integrating equation (4.24) the pressure obtained is:

$$P_V - (P_V)_o = \frac{-c_o^2 \rho_G}{V_c} \left[(V-V_o) - Gt\right] \qquad (4.24a)$$

Since in further calculations the pressure in the gas chamber P_V is a differential pressure related to the hydrostatic pressure above the orifice ($P_{atm} + \rho_L gh$), the pressure can be written as:

$$P_V = \frac{2\sigma}{a_o} - \frac{c_o^2 \rho_G}{V_c} \left[(V-V_o) - Gt\right] \qquad (4.25)$$

c. Pressure in the bubble

Since the bubble is assumed to be spherical, at any point on the interface there is a pressure difference compared to the pressure in the surrounding liquid, due to the surface tension, which is assumed to be equal to $\frac{2\sigma}{a}$.

The pressure in the liquid at any point on the interface is given by the sum of the hydrostatic pressure ($P_{atm} + \rho_L gh$) and the inertia pressure, due to the motion of the liquid (equation 4.17).

The pressure in the bubble is assumed to be invariant across its surface, so the inertia effect, given by equation (4.17), includes only the terms which are independent of θ, for the pressure determination.

Combining all these terms, the pressure in the bubble is given by:

$$P_B = P_{atm} + \rho_L gh + \rho_L \left[a \frac{d^2a}{dt^2} + \frac{3}{2}\left(\frac{da}{dt}\right)^2 - gs\right] + \frac{2\sigma}{a} \qquad (4.26)$$

Similarly, for further calculations, the pressure P_B is a differential pressure related to the hydrostatic pressure, thus:

$$P_B = \rho_L \left[a \frac{d^2a}{dt^2} + \frac{3}{2} \left(\frac{da}{dt}\right)^2 - gs \right] + \frac{2\sigma}{a} \qquad (4.27)$$

It is convenient to disintegrate this equation in its pressure components, thus to find their effect for different dynamic conditions.

II. The equation for the radial expansion of the bubble is found by substituting (4.25) and (4.27) in (4.22), and rearranging:

$$\frac{d^2a}{dt^2} = \frac{2\sigma}{a\rho_L} \left(\frac{1}{a_o} - \frac{1}{a}\right) - \frac{16\pi^2 K a^3}{A_o^2 \rho_L} \left(\frac{da}{dt}\right)^2 - \frac{4\pi c_o^2 \rho_G}{3aV_c \rho_L} (a^3 - a_o^3)$$

$$+ \frac{c_o^2 \rho_G}{aV_c \rho_L} Gt - \frac{3}{2a} \left(\frac{da}{dt}\right)^2 + g \frac{s}{a} \qquad (4.28)$$

For the ' Growing Stage' , s is identical to a, thus the last term in equation (4.28) is replaced by g. This stage is terminated when $F_B = F_I$ (equation 4.19).

For the ' Elongating Stage' , because the last term of (4.28) includes the distance s, the radial expansion equation is solved simultaneously with the equation of motion (4.20). This stage is terminated when $s = a + a_o$ (for 1/4 in. orifice)

$s = a + 2a_o$ (for 1/8 in. orifice).

III. For the ' Waiting Stage' , the recovery of the pressure in the

gas chamber from its value at the detachment of the bubble (P_{Vd}) is given by an equation similar to (4.24), with no flow out of the system:

$$P_V - P_{Vd} = \frac{c_o^2 \rho_G}{V_c} Gt \qquad (4.29)$$

Using equation (4.29) the 'waiting'time (t_ω) is the time necessary for the recovery of pressure from (P_{Vd}) to $\left[(P_V)_o = \frac{2\sigma}{a_o}\right]$.

IV. The mean pressure in the gas chamber is given by integration of its instantaneous value over the entire period of the three stages of the bubbling process:

$$P_{mean} = \frac{1}{T} \int_o^T P_V dT = \frac{1}{t_B + t_\omega} \left[\int_o^{t_B} P_V dt + \int_o^{t_\omega} P_V dt \right] \qquad (4.30)$$

eqn(4.25) eqn. (4.29)

V. In conclusion it can be seen that a dynamic equation for the radial expansion of the bubble (equation 4.28) has been derived from the dynamic pressure equations which represent the bubbling system. The method applied for the solution of this equation and the pressure equations, including all the necessary assumptions and evaluation of the parameters involved, is given in Appendix B.

Results have been obtained for values of a, $\frac{da}{dt}, \frac{d^2a}{dt^2}$, s, $\frac{ds}{dt}$, $\frac{d^2s}{dt^2}$, P_V and P_B (including also the different pressure components from equation 4.22, 4.25, 4.27), all as a function of bubbling time,

and values of t_ω, T and P_{mean} for a whole cycle.

4.2.4. Criterion for Coalescence of Bubbles at the Orifice

When the bubble detaches from the orifice, it leaves behind a small bubble (usually of the diameter of the orifice size). This bubble might either grow immediately, resulting in a secondary bubble which coalesces with the first one, or be pushed back in the gas chamber by the liquid pressure, resulting in a certain amount of dumping through the orifice. The pressure in the liquid behind the bubble at the moment of detachment is found from equation (4.17) by putting $\theta = \pi$:

$$\frac{P_{LD}}{\rho_L} = a\frac{d^2a}{dt^2}\left[1 - \frac{3a^2}{8s^2} - \frac{3a^5}{64s^5}\right] - a\frac{d^2s}{dt^2}\left[\frac{1}{2} + \frac{3a^3}{16s^3} + \frac{3a^6}{128s^6}\right]$$

$$+ \left(\frac{da}{dt}\right)^2\left[\frac{3}{2} - \frac{9a^2}{8s^2} - \frac{9a^5}{32s^5}\right] + \left(\frac{ds}{dt}\right)^2\left[\frac{1}{2} + \frac{9a^4}{16s^4} + \frac{9a^7}{64s^7}\right]$$

$$- \frac{da}{dt}\frac{ds}{dt}\left[\frac{3}{2} - \frac{9a^6}{128s^6}\right] - g(s-a) \qquad (4.31)$$

Since the pressure in the small bubble which remains attached to the orifice is assumed to be equal to the pressure in the gas chamber (P_V) (applying again the initial conditions for the growing of a bubble), this bubble continues to grow and coalesce with the detached bubble, provided its pressure is higher than the pressure in the liquid behind the detached bubble, that is:

$$P_V > P_{LD} \tag{4.32}$$

4.2.5. Dimensionless Form of the Dynamic Equations

A convenient way of presenting the dynamic equations is in a dimensionless form, by using the following non-dimensional variables:

$$\hat{a} = \frac{a}{V_c^{1/3}} \qquad \hat{G} = \frac{G}{c_o V_c^{2/3}}$$

$$\hat{s} = \frac{s}{V_c^{1/3}} \qquad \hat{P} = \frac{P}{\rho_L c_o^2}$$

$$\hat{t} = \frac{t c_o}{V_c^{1/3}} \tag{4.33}$$

$$\hat{Fr} = \text{Froude Number} = \frac{c_o^2}{g V_c^{1/3}}$$

$$\hat{We} = \text{Weber Number} = \frac{\rho_L c_o^2 V_c^{1/3}}{\sigma}$$

Thus the equations derived in (4.22) and (4.2.3) can be presented as follows:

From equation 4.19 (in the form $F_B = F_I$)

$$\frac{\hat{a}}{\hat{Fr}} = 1.13\, a \frac{d^2\hat{a}}{d\hat{t}^2} + 2.13 \left(\frac{d\hat{a}}{d\hat{t}}\right)^2 \tag{4.34}$$

From equation 4.20

$$\frac{d^2\hat{s}}{d\hat{t}^2} = \frac{1}{0.5+0.188\,\frac{\hat{a}^3}{\hat{s}^3} + 0.023\,\frac{\hat{a}^6}{\hat{s}^6}} \left[\frac{1}{\hat{Fr}} - \left(0.375\,\frac{\hat{a}^2}{\hat{s}^2} + 0.047\,\frac{\hat{a}^5}{\hat{s}^5}\right)\frac{d^2\hat{a}}{d\hat{t}^2} \right.$$

$$- \left(1.125\,\frac{\hat{a}^2}{\hat{s}^2} + 0.282\,\frac{\hat{a}^5}{\hat{s}^5}\right)\frac{1}{\hat{a}}\left(\frac{d\hat{a}}{d\hat{t}}\right)^2 + \left(0.563\,\frac{\hat{a}^4}{\hat{s}^4} + 0.141\,\frac{\hat{a}^7}{\hat{s}^7}\right)\frac{1}{\hat{a}}\left(\frac{d\hat{s}}{d\hat{t}}\right)^2$$

$$\left. - \left(1.5 - 0.070\,\frac{\hat{a}^6}{\hat{s}^6}\right)\frac{1}{\hat{a}}\,\frac{d\hat{a}}{d\hat{t}}\,\frac{d\hat{s}}{d\hat{t}} \right] \qquad (4.35)$$

From equation 4.25

$$\hat{P}_V = \frac{2}{\hat{W}_e}\,\frac{1}{\hat{a}_o} - \frac{4}{3}\,\pi\,\frac{\rho_G}{\rho_L}\,(\hat{a}^3 - \hat{a}_o^3) - \frac{\rho_G}{\rho_L}\,\hat{G}\hat{t} \qquad (4.36)$$

From equation 4.27

$$\hat{P}_B = \hat{a}\,\frac{d^2\hat{a}}{d\hat{t}^2} + \frac{3}{2}\left(\frac{d\hat{a}}{d\hat{t}}\right)^2 - \frac{1}{\hat{Fr}}\,\hat{s} + \frac{2}{\hat{We}}\,\frac{1}{\hat{a}} \qquad (4.37)$$

From equation 4.28

$$\frac{d^2\hat{a}}{d\hat{t}^2} = \frac{2}{\hat{We}}\,\frac{1}{\hat{a}}\left(\frac{1}{\hat{a}_o} - \frac{1}{\hat{a}}\right) - 16K\,\frac{\rho_G}{\rho_L}\,\frac{\hat{a}^3}{\hat{a}_o^4}\left(\frac{d\hat{a}}{d\hat{t}}\right)^2 - \frac{4\pi}{3}\,\frac{\rho_G}{\rho_L}\,\frac{1}{\hat{a}}\,(\hat{a}^3 - \hat{a}_o^3)$$

$$+ \frac{\rho_G}{\rho_L}\,\frac{\hat{G}\hat{t}}{\hat{a}} - \frac{3}{2}\,\frac{1}{\hat{a}}\left(\frac{d\hat{a}}{d\hat{t}}\right)^2 + \frac{1}{\hat{Fr}}\,\frac{\hat{s}}{\hat{a}} \qquad (4.38)$$

From equation 4.29

$$\hat{P}_V - \hat{P}_{Vd} = \frac{\rho_G}{\rho_L}\,\hat{G}\hat{t} \qquad (4.39)$$

Since in this dimensionless form, there are still five independent

groups We, $Fr\frac{\rho_G}{\rho_L}$, $\hat{G}$, $\hat{a}_o$ compared to the initial seven variables in the dimensions equations σ, ρ_G, ρ_L, G, V_c, a_o c_o, it is seen that there is not much benefit in solving these dimensionless equations. Nevertheless using such a procedure it is possible to find out the main groups which govern the present set of dynamic equations. While the equation of motion (4.35) is governed only by the Froude Number (Fr) which is a measure of the relative magnitude of dynamic and static pressures, the equation for the radial expansion of the bubble (4.38) is governed, in addition to this group, also by the Weber Number (We) which is a measure of the relative magnitude of dynamic and surface tension pressures.

4.3. Pressure Behind an Accelerating Bubble

As soon as the bubble is detached from the orifice, it accelerates upwards in the liquid, resulting in a change of the liquid pressure in the vicinity of the orifice, which might have an appreciable effect in the dumping studies.

This pressure behind the bubble along the line of motion can be calculated in a similar way as shown in (4.2.2).

A simplified theory for a spherical bubble accelerating from rest, neglecting the effect of the plate on the value of the velocity potential, has been derived by Jameson and Kupferberg (43).

For the present investigation it is assumed that the bubble remains spherical even through this stage of the translating motion. Thus the velocity potential for the flow around the bubble is given by (4.11.a). Using equations (4.13), (4.14), (4.15) and (4.16), the pressure change due to the liquid motion along the vertical path followed by the centre of the bubble (that is for r = s and $\theta = \pi$) is:

$$\frac{\Delta P}{\rho_L} = \left[\frac{a^3}{r^3} - \frac{a^3}{c^3} + \frac{6ra^3}{c^4} + \frac{3a^6}{r^2c^4} - \frac{a^6}{2r^6} + \frac{2a^6}{c^3r^3} - \frac{3a^6}{2c^6} \right] \left(\frac{ds}{dt}\right)^2$$

$$- \left(\frac{a^3}{2r^2} + \frac{ra^3}{c^3} + \frac{ra^6}{c^6} + \frac{a^6}{2r^2c^3}\right) \frac{d^2s}{dt^2} \qquad (4.40)$$

For a spherical bubble accelerating from rest, the acceleration is given approximately by 2g. The validity of this value has been shown by Walters and Davidson (27). Although in the present investigation the bubble at its detachment has an initial velocity U_d, in order to get an approximate dimensionless equation as derived in (43), it is assumed that the initial acceleration is still 2g.

Assuming also that the detachment occurs at a distance a_o from the orifice, the acceleration, velocity and distance travelled by a bubble after a time t from the detachment are:

$$\frac{d^2s}{dt^2} = 2g$$

$$\frac{ds}{dt} = 2\,gt + U_d \qquad (4.41)$$

$$s = gt^2 + U_d t + a + a_o$$

Defining the dimensionless distance:

$$\tilde{s} = \frac{s}{a} = 1 + \frac{a_o}{a} + \frac{U_d t}{a} + \frac{gt^2}{a} \qquad (4.42)$$

and substituting (4.42) and (4.41) in (4.40) we find:

$$\frac{\Delta P}{\rho_L ga} = \frac{3.75}{\tilde{s}^2} - \frac{5}{\tilde{s}^3} - \frac{0.5}{\tilde{s}^4} + \frac{0.344}{\tilde{s}^6} + \left(\frac{1.25}{\tilde{s}^3} - \frac{0.086}{\tilde{s}^6}\right)\left(\frac{U_d^2}{ga} - 4\frac{a_o}{a}\right) \qquad (4.43)$$

Figure 4.3 shows the magnitude of the group $\frac{\Delta P}{\rho_L ga}$ for different values of $\left(\frac{U_d^2}{ga} - 4\frac{a_o}{a}\right)$. This expression for ΔP is subject to two main sources of error, as mentioned above: a) the bubble tends to stop accelerating as its velocity increases; b) the bubble tends to deform quite rapidly from its assumed spherical shape.

Walters and Davidson (27) have shown in their analysis for three dimensional bubbles accelerating from rest that an acceleration of 2g is valid up to $\tilde{s} = 1.65$ approximately, although a tongue of liquid might begin to penetrate the rear of the bubble (bubble ceasing to remain spherical) at $\tilde{s} = 1.36$ approximately. So the shape of the curves beyond $\tilde{s} = 1.65$ are slightly in doubt, and the values of $\frac{\Delta P}{\rho_L ga}$ probably subside to zero rather more rapidly than shown in figure 4.3. More details about the properties of such curves are given in (43).

Some calculations of the pressure distribution along a horizontal line (i. e. perpendicular to the line of motion) found by introducing

FIG. 4.3.

PRESSURE AT THE ORIFICE PLANE BEHIND THE LINE OF MOTION OF AN ACCELERATING SPHERICAL BUBBLE.

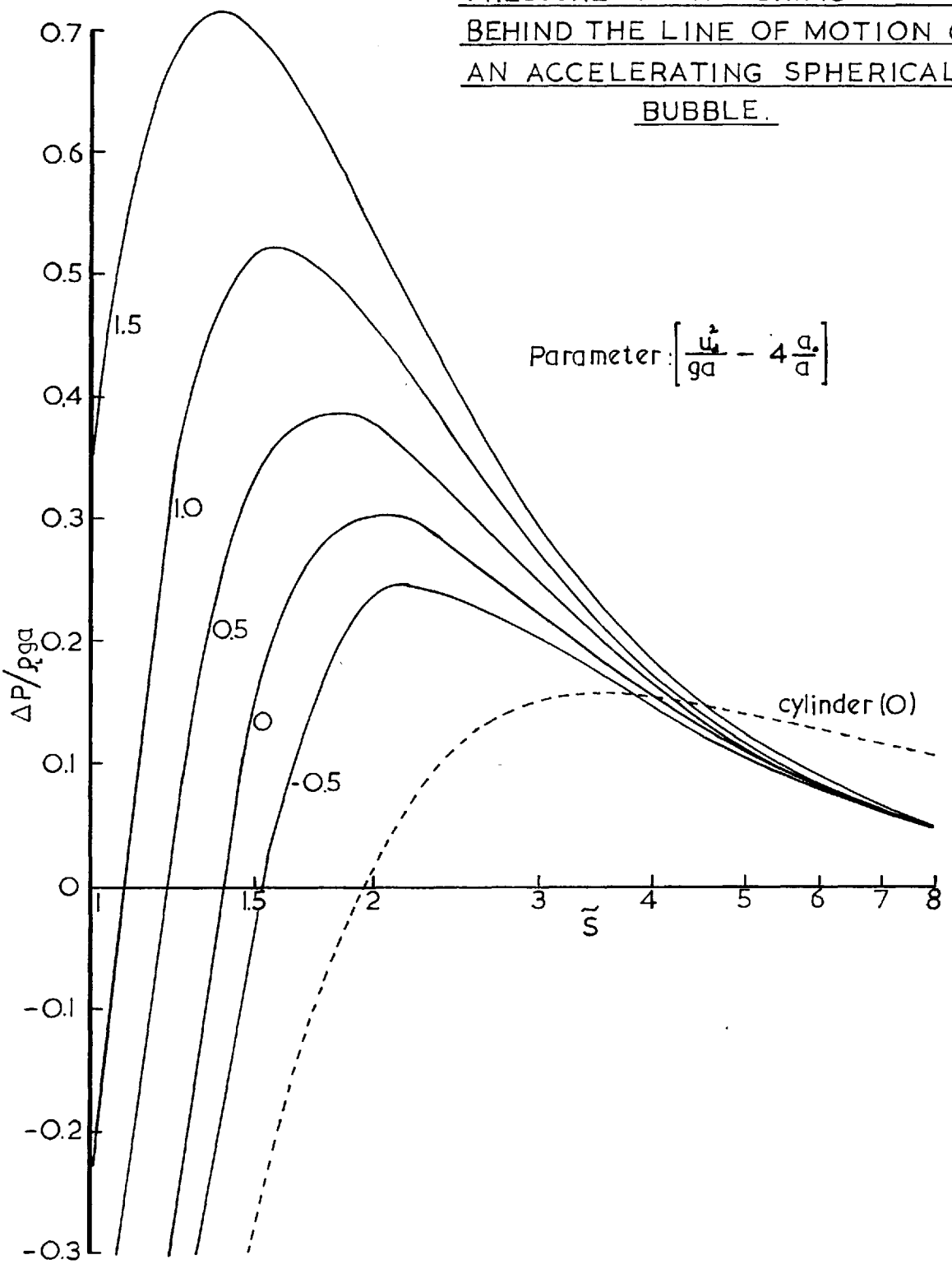

$\theta = \pi \pm \alpha$ for several small angles α, thus obtaining an equation similar to (4.40), have shown a negligible change compared to the values obtained along the line of motion.

Mainly for comparison purposes the pressure behind an accelerating cylindrical (two dimensional) bubble has also been investigated. The velocity potential for the flow around a translating cylinder in an inviscid liquid is given by Lamb [40], p. 76):

$$\phi_T = \frac{ua^2}{r} \cos\theta \tag{4.44}$$

Using the similar 'Method of Images' as described in Appendix A, the effect of the plate on the velocity potential is given by:

$$\phi_T = \frac{ds}{dt}\left(\frac{a^2}{r} + \frac{a^2 r}{c^2} + \frac{a^4}{c^2 r} + \frac{a^4 r}{c^4} + \frac{a^6}{c^4 r} + \frac{a^6 r}{c^6}\right) \cos\theta \tag{4.45}$$

Using the same procedure as for a spherical bubble, the pressure behind such a cylinder starting from rest (i.e. neglecting U_d and a_o and assuming an acceleration of g [26]):

$$\frac{\Delta P}{\rho_L g a} = \frac{1.19}{\tilde{s}} - \frac{2.38}{\tilde{s}^2} + \frac{0.58}{\tilde{s}^3} - \frac{0.88}{\tilde{s}^4} + \frac{0.17}{\tilde{s}^5} - \frac{0.25}{\tilde{s}^6} \tag{4.46}$$

The values of $\frac{\Delta P}{\rho_L g a}$ are also shown in figure 4.3 by a dotted line.

CHAPTER 5

DISCUSSION OF THE EXPERIMENTAL RESULTS AND COMPARISON TO THE PROPOSED MECHANISM

5.1. General Description of Bubble Formation

As has already been stated the investigation of the bubble formation was mainly in the range in which reasonable rate of dumping has occurred.

Although it is quite clear that an increase in the orifice diameter leads to an increase in the rate of dumping, there is an upper limit to the orifice diameter for formation of stable bubbles, with a steady increase in the distortion of the bubble. It is most likely that for very large diameters, the mechanism of dumping (Chapter 6) is different, resulting in a continuous two-phase flow. Thus, to ensure a reasonable agreement with the proposed mechanism the largest orifice diameter used was 1/4 in.

Similarly, it was found for the air-water system that dumping did not occur to any extent with 1/16 in. orifice. Reasonable dumping was first observed with 1/8 in. orifice, which was chosen as the small orifice diameter for the present investigation.

Some typical photographs of the bubble formation in an air-

water system, for these two orifice diameters are given in figures 5.1 - 5.6. Throughout the different conditions it is possible to observe quite clearly the two different stages in the formation of the bubble, that is, the 'Growing Stage' and the 'Elongating Stage'.

The trace observed on the left side of each photograph represents the relative pressure in the gas chamber, as was recorded simultaneously by the oscilloscope.

In every case when a bubble detaches from the orifice, it leaves behind a small nucleus which can form another bubble. Provided the pressure in the gas chamber is larger than the pressure in the liquid behind the bubble at detachment (equation 4.32), another bubble starts to form and coalesce with the previous one. The secondary bubble might be very small compared to the first one (Figure 5.2, 5.5, 5.6) or slightly larger (Fig. 5.3). Single bubble formation is seen clearly in figures 5.1 and 5.4.

The effect of pressure behind an accelerating bubble (equation 4.43) might be seen in figure 5.4. Although immediately after detachment there is a tendency for the growing of the secondary bubble, the increase in liquid pressure tends to push back this small bubble, until it disappears from above the orifice.

Some typical measurements of pressure fluctuations in the gas chamber as were recorded by the U.V. recorder, for both the systems

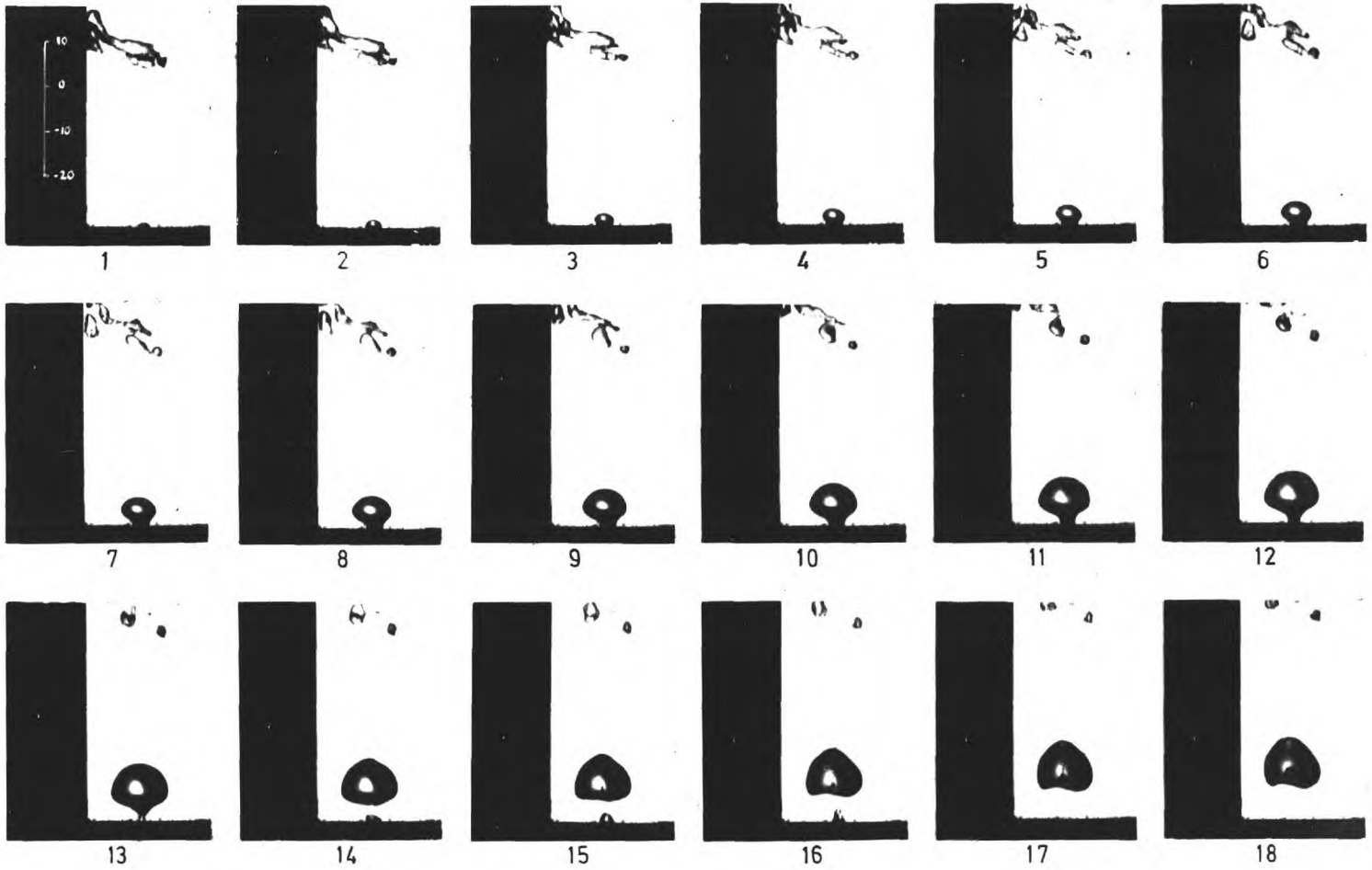

FIG. 5.1.

STAGES DURING A BUBBLE FORMATION, AIR-WATER SYSTEM.

(Cine pictures at 200 frames/sec - On l.h.s. of picture : P_V [mm H_2O]).

D_o = 0.25 in. , V_c = 2250 cc. , G = 16.7 cc/sec.

Frames 2-7: 'GROWING' Stage. ; Frames 8-13: 'ELONGATING' Stage.

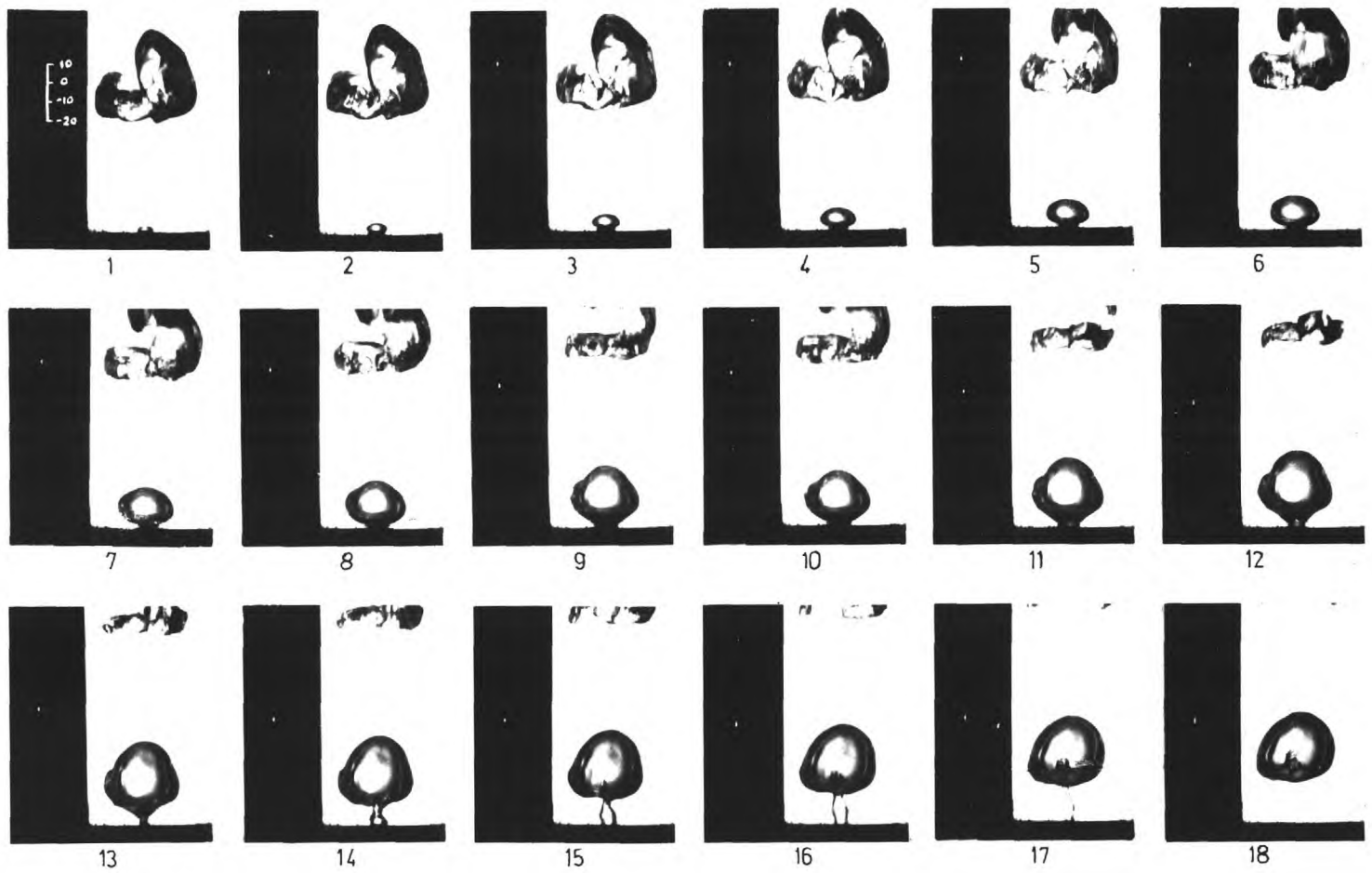

FIG. 5.2.

STAGES DURING A BUBBLE FORMATION, AIR-WATER SYSTEM.

(Cine pictures at 200 frames/sec– On l.h.s. of picture: P_V [mm H_2O]).

D_o = 0.25 in., V_c = 2250 cc., G = 66.7 cc/sec.

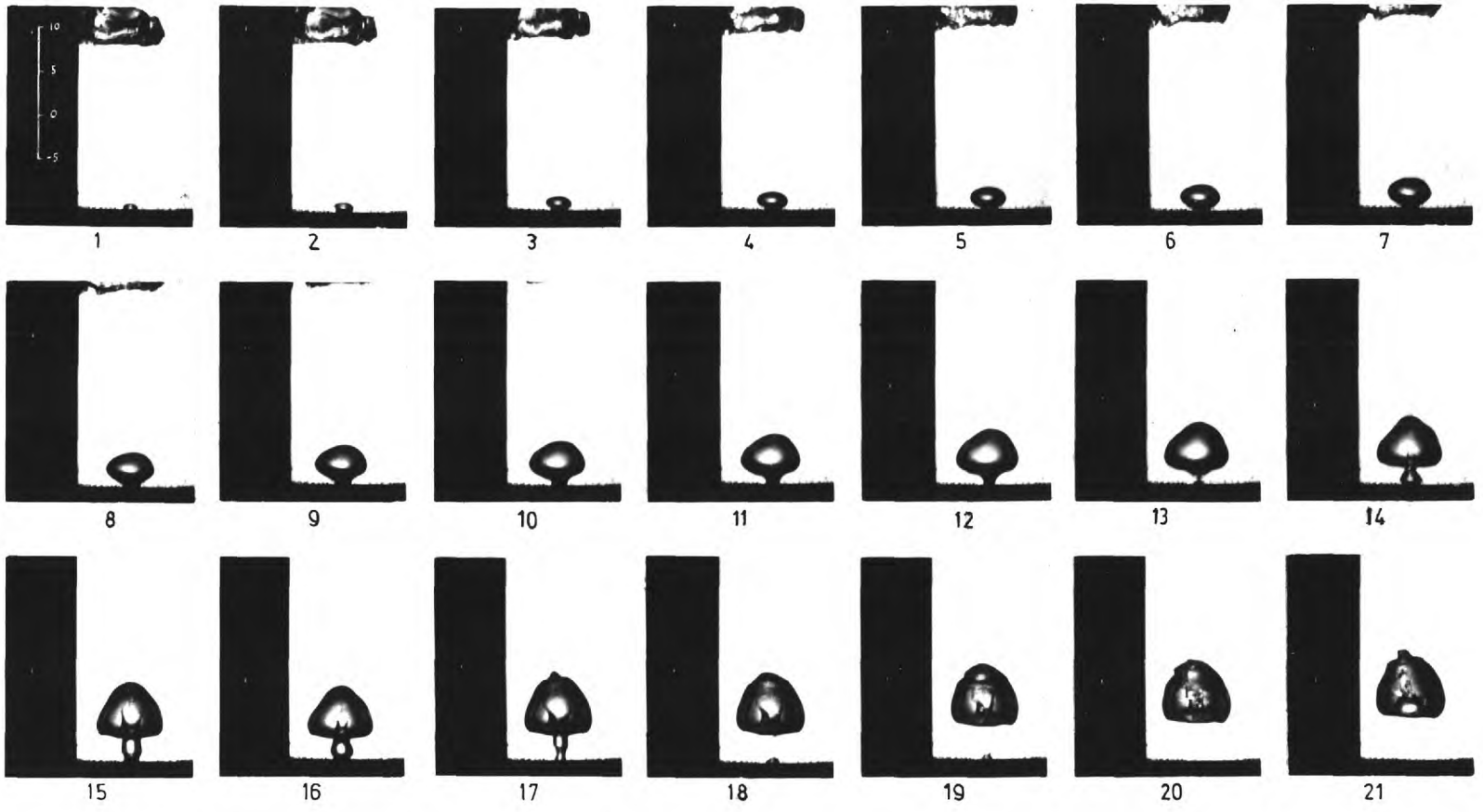

STAGES DURING A BUBBLE FORMATION, AIR-WATER SYSTEM.

(Cine pictures at 200 frames/sec – On l.h.s. of picture: P_V [mm H_2O]).

D_o = 0.25 in., V_c = 5000 cc., G = 35.0 cc/sec.

FIG. 5.3.

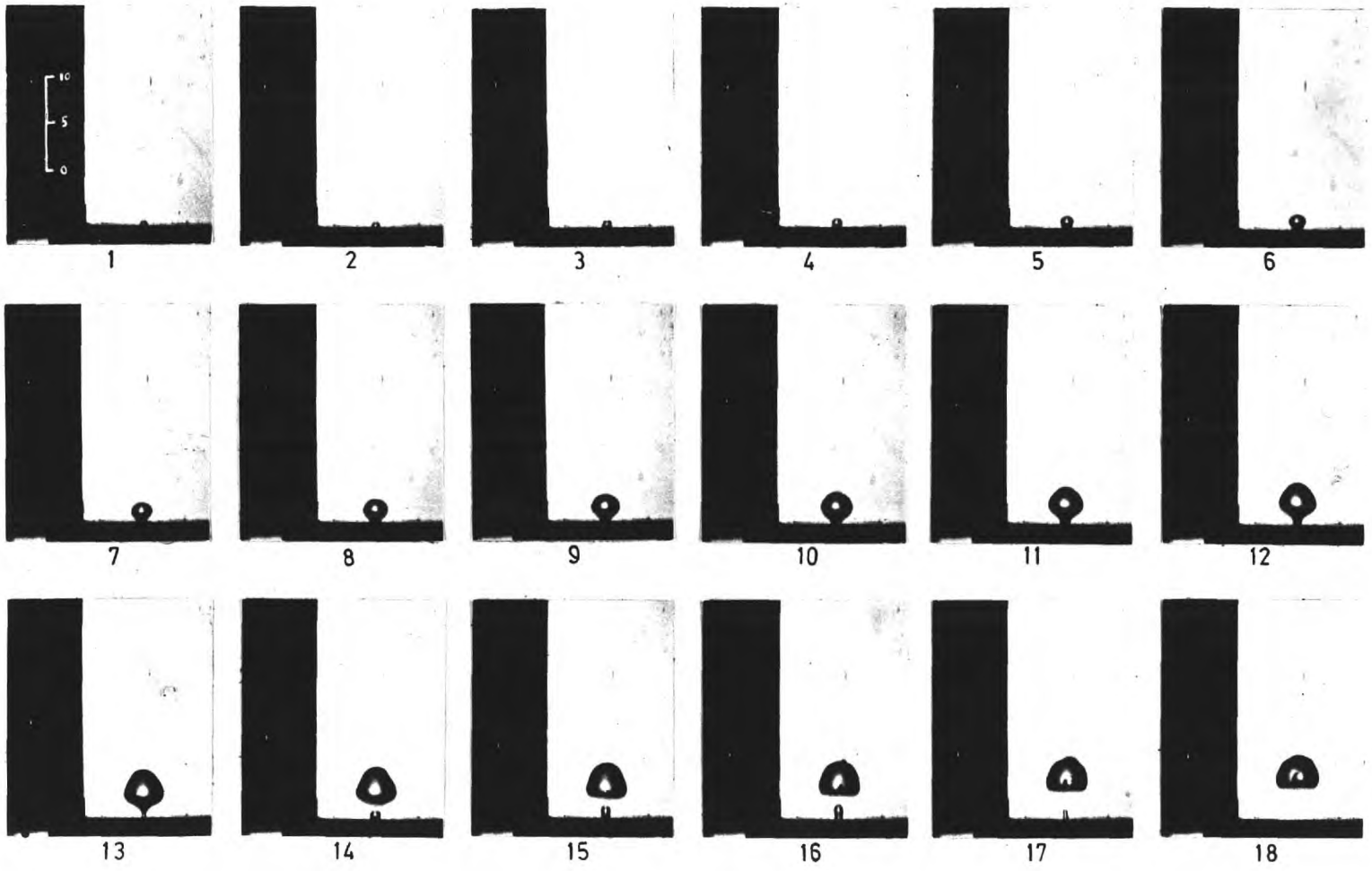

FIG. 5.4.

STAGES DURING A BUBBLE FORMATION, AIR-WATER SYSTEM.

(Cine pictures at 200 frames/sec—On l.h.s. of picture : P_V [mm H_2O]).

D_o=0.125 in., V_c = 2250 cc., G = 2.0 cc/sec.

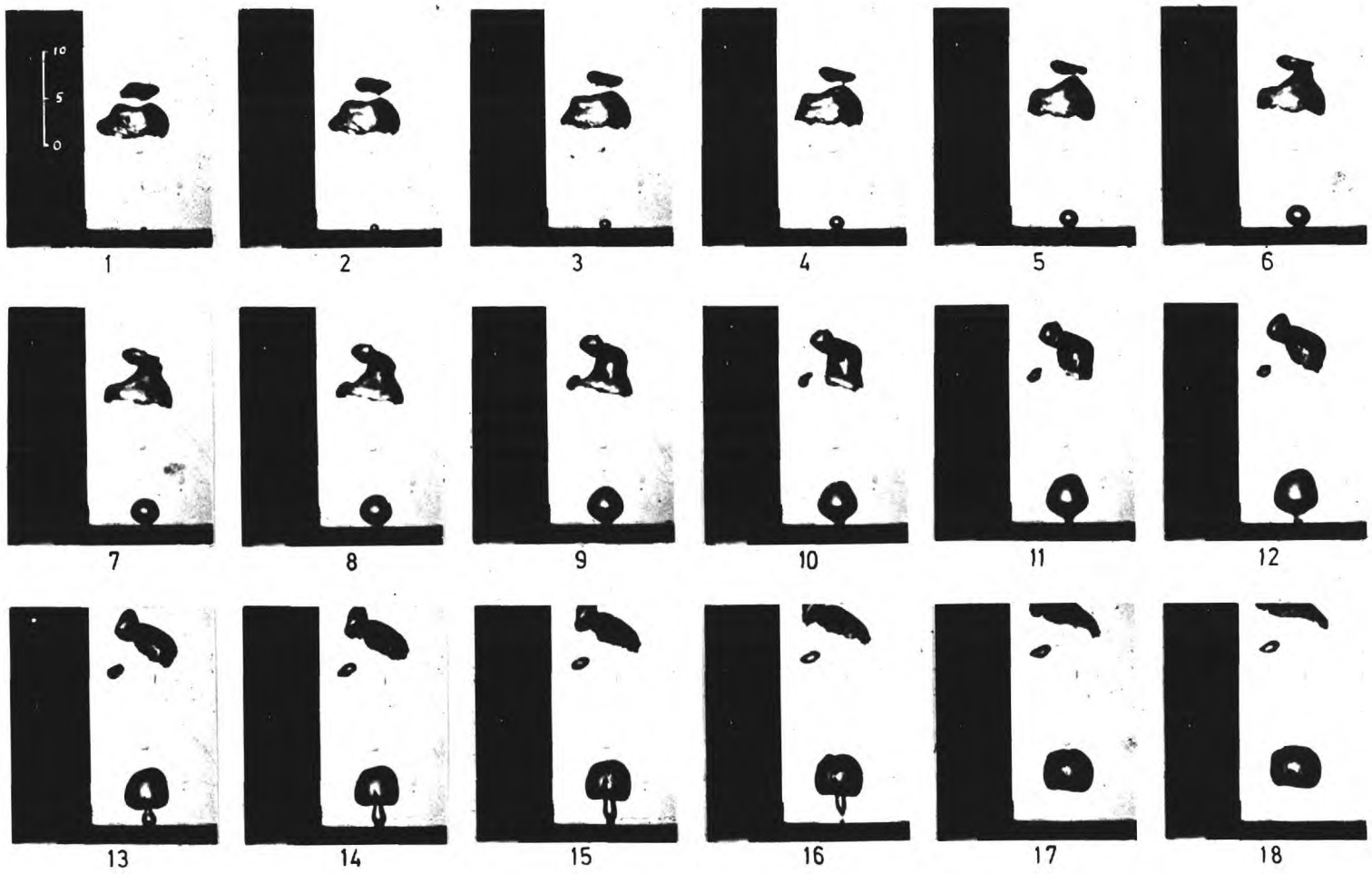

STAGES DURING A BUBBLE FORMATION, AIR-WATER SYSTEM.

(Cine pictures at 200 frames/sec - On l.h.s. of picture : P_V [mm H_2O]).

D_o = 0.125 in. , V_c = 2250 cc. , G = 16.7 cc/sec.

Frames 2-7 : 'GROWING' Stage. ; Frames 8-12 : 'ELONGATING' Stage.

FIG. 5.5.

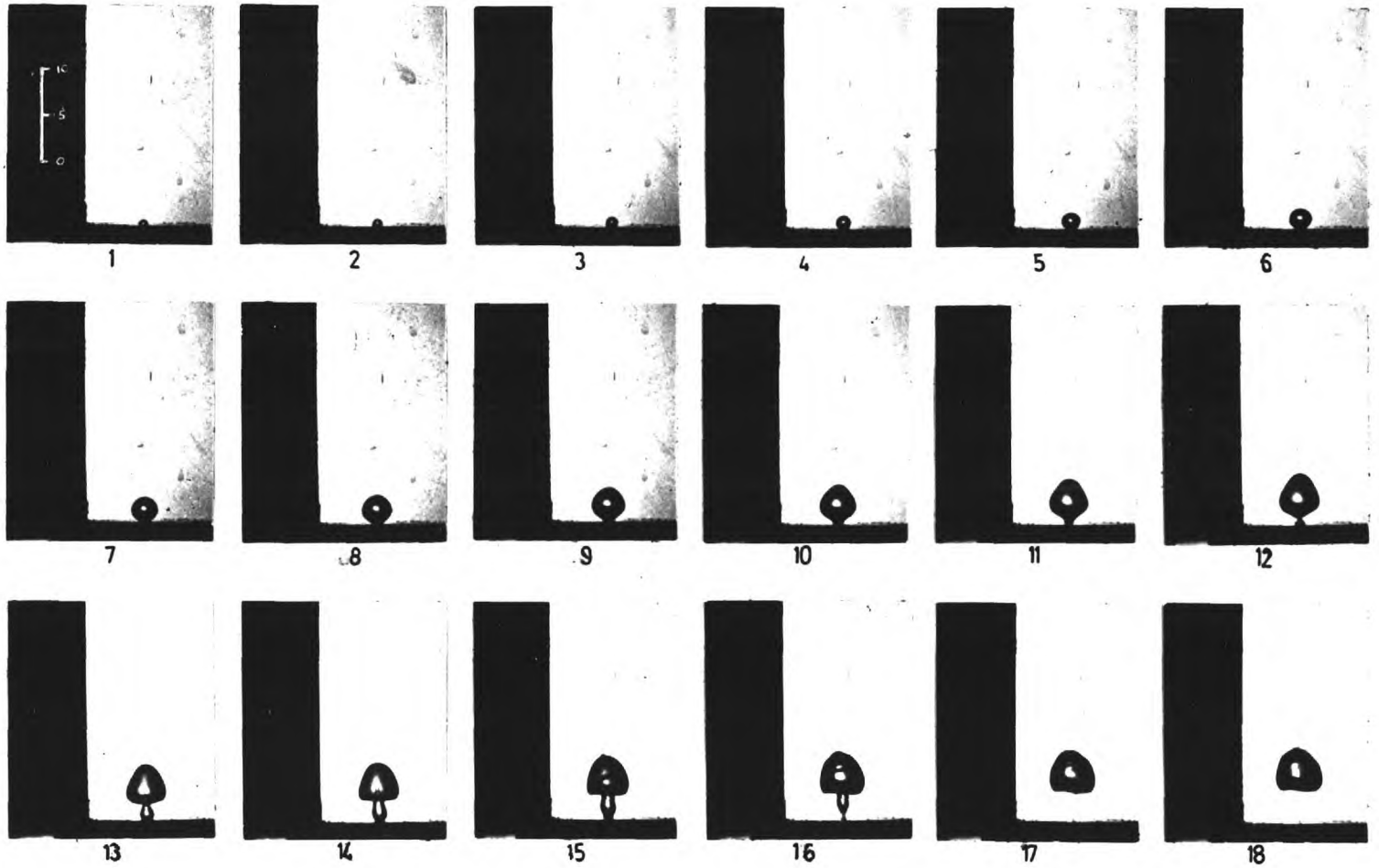

FIG. 5.6.

STAGES DURING A BUBBLE FORMATION, AIR-WATER SYSTEM.

(Cine pictures at 200 frames/sec – On l.h.s. of picture : P_V [mm H_2O]).

D_o = 0.125 in. , V_c = 5000 cc. , G = 5.0 cc / sec.

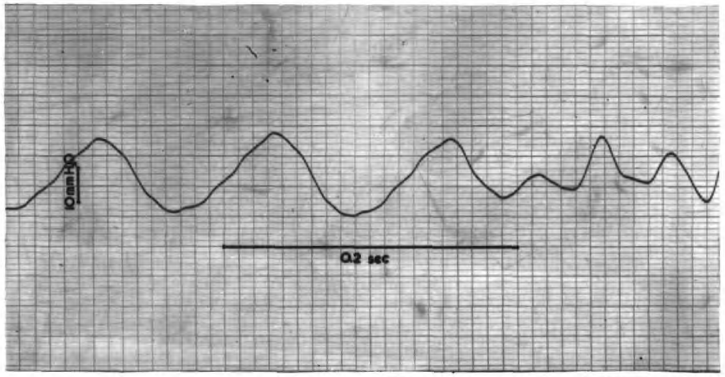

a. AIR-WATER V_c = 500 cc. G= 35.0 cc/sec

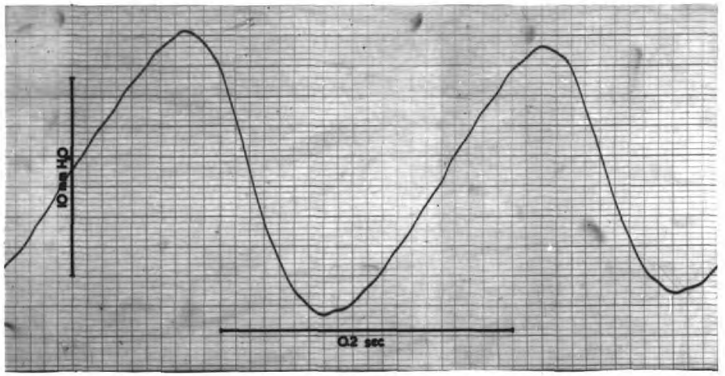

b. AIR-WATER V_c = 2250 cc G=17.2 cc/sec.

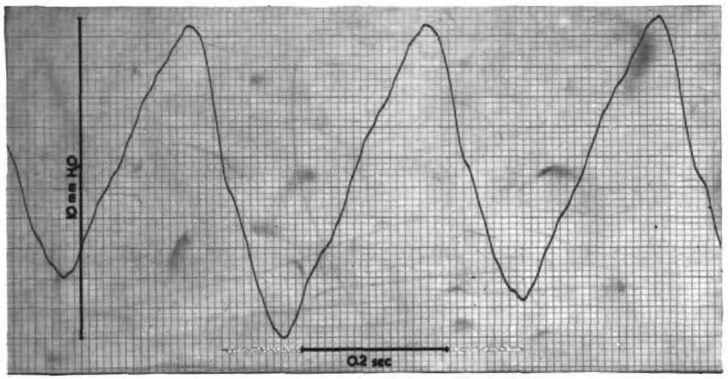

c. AIR-WATER V_c = 5000 cc. G = 17.5 cc/sec.

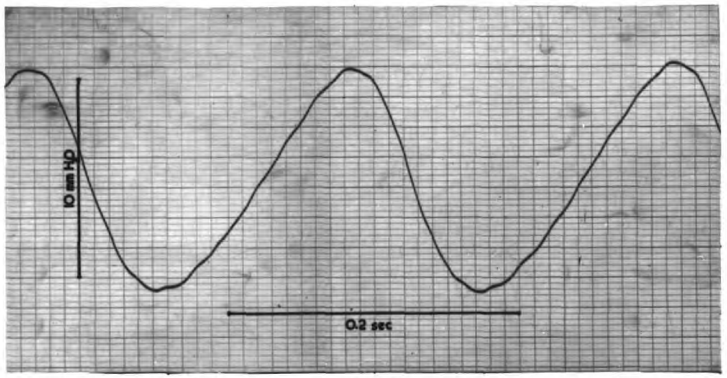

d. AIR-ETHANOL V_c = 2250 cc G=17.5 cc/sec

PRESSURE FLUCTUATIONS IN GAS CHAMBER BELOW A 0.25 in. ORIFICE DIAMETER.

FIG. 5.7.

FIG 58

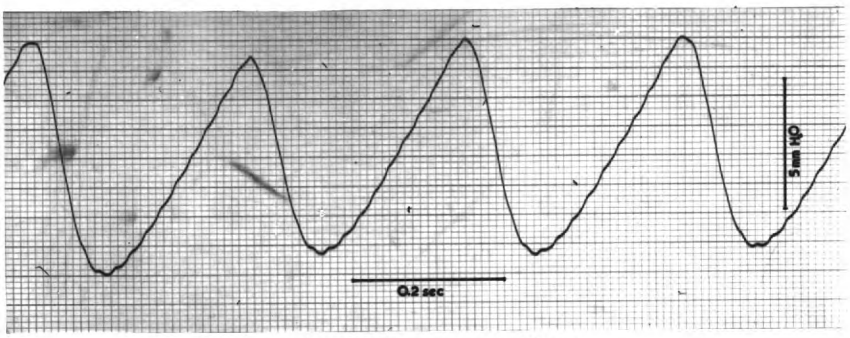

a. AIR-WATER V_c = 2250 cc. G = 8.0 cc/sec.

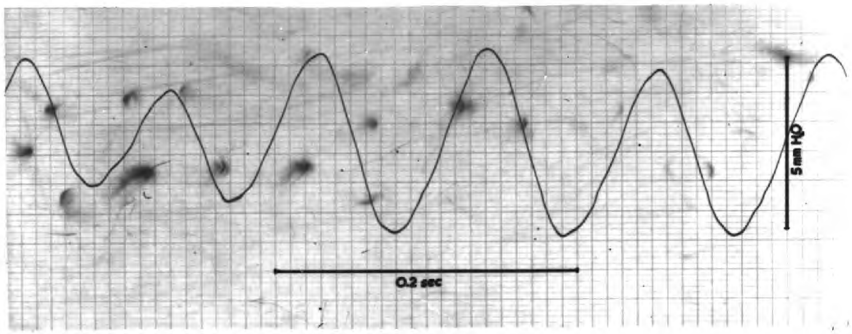

b. AIR-WATER V_c = 2250 cc. G = 24.3 cc/sec.

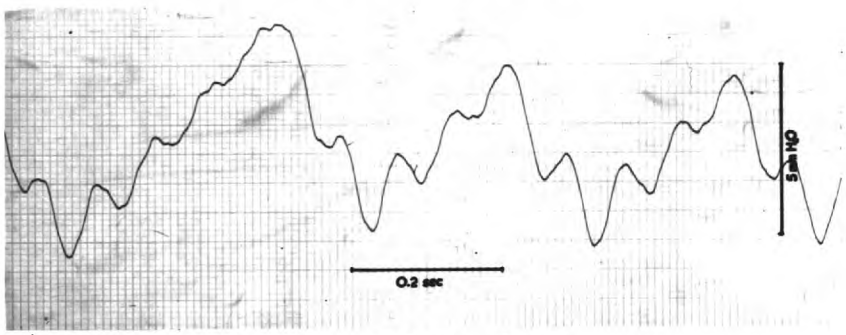

c. AIR-WATER V_c = 5000 cc. G = 8.0 cc/sec.

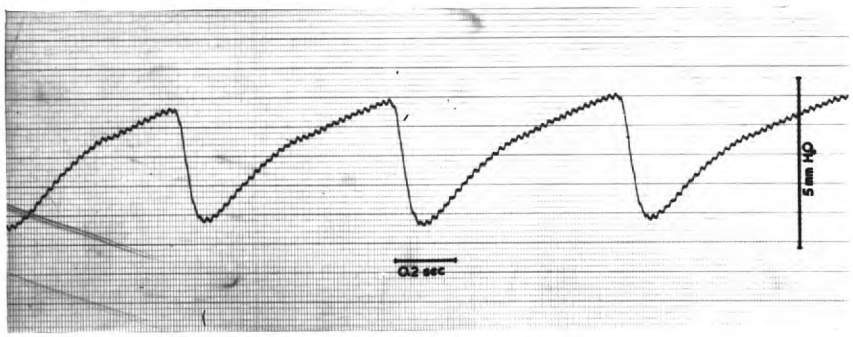

d. AIR-ETHANOL V_c = 2250 cc. G = 1.4 cc/sec

PRESSURE FLUCTUATIONS IN GAS CHAMBER BELOW A 0.125 in. ORIFICE DIAMETER.

air-water and air-ethanol, are given in figures 5. 7 and 5. 8.

5. 2. Effect of Gas Flow Rate and Geometrical Properties of the System (Air-Water System)

The range of air flow rates investigated was 0. 1 - 2. 0 liter/min (i. e. 1. 7 - 33. 3 cc/sec) for an 1/8 in. orifice and 0. 4 - 8. 0 liter/min (i. e. 6. 7 - 133. 3 cc/sec) for an 1/4 in. orifice. The corresponding linear gas velocities $(\frac{G}{A_o})$ were 21 - 416 cm/sec for both orifices.

In each of the graphs shown in figures 5. 9 - 5. 12 the continuous lines represent the theoretical values as calculated from the equations derived in Chapter 4.

The experimental results are represented by the respective points. Since the bubble frequency for different conditions was measured by three different methods as described in (3. 3. 3), the points represent usually an average of the values obtained.

The dotted lines represent the distinction between single and double bubble formation as described by equation (4. 32).

A steady increase in volume of the bubble with increase of gas flow rate and increase of gas chamber volume is observed, both for 1/4 in. and 1/8 in. orifice diameters (Fig. 5. 9 - 5. 10). As a general trend it agrees quite well with the previous work in this field. Referring

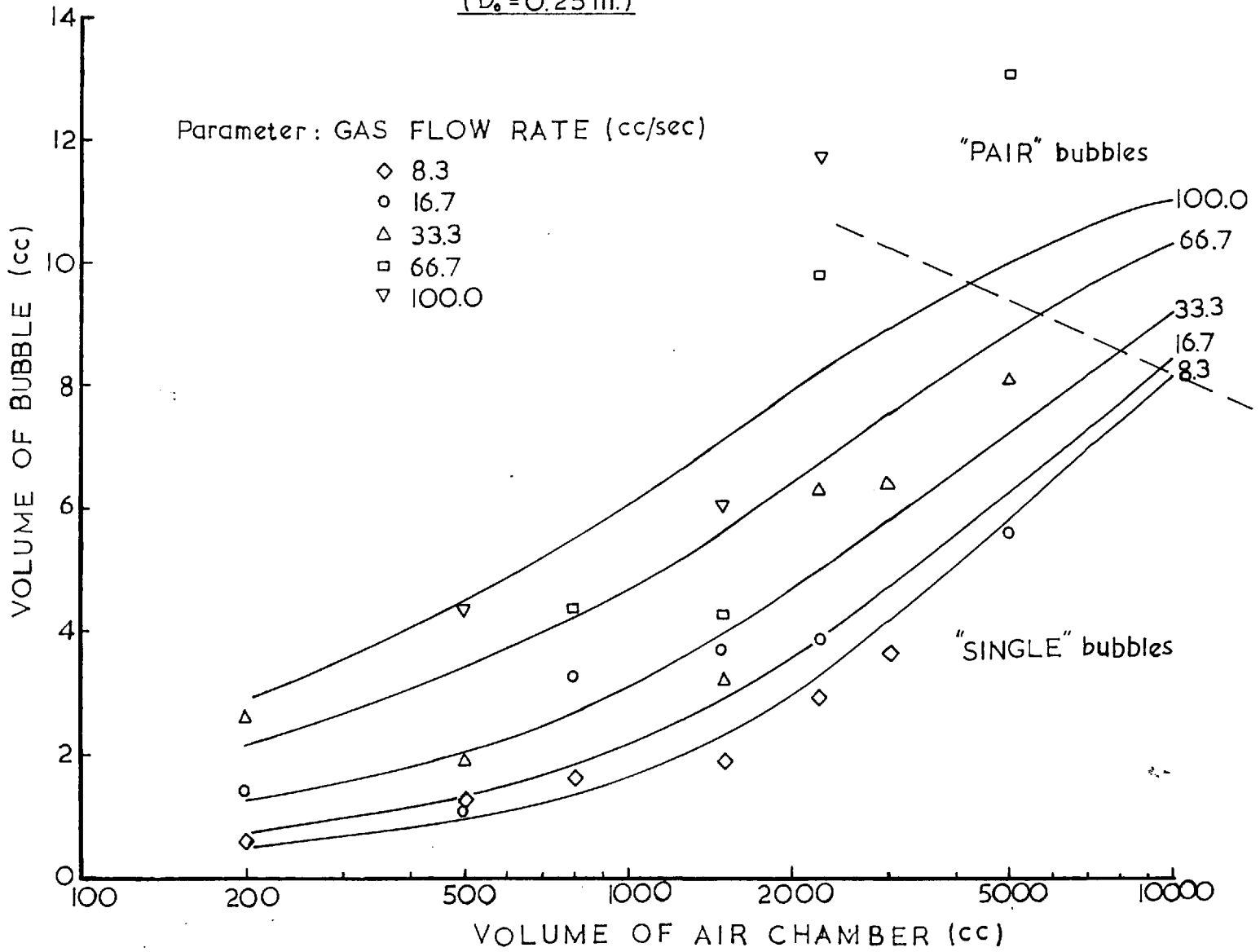
EFFECT OF AIR CHAMBER ON VOLUME OF BUBBLES.
(D₀ = 0.25 in.)
Parameter: GAS FLOW RATE (cc/sec)
8.3
16.7
33.3
66.7
100.0
"PAIR" bubbles
"SINGLE" bubbles
VOLUME OF BUBBLE (cc)
VOLUME OF AIR CHAMBER (cc)
0
2
4
6
8
10
12
14
100
200
500
1000
2000
5000
10000

FIG. 5.9.

EFFECT OF AIR CHAMBER VOLUME ON VOLUME OF BUBBLES.
(D_o = 0.125 in.)

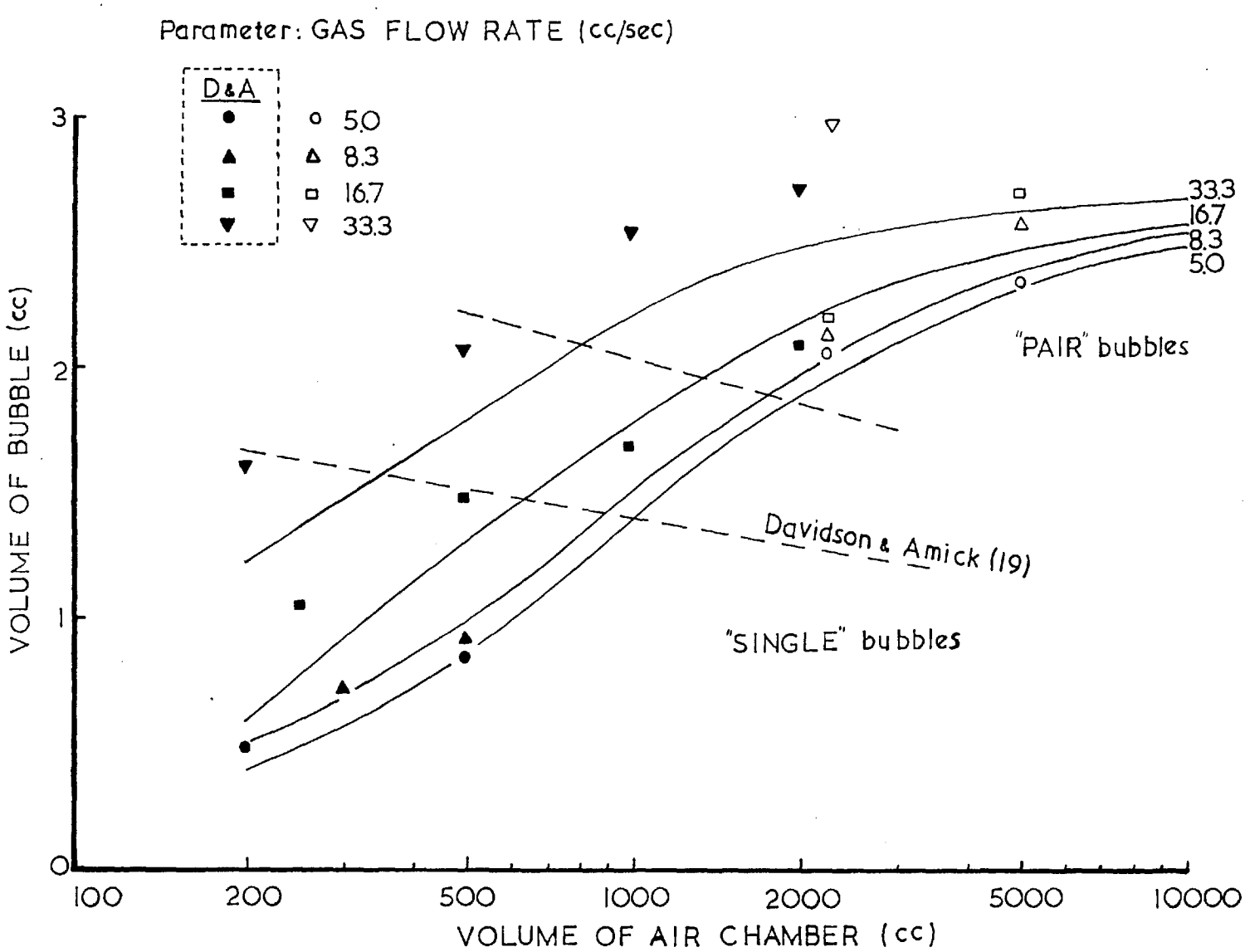

FIG. 5.10.

FIG. 5.11.

EFFECT OF GAS FLOW RATE ON FREQUENCY OF BUBBLES. (D_o = 0.25 in.)

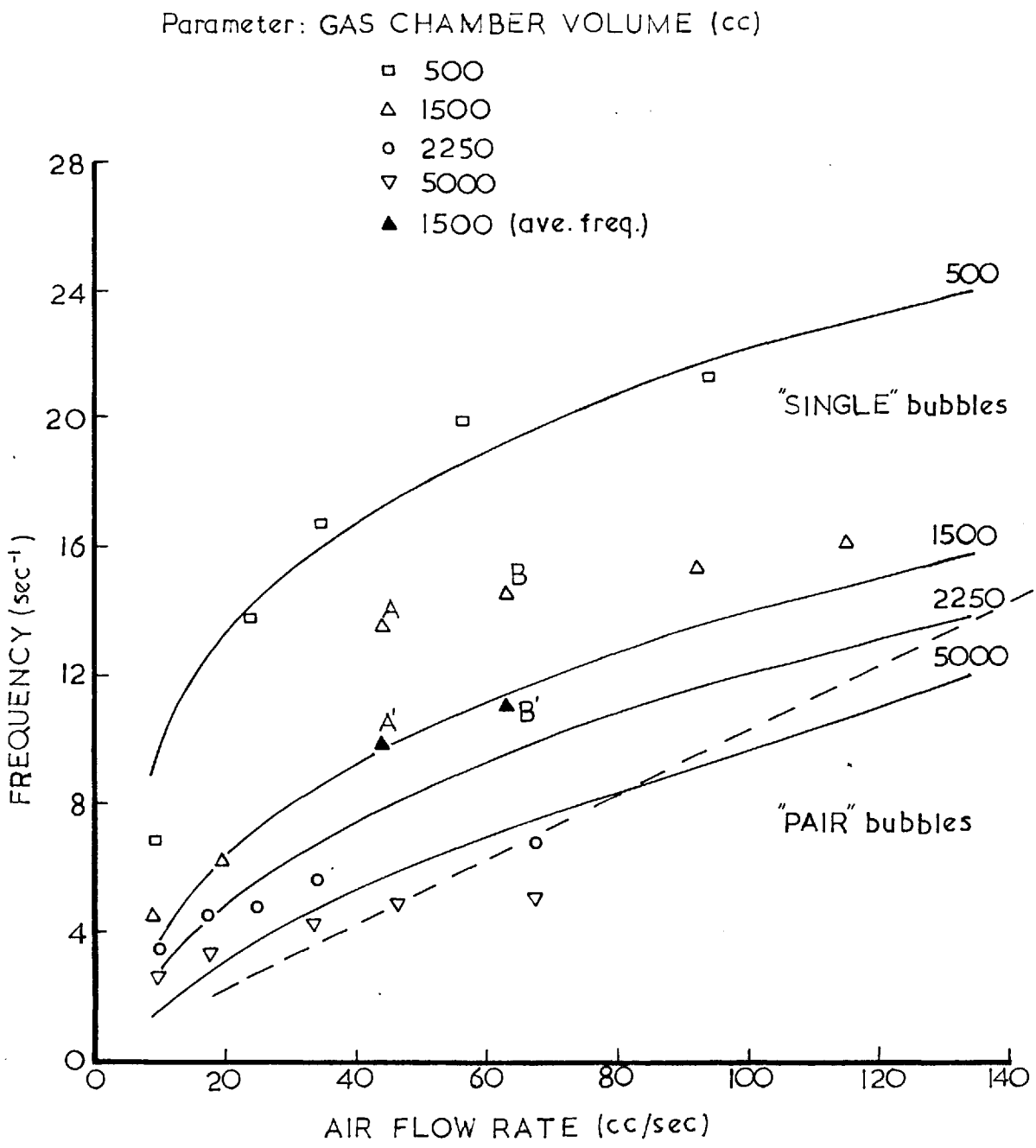

FIG. 5.12.

EFFECT OF GAS FLOW RATE ON FREQUENCY OF BUBBLES. (D_o = 0.125 in.)

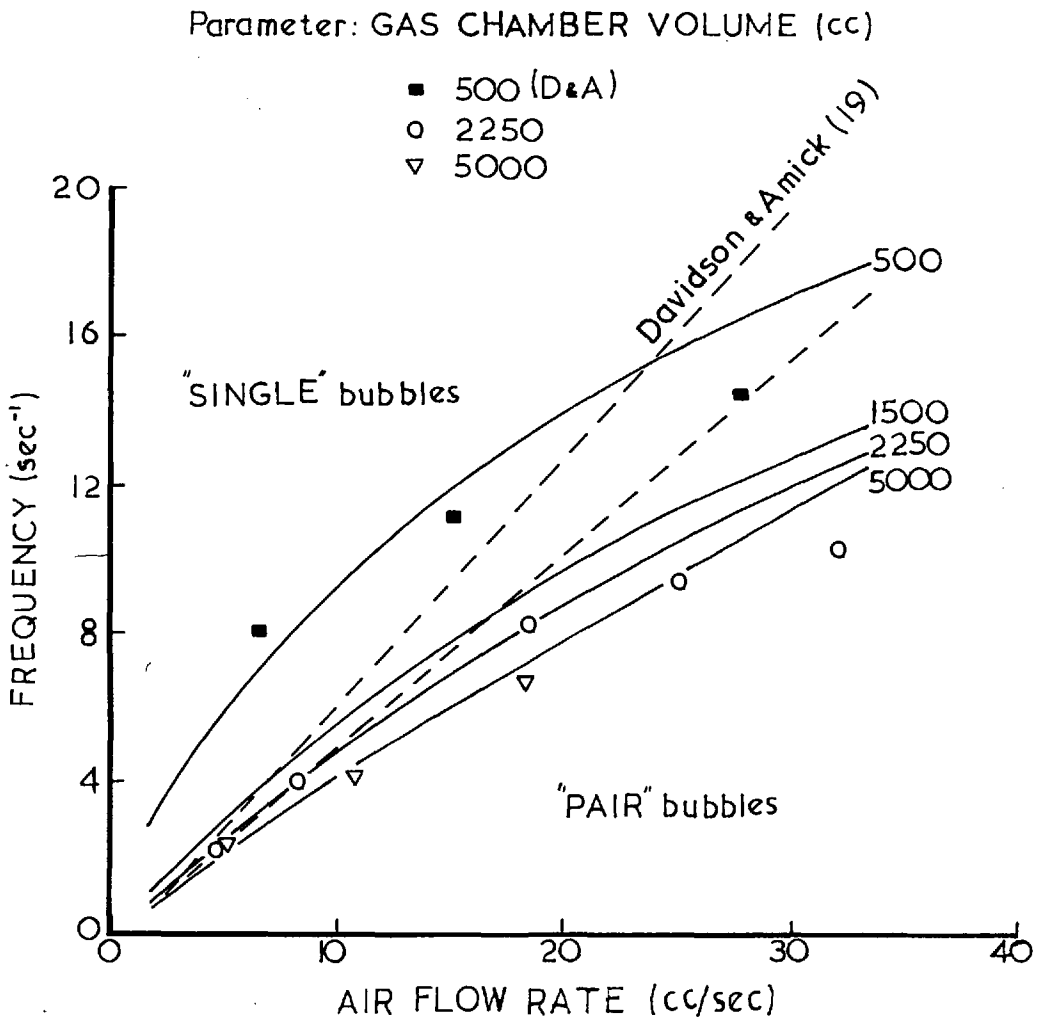

FIG. 5.13.

EFFECT OF GAS FLOW RATE ON VOLUME OF BUBBLE UNDER "CONSTANT FLOW RATE" CONDITIONS.

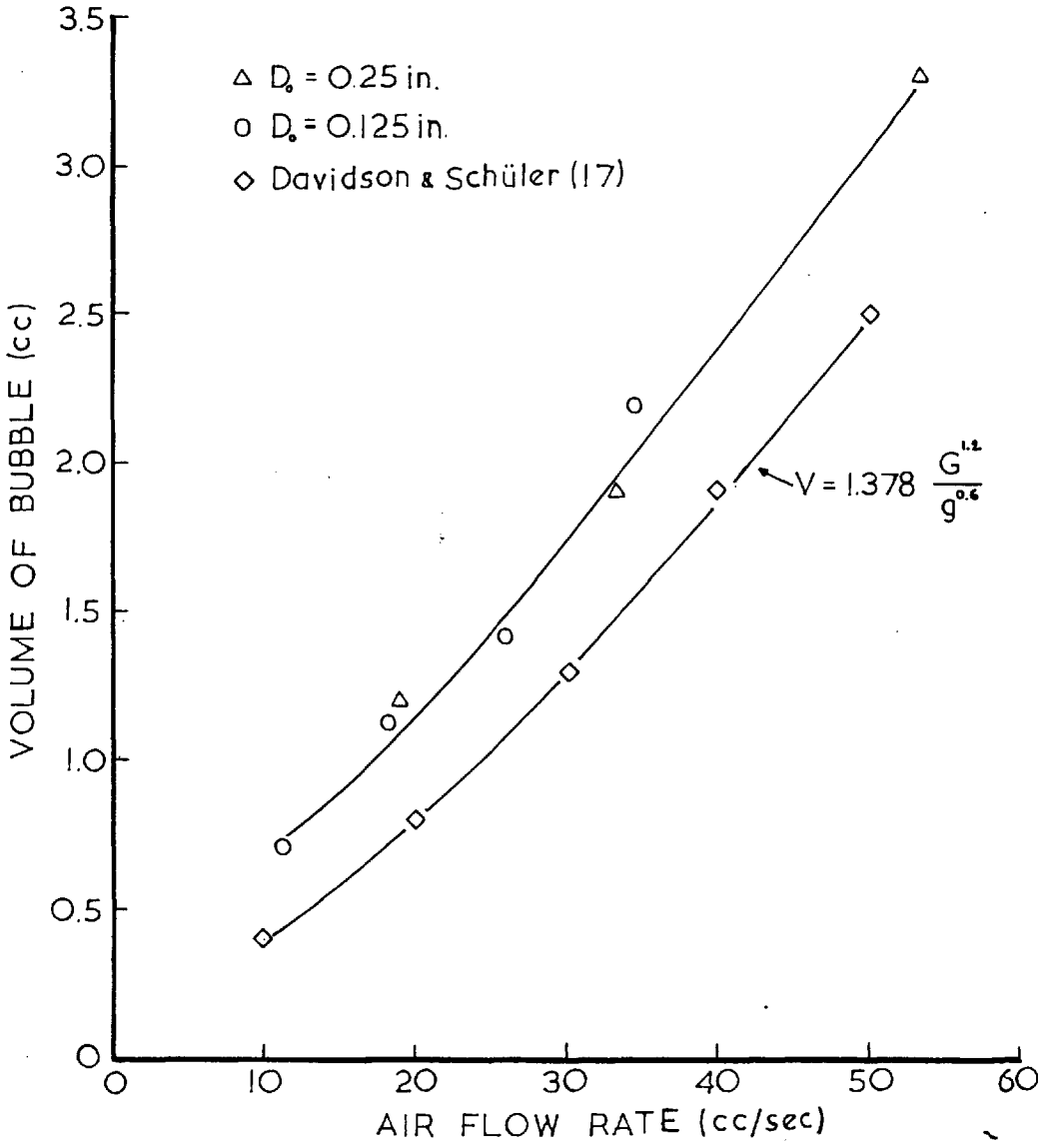

to (2. 11) the main part of the experiments were indeed carried out in the 'slowly increasing volume region'. Values of Reynolds Number given in the literature for this region, corresponds to 7. 5 - 37. 5 cc/sec for 1/8 in. and 15 - 75 cc/sec for 1/4 in.

For higher gas flow rates at a 1/4 in. orifice, the frequency is observed to increase asymptotically to a maximum value, which is again well in agreement with previous work, being mainly in the 'constant frequency region' (Fig. 5. 11).

5. 2. 1. Bubbling at a 1/4 in. Orifice

For very low air flow rates (up to about 20 cc/sec) there is a very good agreement to the theoretical equations, shown by Fig. 5. 9 and 5. 11. Above this range it seems that the gas chamber volume has a more complex effect, than purely increasing the volume of the individual bubbles.

It has been observed, either by photographs or by recorded pressure fluctuations (Fig. 5. 7a) that for moderate flow rates in the range of 30 - 70 cc/sec and for low gas chamber volumes up to about 1500 cc, there is a periodical oscillation of bubble formation, resulting either in smaller bubbles with a higher frequency or larger bubbles with a lower frequency. Such type of behaviour has been observed also by Davidson and Amick (19). For larger gas chamber volumes

this effect has disappeared. A decrease in volume of the gas chamber decreases the volume of the individual bubble, that is increases the bubbling frequency. It might be possible that the frequency of the bubbles becomes so high that the assumption of the liquid in the vicinity of the orifice being at rest is invalid and the different states of liquid motion might cause the alternative behaviour, as stated also by Davidson and Amick (19).

For a consistent representation of the experimental results, the values used are for the smaller bubbles with higher frequency. Thus for a low gas chamber volume of this range (500 cc), the agreement with the theory becomes quite good, while a discrepancy exists with a higher volume (1500 cc), as seen in Fig. 5.11.

It is worth observing the two experimental points A and B, referring to a gas chamber volume of 1500 cc (Fig. 5.11). Calculating an average frequency due to the two possible frequencies of bubbling, the respective points A' and B' fit well with the theoretical line.

The discrepancies observed for very large gas chamber volumes or for higher air flow rates (above 70 cc/sec), where the volume of the bubble is larger, is due either to the formation of a secondary bubble represented by the dotted line or to the limitation of the theory due to its initial assumptions, or to the both effects. The degree of the discrepancy depends on the magnitude of such a secondary bubble

or the rate of distortion of the bubble from a spherical shape.

The extremely good agreement with the theory for certain conditions in the lower range of gas flow rate can be seen in the rate of growth of the bubble (Fig. 5.14) and in the pressure change in the gas chamber (Fig. 5.15a). As can be seen in Fig. 5.1 which shows the bubble formation for the above conditions, the corresponding bubble is not completely spherical. To get a better value for the average radius during its growth (Fig. 5.14) the bubble was treated as a spheroid, thus the diameter of an equi-volume sphere was calculated from:

$$\frac{\pi}{6} \bar{D}_B^{\,3} = \frac{\pi}{6} a^2_x \, b_x \qquad (5.1)$$

Where a_x, b_x are the axis of the spheroid.

The discrepancy in the values of the pressure in the gas chamber compared to the theory, for the 'waiting stage', as shown in fig. 5.15a, can be due to the changes of chamber volume which are not considered in the theoretical equations. Immediately after the detachment of the bubble, the remaining small bubble which is attached to the orifice tends to grow, thus the system (bubble and chamber) tends to expand, resulting in a lower increase in pressure compared to the theory. Once the pressure behind the accelerating bubble is large enough to push this small bubble back through the orifice, with a possibility of

FIG. 5.14.

RADIUS AND VERTICAL DISTANCE OF CENTRE OF BUBBLE FOR "BUBBLING PERIOD". (D_o=0.25 in.)

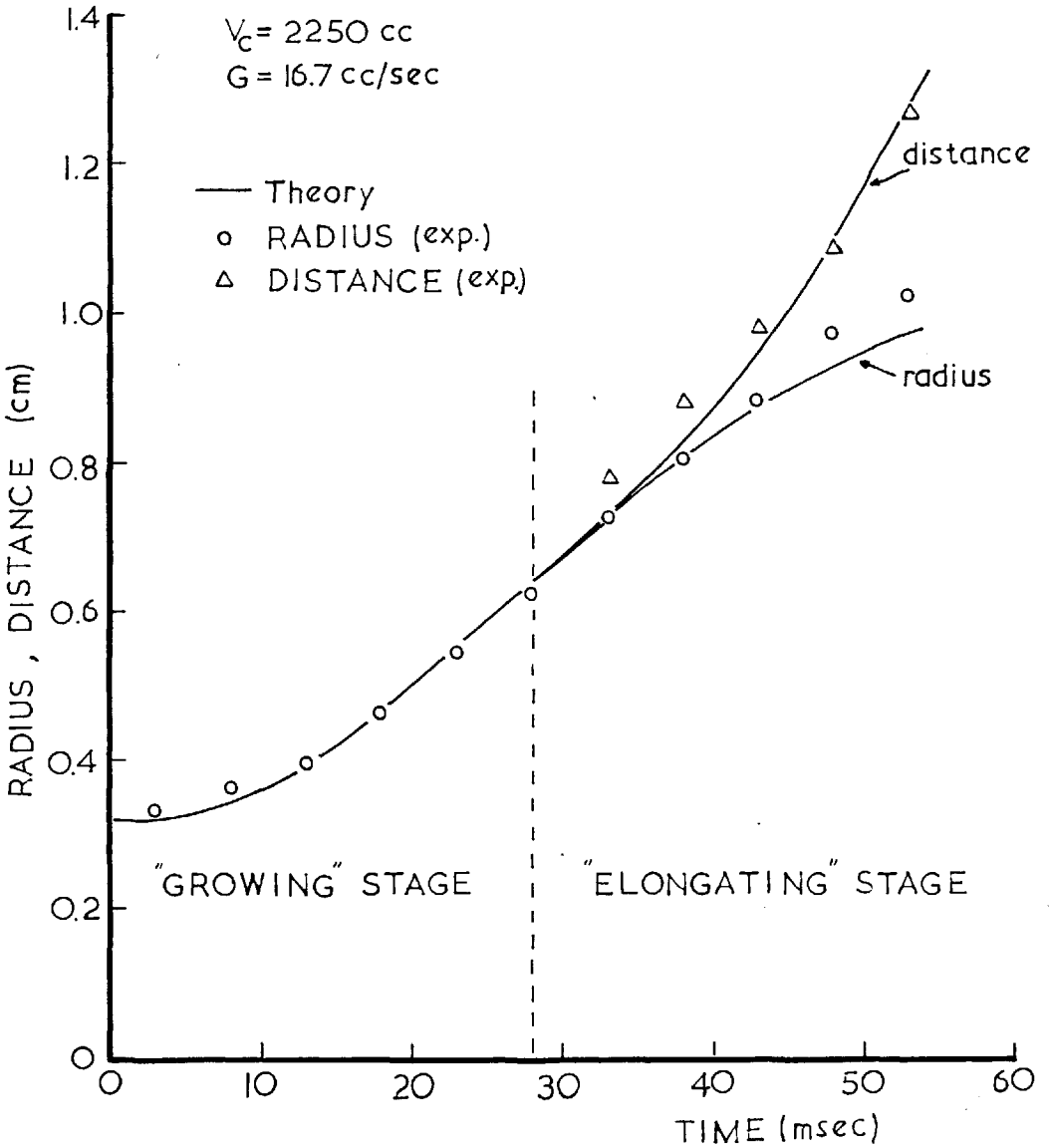

FIG. 5.15.

GAS CHAMBER PRESSURE FOR A CYCLE OF BUBBLE FORMATION. (D_o = 0.25 in.)

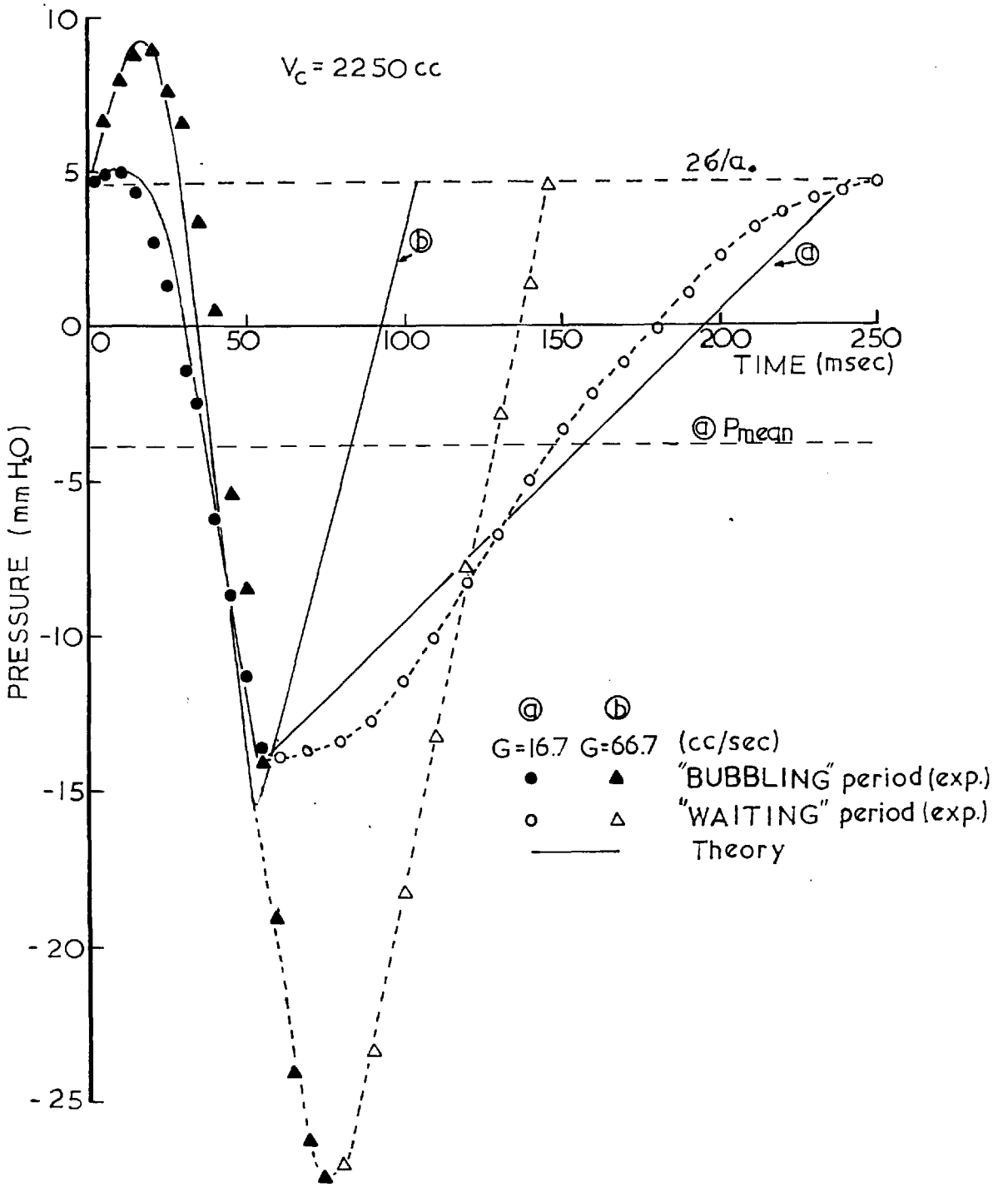

FIG. 5.16.

RADIUS AND VERTICAL DISTANCE OF CENTRE OF BUBBLE FOR "BUBBLING PERIOD". (D_o=0.125 in.)

V_c = 2250 cc
G = 16.7 cc/sec

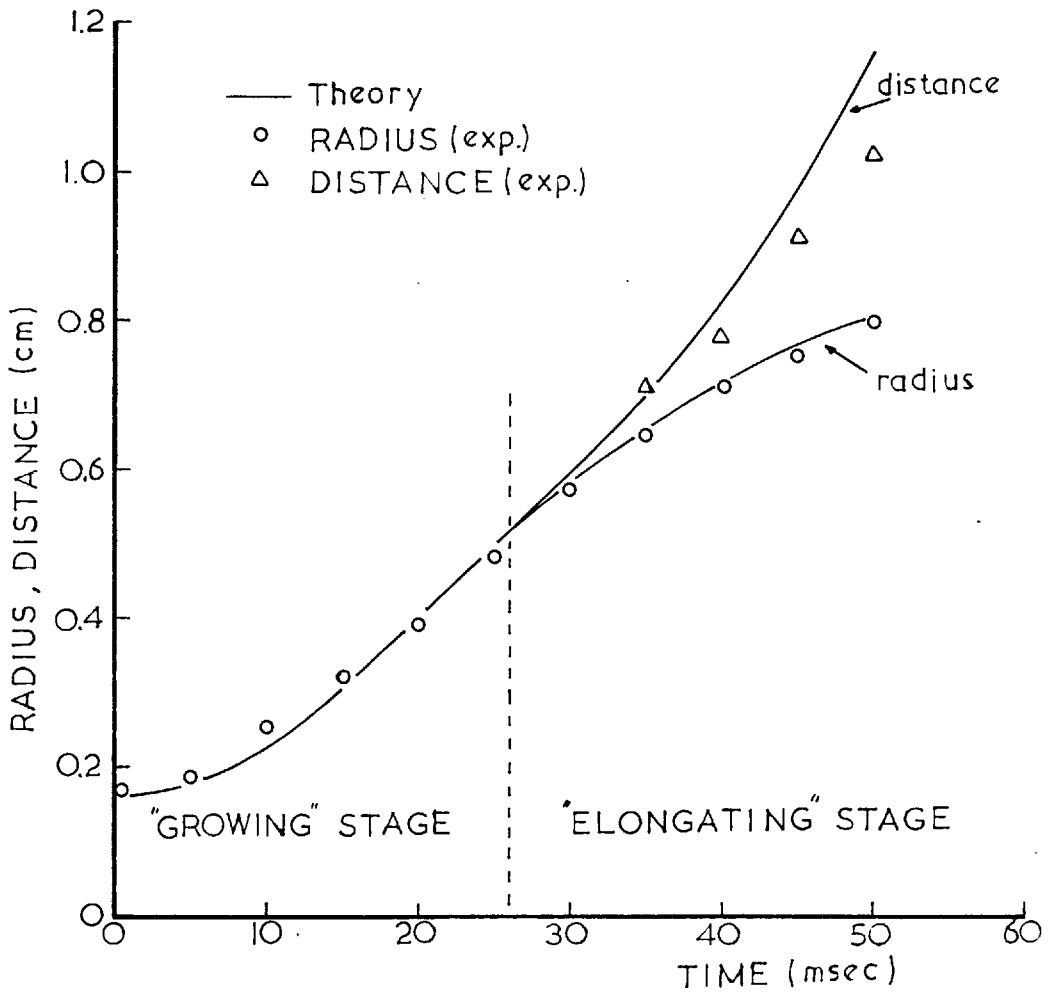

FIG. 5.17.

GAS CHAMBER PRESSURE FOR A CYCLE OF BUBBLE FORMATION. (D_o = 0.125 in.)

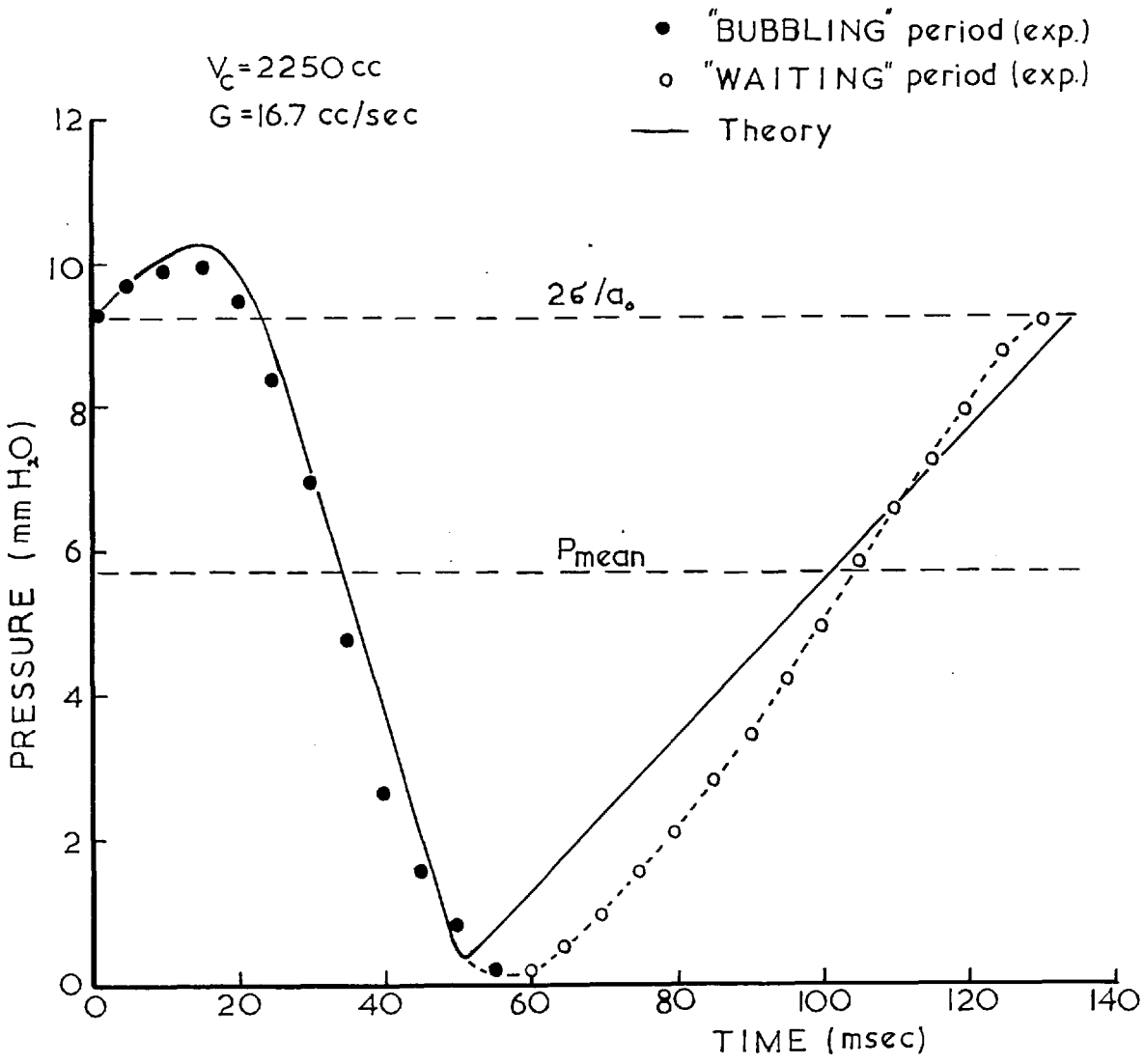

dumping, the system tends to contract, resulting in a larger increase in pressure. When the next bubble starts forming, the system tends to expand, resulting again in a lower increase in pressure compared to the theory.

The presence of a small secondary bubble can be seen in fig. 5.15b. Although for the initial stages there is quite a good agreement for the pressure change in the gas chamber, the pressure continues to decrease due to the secondary bubble.

5.2.2. Bubbling at an 1/8 in. Orifice

The general trend of behaviour is similar to bubbling at the 1/4 in. orifice (Fig. 5.10).

Although no experiments were carried out for gas chamber volumes lower than 2250 cc, using Davidson and Amick (19) results for this range, there is a good agreement with the present theory. Also the criterion between 'single' and 'pair' bubble formation is reasonably in agreement. This criterion is for much lower gas flow rates and gas chamber volumes, compared to bubbles at a 1/4 in. orifice.

Since the secondary bubble which might form is usually quite small and the bubbles have in general a lower volume, the discrepancy of the results for this range is in general lower than in the case of bubbling at a 1/4 in. orifice.

Comparing the gas chamber volume effect on the volume of bubbles formed at an 1/8 in. orifice (Fig. 5. 10) to those formed at a 1/4 in. orifice (Fig. 5. 9) it can be seen that for very small chamber volumes (up to 500 cc.) there is no difference between the bubbles volume, for the range of flow rates investigated (the range for 1/8 in. orifice). The difference starts to be more significant for chamber volumes above 800 cc., resulting in a larger volume for bubbles formed at a 1/4 in. orifice.

Those results are quite well in agreement with Davidson and Schüler (17) theory for bubbling under 'constant flow rate' condition, for which the gas chamber volume effect is eliminated (one might postulate an infinite small gas chamber volume). Some experimental results which were carried out for 'constant flow rate' conditions, and the calculated values from Davidson and Schüler theory are shown in fig. 5. 13. Comparison to fig. 5. 9 and 5. 10 shows the agreement with the behaviour of the small chamber volumes.

There is no considerable effect of gas chamber volumes above 1500 cc. on bubble volume or frequency for bubbles formed at an 1/8 in. orifice. An increase in gas flow rate has only a very slight effect of increasing the volume of the bubble, resulting in a steady increase in their frequency, probably to a maximum value of about 17 bubbles/sec, as has been observed by Calderbank (24).

The agreement with the theory can be seen also for the growth rate of a bubble (Fig. 5.16) using the same method as in (5.2.1), or pressure change in the gas chamber (Fig. 5.17).

5.3. Effect of Physical Properties of the System

The air-ethanol system was investigated under the same conditions as the air-water system, using the same range of gas flow rates. The experimental results compared to the theoretical ones are given in figures 5.18 and 5.19.

In general it has been observed the same trend of behaviour as for the air-water system, with a similar degree of discrepancy between the theoretical and experimental results.

The theoretical values of bubble volumes are shown in comparison to some of the air-water systems. It can be seen that all over the range investigated and under similar conditions the volume of the bubble is larger for the air-water system.

The dotted line represents again the distinction between single and double bubble formation as described by equation (4.32). Comparing to Fig. 5.9 and 5.10, it can be seen that although the appearance of a secondary bubble for the air-ethanol system is for slightly higher gas flow rates or slightly larger chamber volumes, the volume of the bubble for these conditions is slightly lower than that for the air-water system.

FIG. 5.18.

EFFECT OF GAS FLOW RATE ON VOLUME OF BUBBLE FOR AIR-ETHANOL SYSTEM. (D_o = 0.25 in.)

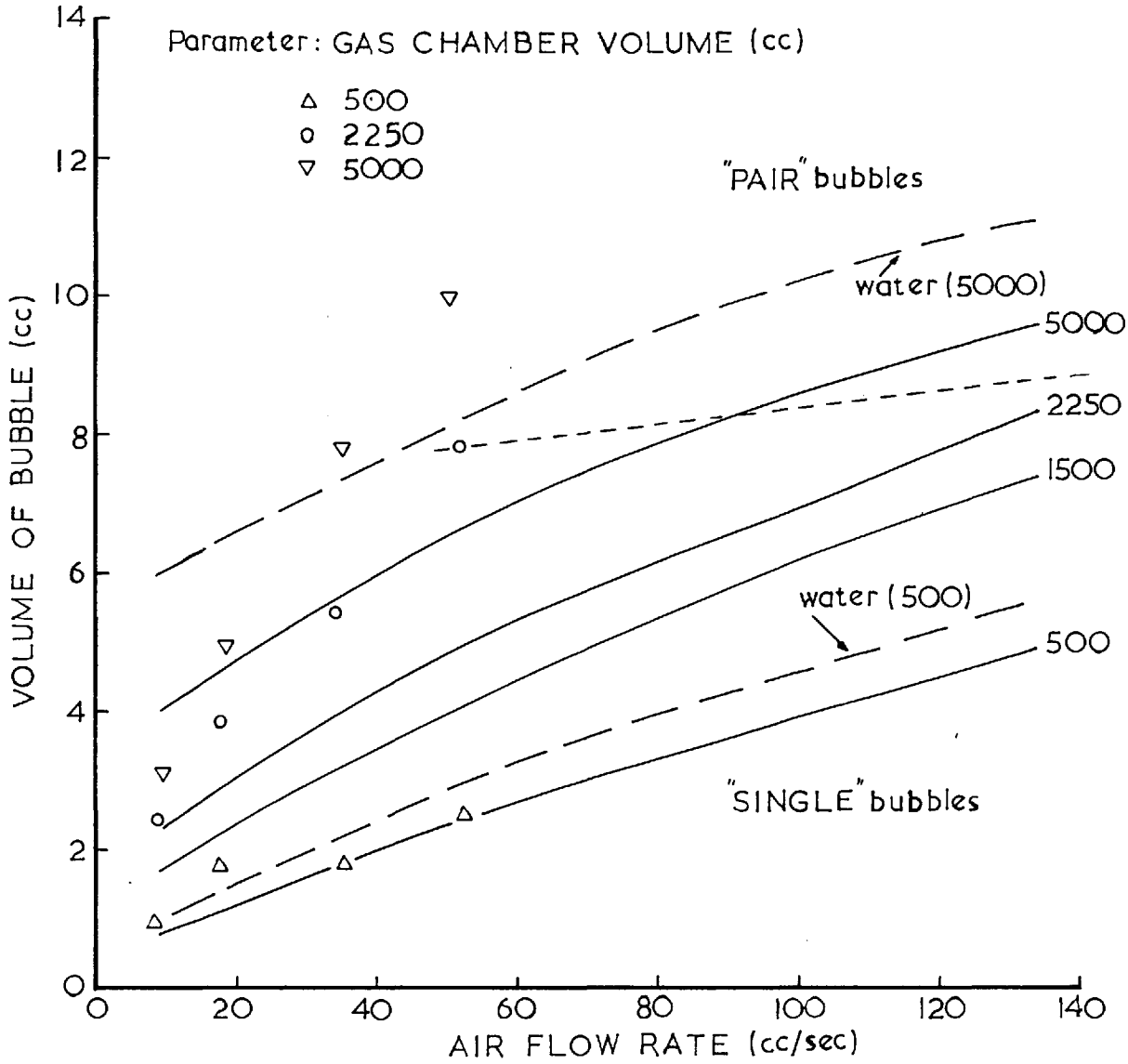

FIG. 5.19.

EFFECT OF GAS FLOW RATE ON VOLUME OF BUBBLE FOR AIR-ETHANOL SYSTEM. (D_o = 0.125 in.)

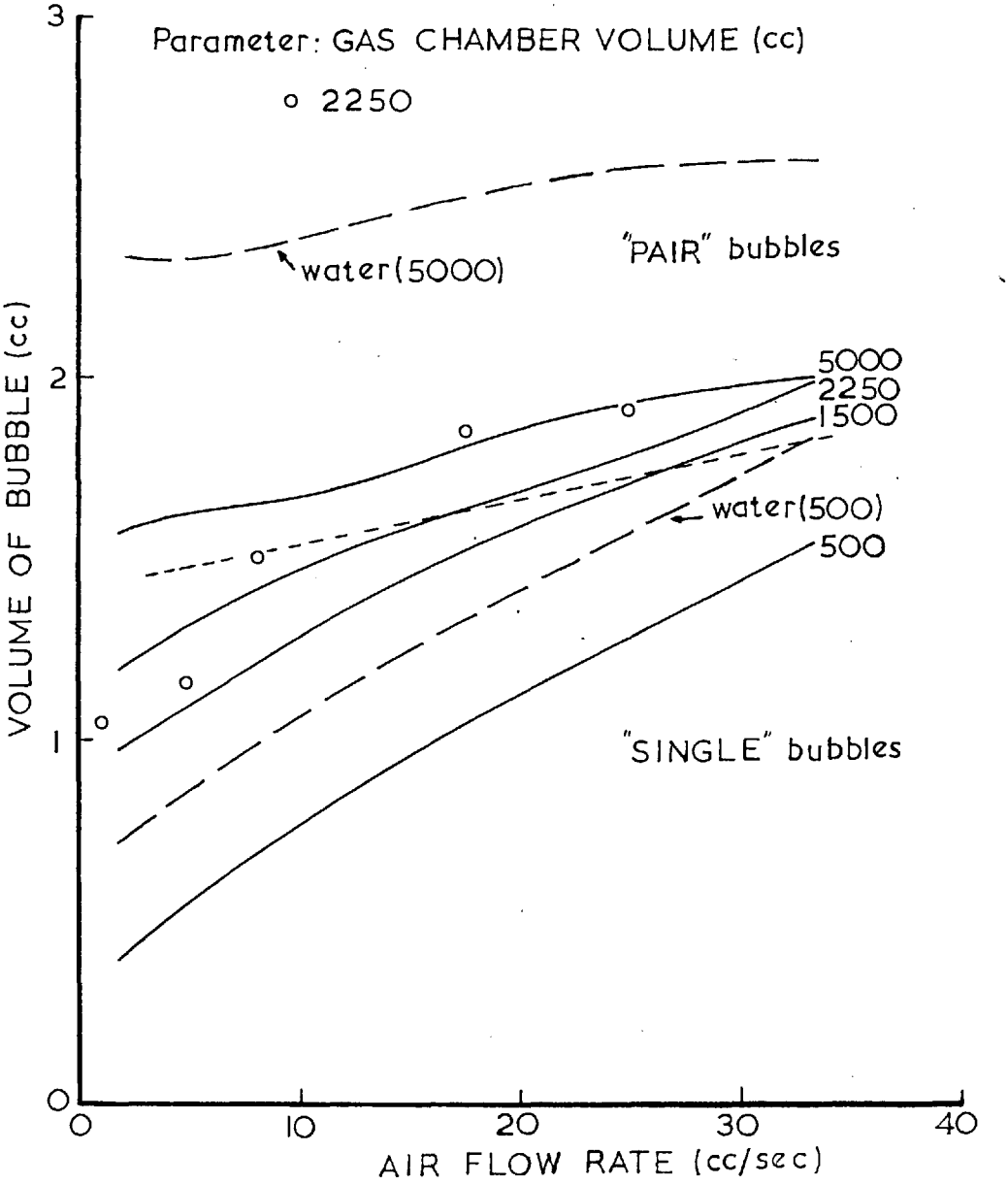

5.4. Analysis of the Theoretical Equations

Analysis of several equations derived in (4.2.3) and (4.2.5) can explain the general trend of behaviour of a bubbling system as observed in (5.1), (5.2) and (5.3), by investigating the effects of each of the components involved in the pressure equations. Some examples of such an analysis for the volume of the bubbles is given below.

5.4.1. Effect of Gas Chamber Volume (Fig. 5.20)

Considering the three components of the pressure in the bubble (equation 4.27) it can be seen that the effect of chamber volume on $\frac{2\sigma}{a}$ and $\rho_L gs$ is negligible compared to its effect on the inertia term $\rho_L \left[a\frac{d^2a}{dt^2} + \frac{3}{2}\left(\frac{da}{dt}\right)^2 \right]$.

As the bubble starts growing the flow rate through the orifice is smaller compared to the mean gas flow rate in the chamber (according to the assumption that the initial growth rate is zero). Thus for a small chamber volume the pressure in the chamber will increase quicker than for a large chamber volume. So a slight increase in the flow rate through the orifice is expected for the small chamber volume, compared to the large one, resulting in a higher value for the inertia term.

As soon as the flow rate through the orifice exceeds the value

FIG. 5.20.

VARIOUS PRESSURE COMPONENTS FOR THE "BUBBLING PERIOD".

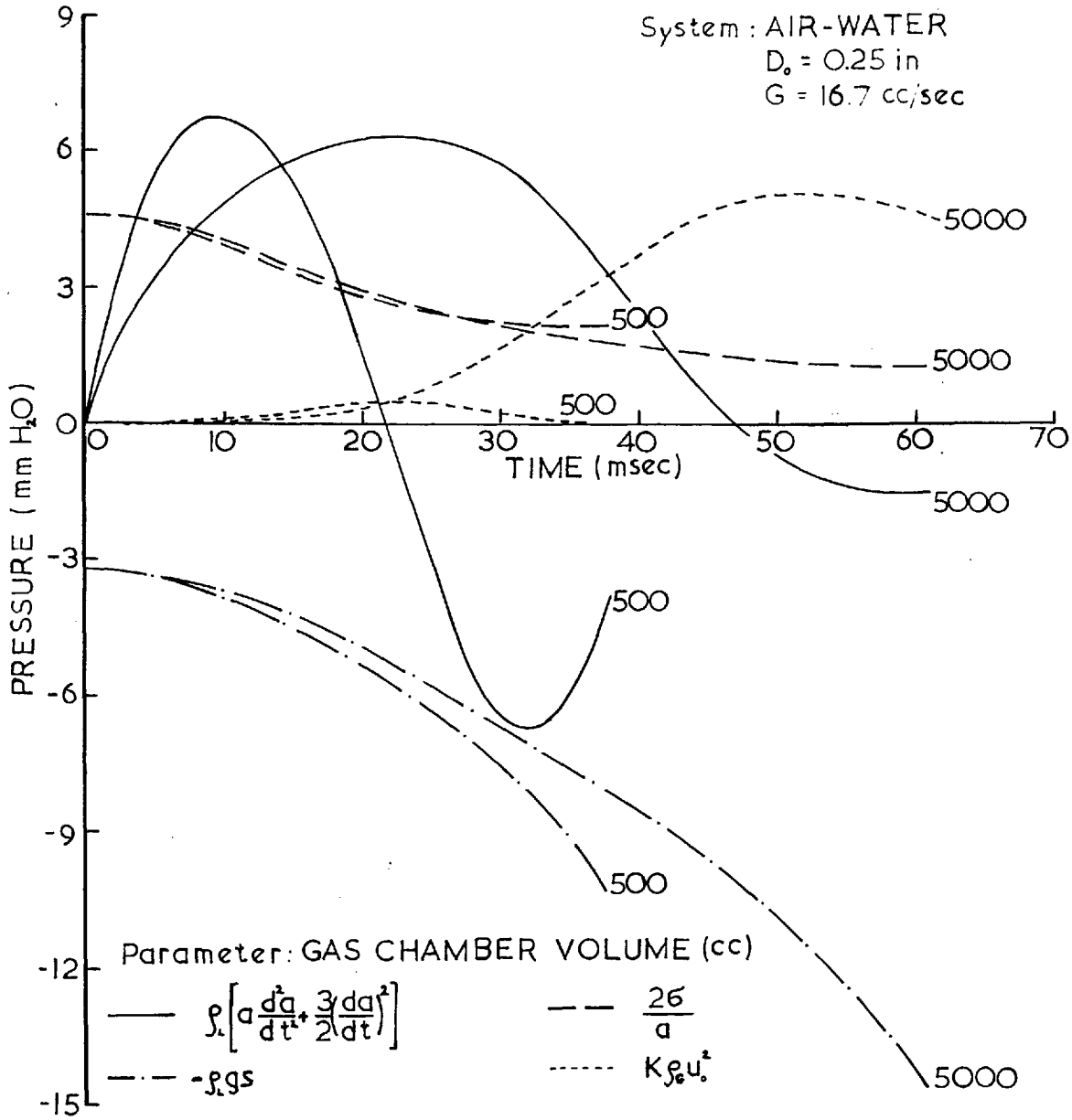

FIG. 5.21.

VARIOUS PRESSURE COMPONENTS FOR THE "BUBBLING PERIOD".

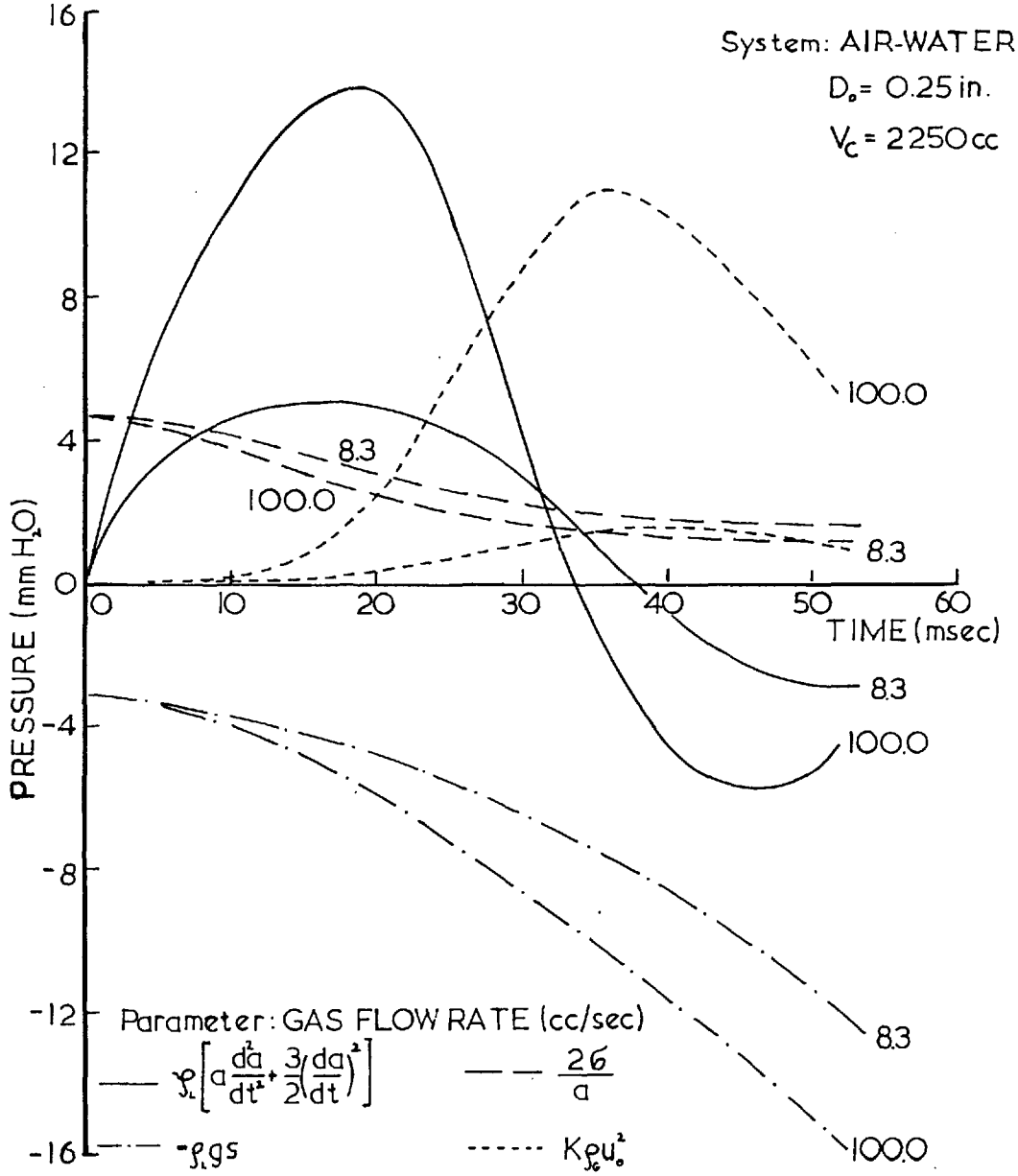

FIG. 5.22.

VARIOUS PRESSURE COMPONENTS FOR THE "BUBBLING PERIOD".

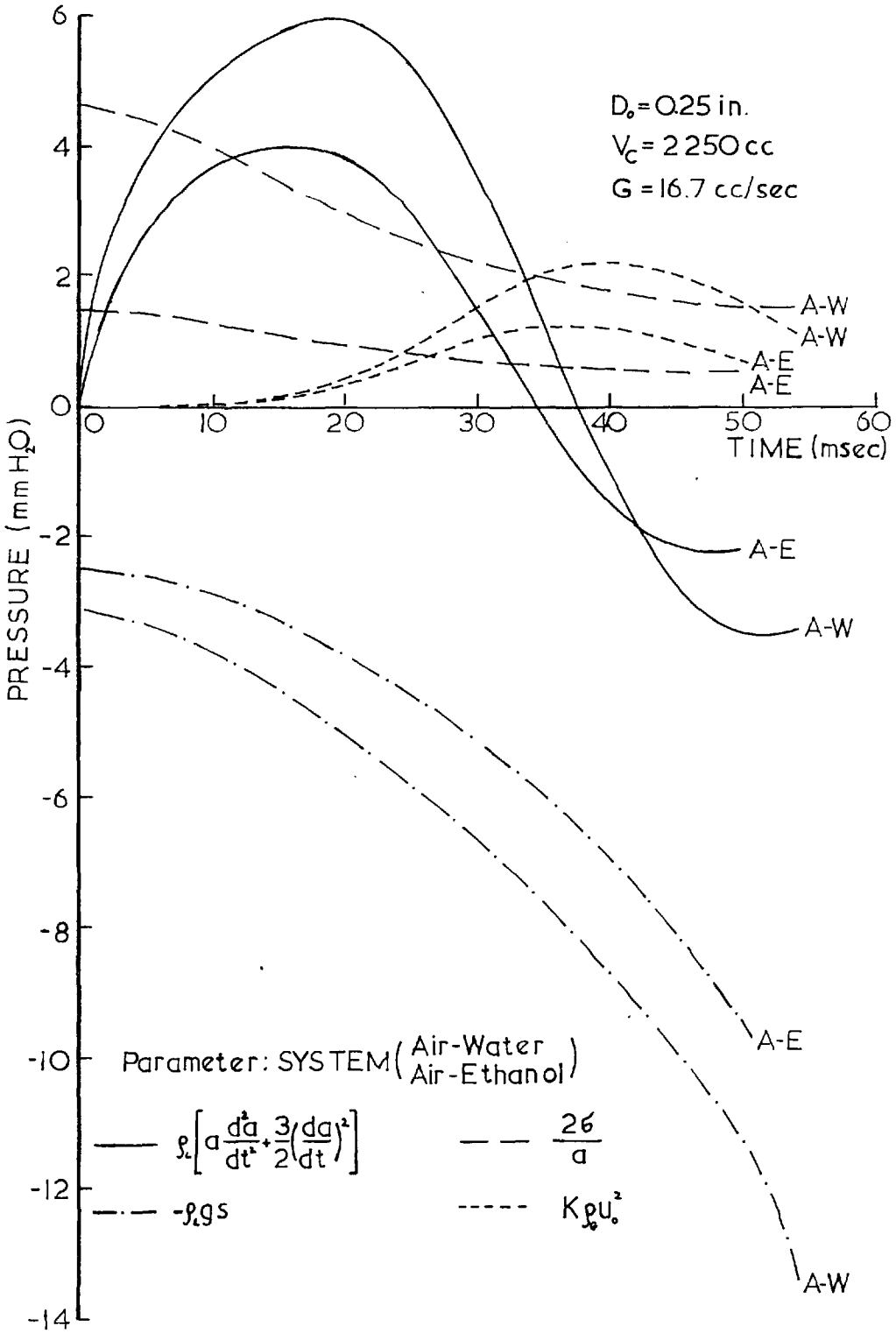

of the mean flow rate in the chamber, the pressure in the small chamber decreases quicker than in the large chamber. So a decrease in flow rate through the orifice (pressure term $K\rho_G u_o^2$) is expected for the small chamber, resulting in a lower value of the inertia term.

From the $\rho_L gs$ term it can be seen that the velocity of rise of the bubble is lower for a large chamber, thus the period of bubbling (for moving a distance equal to a_o) is longer.

Both factors of longer bubbling time and higher flow rate through the orifice tend to increase the bubble volume formed above a large chamber.

5.4.2. Effect of Gas Flow Rate (Fig. 5.21)

Considering again the components of the pressure (equation 4.27) it can be seen that the effect of gas flow rate is also mainly on the inertia term $\rho_L \left[a\frac{d^2a}{dt^2} + \frac{3}{2}\left(\frac{da}{dt}\right)^2 \right]$.

An increase in the gas flow rate in the chamber tends to increase the pressure in the chamber, thus a higher gas flow rate is expected through the orifice, resulting in a higher value for the inertia term.

Since the bubbling time is nearly the same, this higher gas flow rate through the orifice causes the formation of a larger bubble volume for the high gas flow rate.

5.4.3. Effect of Physical Properties of the System (Fig. 5.22)

Using the system air-ethanol in comparison to the air-water system, and considering again the pressure components (equation 4.27) it can be seen that the stronger effect is in the surface tension term $(\frac{2\sigma}{a})$.

The difference in $\rho_L gs$ terms which is nearly constant, is mainly due to the density difference between water and ethanol. Thus the velocity of rise is nearly the same, resulting in nearly the same bubbling time.

Considering the dimensionless equation for the radial expansion of the bubble (equation 4.38), provided the only variable is the surface tension, the inertia term is inversely proportional to the Weber Number, i.e. it is proportional to the ratio of surface tension pressure $(\frac{2\sigma}{a})$ and dynamic pressure $(\rho_L u^2)$. Since the velocity of rise is nearly the same, and since the $\frac{2\sigma}{a}$ ratio is larger than $\rho_L u^2$ ratio, a higher value of $\frac{1}{We}$ is expected for the air-water system, resulting in a higher value for the inertia term.

A higher gas flow rate through the orifice is observed for the air-water system, resulting in a larger bubble volume.

5.5. Formation of Bubbles on a Sieve Tray

5.5.1. Behaviour of a Sieve Tray

As described in (2.2) it is convenient to consider the bubble formation on a sieve tray as a similar process to the bubbling at a single orifice. Thus in addition to most of the factors which might affect bubble formation at an orifice, it is necessary to take into consideration also the plate geometry, for an accurate analysis of the bubble formation on a sieve tray.

A limited number of experiments were carried out with two small sieve trays, 0.25 in. and 0.125 in. diameter of perforations, for which the distance between each two neighbouring holes was large enough to eliminate to a certain extent the interaction of bubbles during formation.

The general trend of behaviour of those trays, working in the 'dumping range' agree quite well with the work published in this field. As stated by Chan and Prince (15) the pressure in the gas chamber underneath the tray fluctuates in a periodic manner. Since these pressure fluctuations are responsible for the flow of liquid or gas through the holes, for a stable operation, their amplitude is the minimum required to obtain the overall fluid flow through the holes. Thus, an increase in gas flow rate or an increase in the number of holes both have the similar effect of decreasing the amplitude of the pressure

fluctuations. (Since the random formation of bubbles one may postulate for an infinite number of holes that at any instant the nett effect of pressure variations under the individual holes is zero.)

For the present investigation figure 5. 23 shows the effect of number of holes and figure 5. 24 shows the effect of gas flow rate on pressure fluctuations. A similar effect of the gas flow rate is reported also by Davies and Porter (44).

For a limited number of holes, an increase in gas flow rate tends to increase the frequency of pressure fluctuations, as seen in figures 5. 25 and 5. 26. An increase in the number of holes has no appreciable effect for 1/8 in. holes (Fig. 5. 26), but tends to increase the pressure fluctuations for 1/4 in. holes (Fig. 5. 25), as reported also by Chan and Prince (15). Nevertheless the frequency reaches a constant value, already for a limited number of holes.

For a constant volume of gas chamber it seems that there is almost no effect of the hole diameter on the maximum frequency, provided the gas flow rate is high enough to ensure bubbling through any of the perforations.

However the volume of the gas chamber has an appreciable effect on the frequency. Although this effect has not been studied in the present investigation, Chan and Prince (15) have derived a theoretical model for which the frequency is dependent upon $V_c^{-0.50}$,

FIG. 5.23

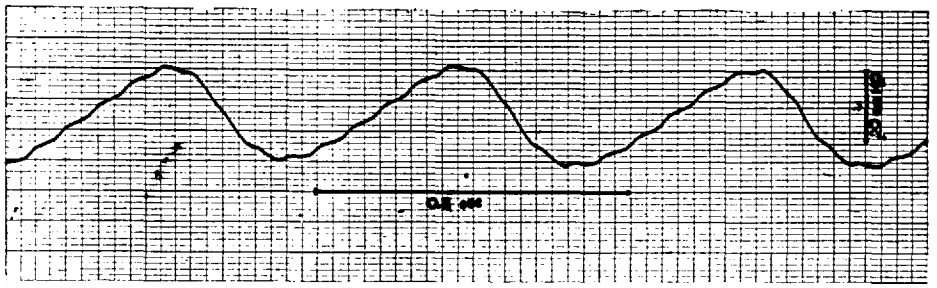

a. 1 HOLE

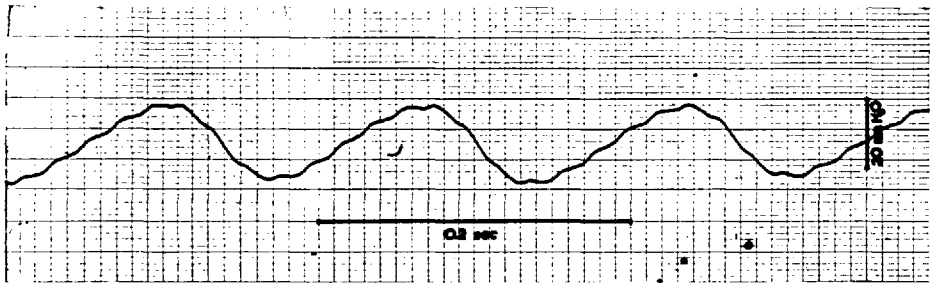

b. 3 HOLES

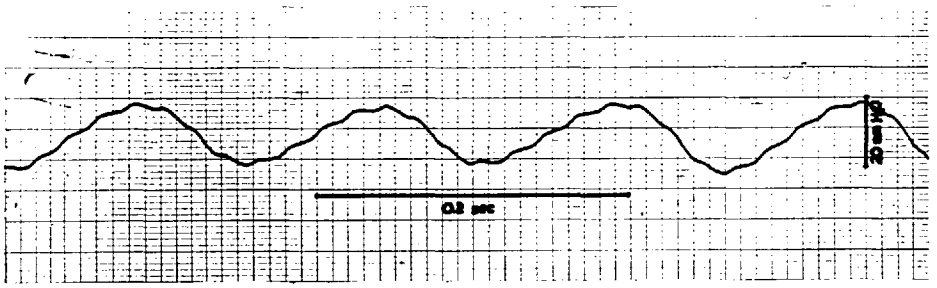

c. 5 HOLES

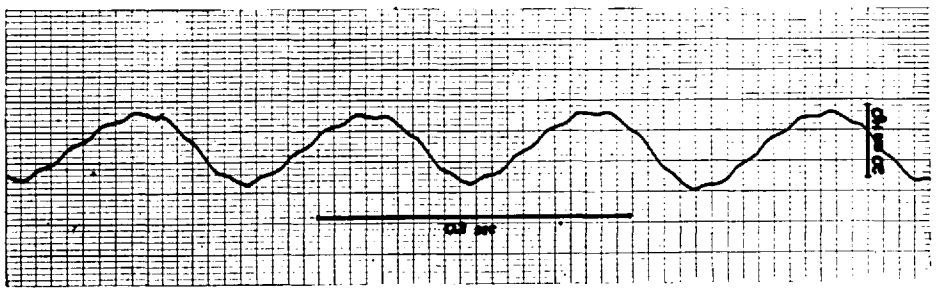

d. 7 HOLES

PRESSURE FLUCTUATIONS IN GAS CHAMBER BELOW A SIEVE TRAY.

(D_0 = 0.25 in. , V_c = 2250 cc. , G = 33.3 cc/sec)

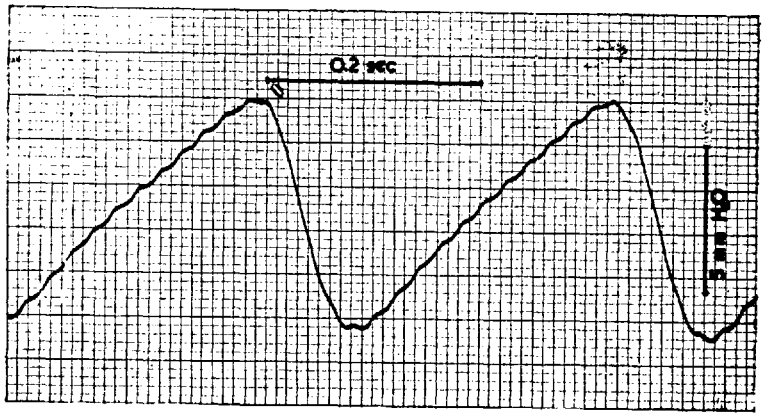

a. G = 8.0 cc/sec

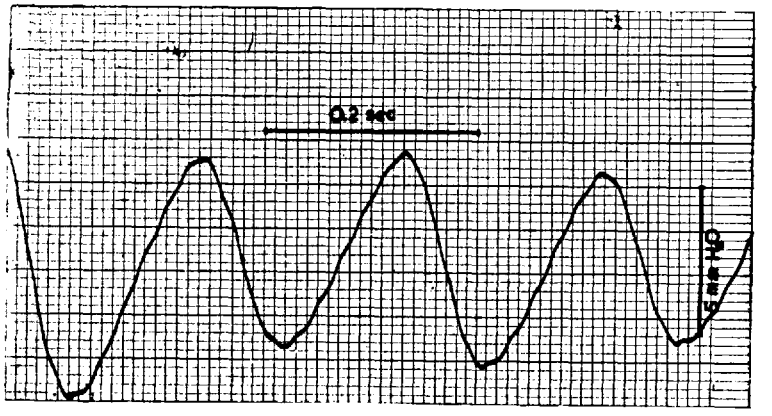

b. G = 16.2 cc/sec

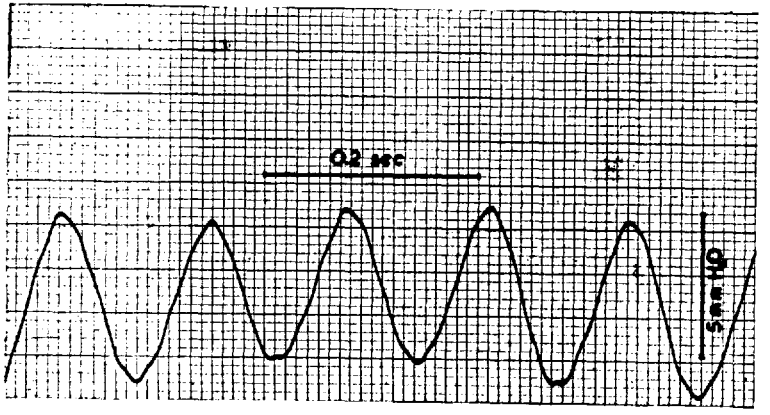

c. G = 33.2 cc/sec

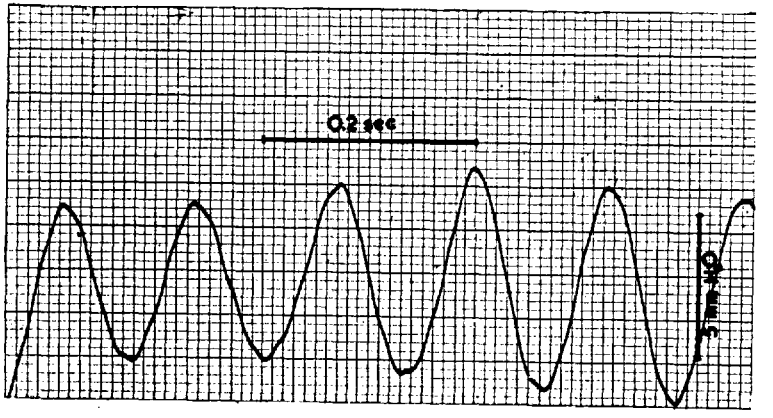

d. G = 51.5 cc/sec

PRESSURE FLUCTUATIONS IN GAS CHAMBER BELOW A SIEVE TRAY.
(D_o = 0.125 in. , V_c = 2250 cc. , 19 HOLES)

FIG. 5.24.

FIG. 5.25.

MEAN FREQUENCY OF BUBBLES AND FREQUENCY OF PRESSURE FLUCTUATIONS IN A SIEVE TRAY.
(0.25 in. PERFORATIONS)

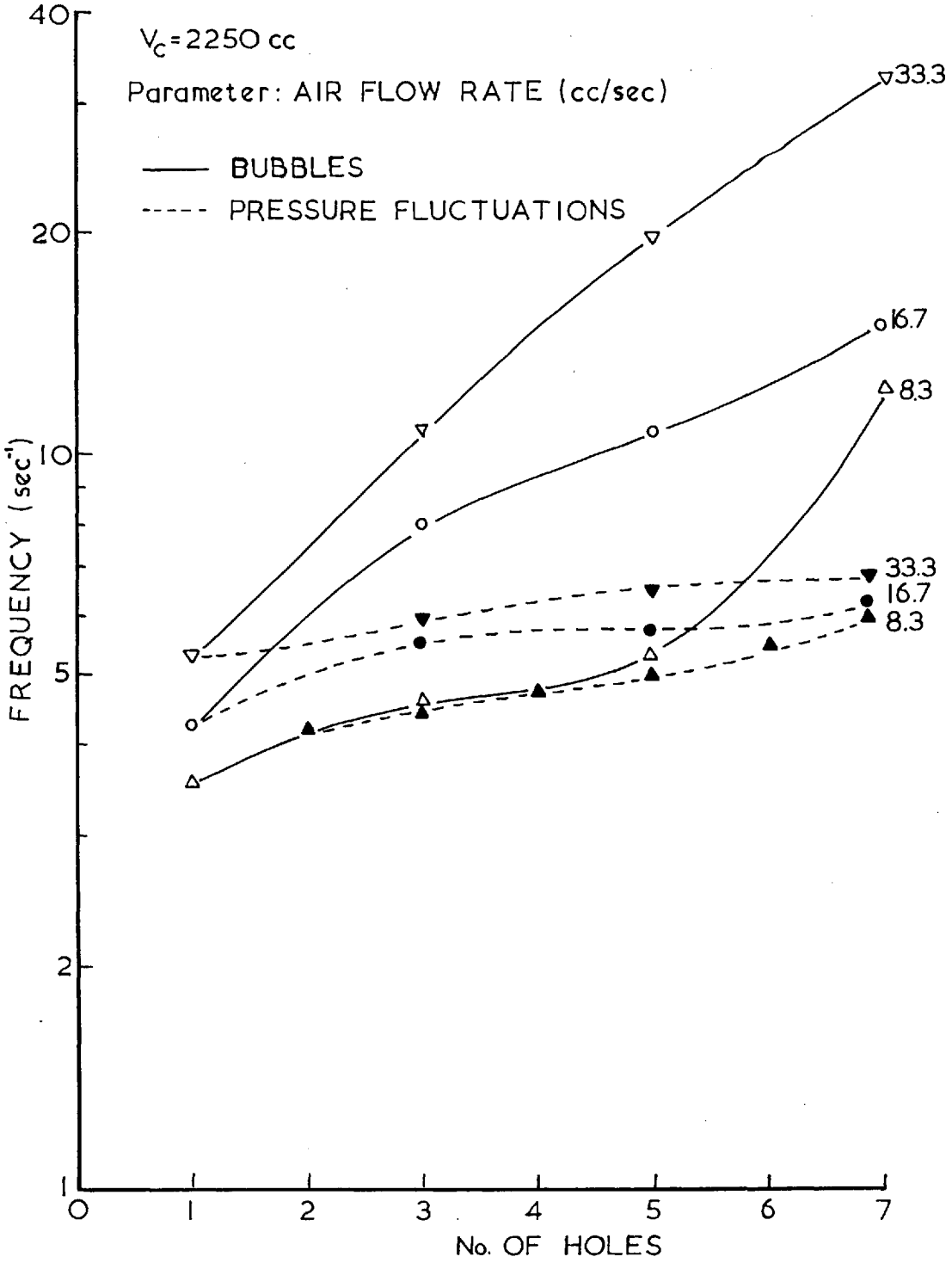

FIG. 5.26.

MEAN FREQUENCY OF BUBBLES AND FREQUENCY OF PRESSURE FLUCTUATIONS IN A SIEVE TRAY. (0.125 in. PERFORATIONS)

V_c = 2250 cc

Parameter: AIR FLOW RATE (cc/sec)

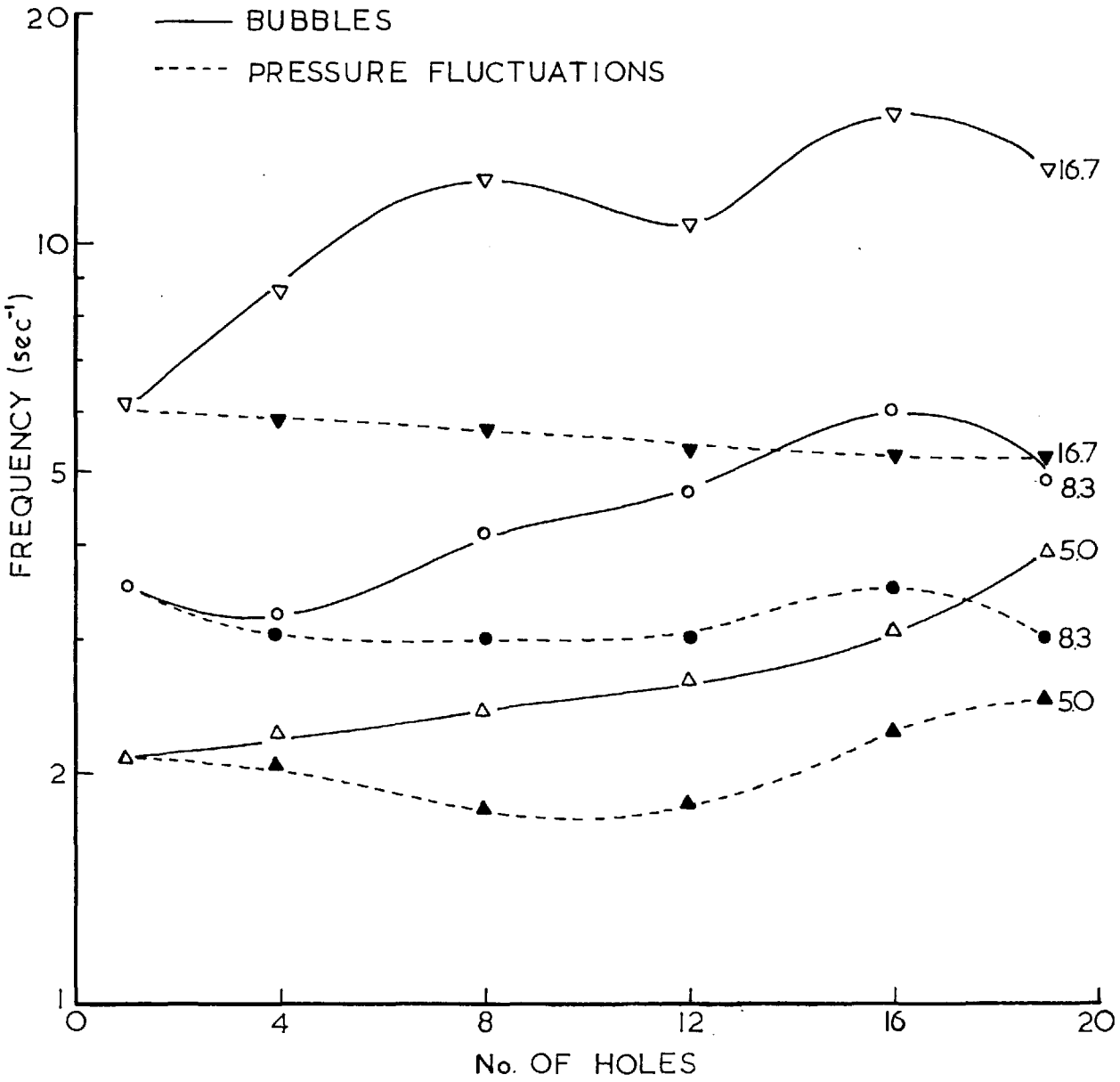

which is well in agreement with Brown's correlation (15) which shows a dependence of $V_c^{-0.46}$.

5.5.2. Simplified Model for Bubble Formation

Although there is a random distribution in the number of holes bubbling per unit time for a sieve tray working in the 'dumping range', there are several possible models for visualising such a behaviour, some of which have been described also by Prince and Chan (14, 15).

The most useful theoretical model for determining the behaviour of such a sieve tray might be to isolate one arbitrary orifice in the tray and to study its behaviour in a similar way as for single orifice studies. The difference in this case, compared to a single orifice lies in the fact that the gas flow rate supplied to such an arbitrary orifice and the pressure under the orifice, both vary periodically, being affected by the overall behaviour of the other orifices in the tray.

Because the complexity of the equations necessary to describe such a behaviour, this model has been abandoned for the present investigation.

A much more simplified model is to assume an identical behaviour of the system for each cycle of the pressure fluctuations in the gas chamber. Thus, if n is the mean frequency of bubbles formed and f is the frequency of pressure fluctuations, a value β might be defined

as:

$$\beta = \frac{n}{f} \tag{5.2}$$

(One might regard this value as the number of orifices bubbling for each cycle.)

Further postulating that the bubbles formed are identical and there is no interaction between neighbouring bubbles during their formation, it is possible to assume that the gas chamber is composed of a series of β chambers; thus each chamber volume becomes $\frac{V_c}{\beta}$ and the gas flow rate in each of them is $\frac{G}{\beta}$.

Therefore it is assumed that the mean volume of the bubbles is identical to the volume of a bubble formed above a gas chamber of volume $\frac{V_c}{\beta}$, while the gas flow rate is $\frac{G}{\beta}$.

Although such a simple model might represent the actual behaviour of a sieve tray provided the number of the holes and the gas flow rate are large enough, a fair agreement with the theory for single orifice behaviour has been obtained even for the small number of holes in the present investigation.

Figures 5.25 and 5.26 show the average number of bubbles formed per unit time, obtained experimentally.

Tables 5.1 and 5.2 show the experimental average volume of bubbles (gas flow rate/frequency) compared to a theoretical average

TABLE 5.1. Mean Volume of Bubbles Formed on a Sieve Tray

(0.125 in. perforations)

Gas flow rate (cc/sec)	Number of holes on tray	β	Theoretical Volume (cc)	Experimental Volume (cc)
5.0	1	1.0	2.0	2.4
5.0	4	1.1	1.9	2.1
5.0	8	1.4	1.7	2.0
5.0	12	1.4	1.7	1.9
5.0	16	1.3	1.7	1.6
5.0	19	1.6	1.6	1.2
8.3	1	1.0	2.1	2.2
8.3	4	1.1	2.0	2.6
8.3	8	1.4	1.8	1.9
8.3	12	1.6	1.7	1.7
8.3	16	1.7	1.6	1.4
8.3	19	1.6	1.7	1.6
16.7	1	1.0	2.3	2.6
16.7	4	1.5	1.9	1.9
16.7	8	2.1	1.6	1.3
16.7	12	2.0	1.6	1.5
16.7	16	2.9	1.2	1.1
16.7	19	2.4	1.4	1.3
33.2	19	6.4	0.7	0.7
51.5	19	7.8	0.6	0.9
86.7	19	8.0	0.8	1.4

TABLE 5.2. Mean Volume of Bubbles Formed on a Sieve Tray

(0.25. in. perforations)

Gas flow rate (cc/sec)	Number of holes on tray	β	Theoretical Volume (cc)	Experimental Volume (cc)
8.3	1	1.0	3.3	2.7
8.3	3	1.0	3.3	2.1
8.3	5	1.1	2.8	1.6
8.3	7	2.0	1.3	0.7
16.7	1	1.0	4.0	4.0
16.7	3	1.5	2.5	2.1
16.7	5	1.9	2.0	1.7
16.7	7	2.4	1.3	1.2
33.3	1	1.0	5.1	6.1
33.3	3	1.8	2.7	3.0
33.3	5	3.0	1.5	1.7
33.3	7	4.8	0.9	1.0
66.7	7	5.1	1.2	1.7

volume calculated by the method described above.

Since it is not possible to derive any simple method for a theoretical prediction of β, it has been found rather difficult to extend this model for further investigation of sieve tray behaviour.

5.6. Mean Pressure in Gas Chamber

The total plate pressure drop on a plate (h_T) can logically be split between that due to liquid on the plate (h_l) and that due to passage of vapour through the plate (h_v):

$$h_T = h_l + h_v \qquad (5.3)$$

If Z_F is the foam height and ρ_F its relative density, some workers (2, 3) have calculated h_l by assuming that it is equal to $\rho_F Z_F$. However, others (6, 46) have found that usually $h_l < Z_F \rho_F$. Bernard (46) has suggested that the discrepancy may be due to a pressure drop in the foam equivalent to the change of momentum of the high velocity vapour emerging from the sieve tray perforations.

Similarly, previous workers have assumed that h_v was simply equivalent to the pressure drop due to the flow of a same vapour rate through a dry plate (h_{dp}), while others (1, 2, 3, 4) have found that the term h_v was always greater than the dry plate pressure drop by a small amount termed the 'residual head' (h_r) :

$$h_v = h_{dp} + h_r \qquad (5.4)$$

Those measurements were carried out for gas velocities above or at a critical value, which is the minimum gas flow rate to prevent any dumping through the perforations.

Mayfield et al. (1) have found that h_r was about 0.1 - 0.2 in. water and was considered to be within the accuracy of the measurements. Arnold et al. (2) have found a larger value of 0.1 - 0.5 in. water which was about 10% of the total pressure drop. Hunt et al. (3) have found values of approximately 0.3 - 0.5 in. assuming that viscosity, surface tension, density and hydrostatic head have no appreciable effect on h_r. McAllister et al. (4) have found that an increase in gas flow rate has no effect on the ratio of $\frac{h_r}{h_{dp}}$ for thin plates, whereas the ratio decreases for thick plates.

Some of the discrepancies in the values of h_r calculated by different workers may be due to the momentum effect, as stated above, which varies for the different conditions investigated and has been neglected by those workers. However, it seems that such a residual pressure drop is mainly a function of different bubbling conditions, as is shown in the present investigation.

It is reasonable to assume for the present studies which are in the 'dumping range', that the gas flow rates used are low enough to neglect momentum effects, thus h_1 is identical to the hydrostatic pressure above the orifice. Referring to equation (5.3) the value of

h_v is therefore identical to the mean pressure in the gas chamber (P_{mean}) as calculated by equation (4. 30), thus the magnitude of h_r is given by the difference between P_{mean} and h_{dp} (equation 5. 4).

Figures 5. 27 and 5. 28 show the theoretical values of P_{mean} (including respective experimental values) in comparison to the dry pressure drop for 1/4 in. and 1/8 in. orifice, whereas figure 5. 29 shows the same type of comparison for the sieve trays investigated (only experimental values).

An increase in the gas flow rate tends to increase the mean pressure; however for a 1/4 in. orifice a minimum P_{mean} has been observed in the range of low gas flow rates. This minimum tends to disappear as the chamber volume increases. The mean pressure also increases with the increase in chamber volume; however for a 1/4 in. orifice there is a 'critical' chamber volume for which a minimum P_{mean} has been observed in the range of low gas flow rates. These conclusions can be explained by a similar analysis as in (5. 4), by studying the effect of the various parameters on the value of pressure in gas chamber at the moment of bubble detachment and the ratio between bubbling and waiting time, which are the main factors in determining the ultimate value of the mean pressure in the system (equation (4. 30).

For a 1/4 in. orifice, the mean value is observed to be lower

FIG. 5.27.

EFFECT OF GAS FLOW RATE ON MEAN PRESSURE IN THE GAS CHAMBER. (D_o = 0.25 in.)

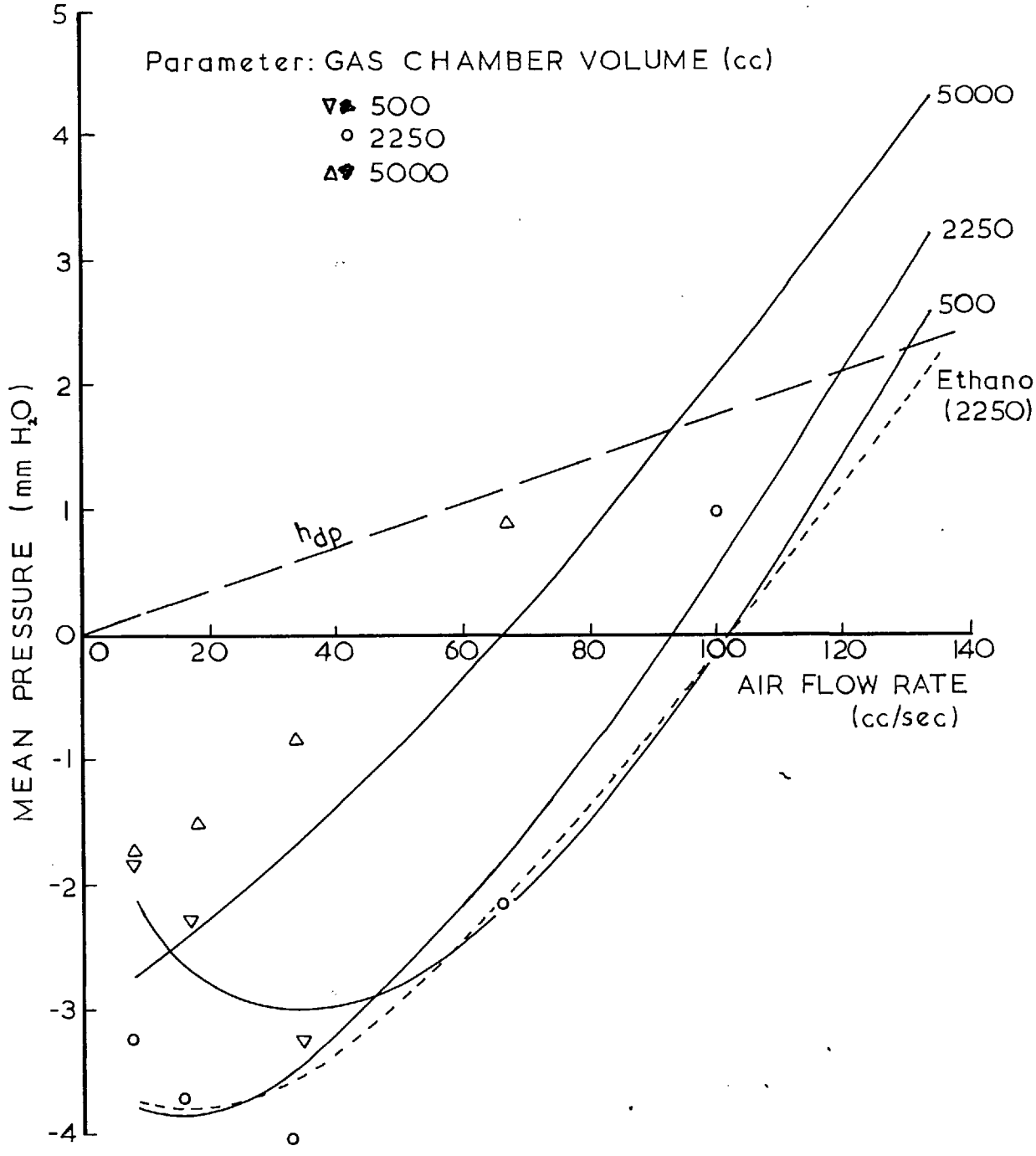

FIG. 5.28.

EFFECT OF GAS FLOW RATE ON MEAN PRESSURE IN THE GAS CHAMBER. (D_o = 0.125 in.)

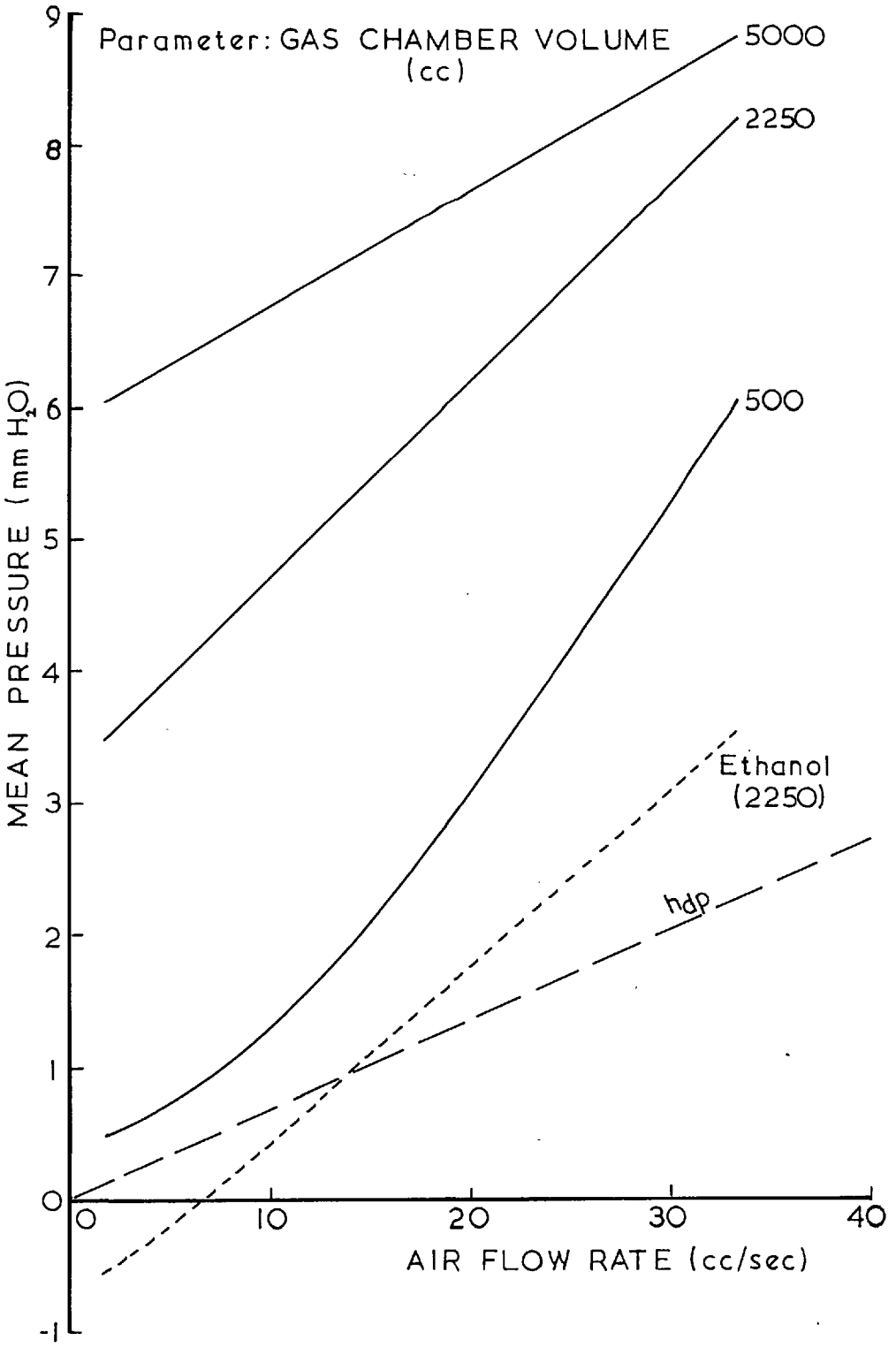

EFFECT OF GAS FLOW RATE ON MEAN PRESSURE IN THE GAS CHAMBER FOR A SIEVE TRAY.

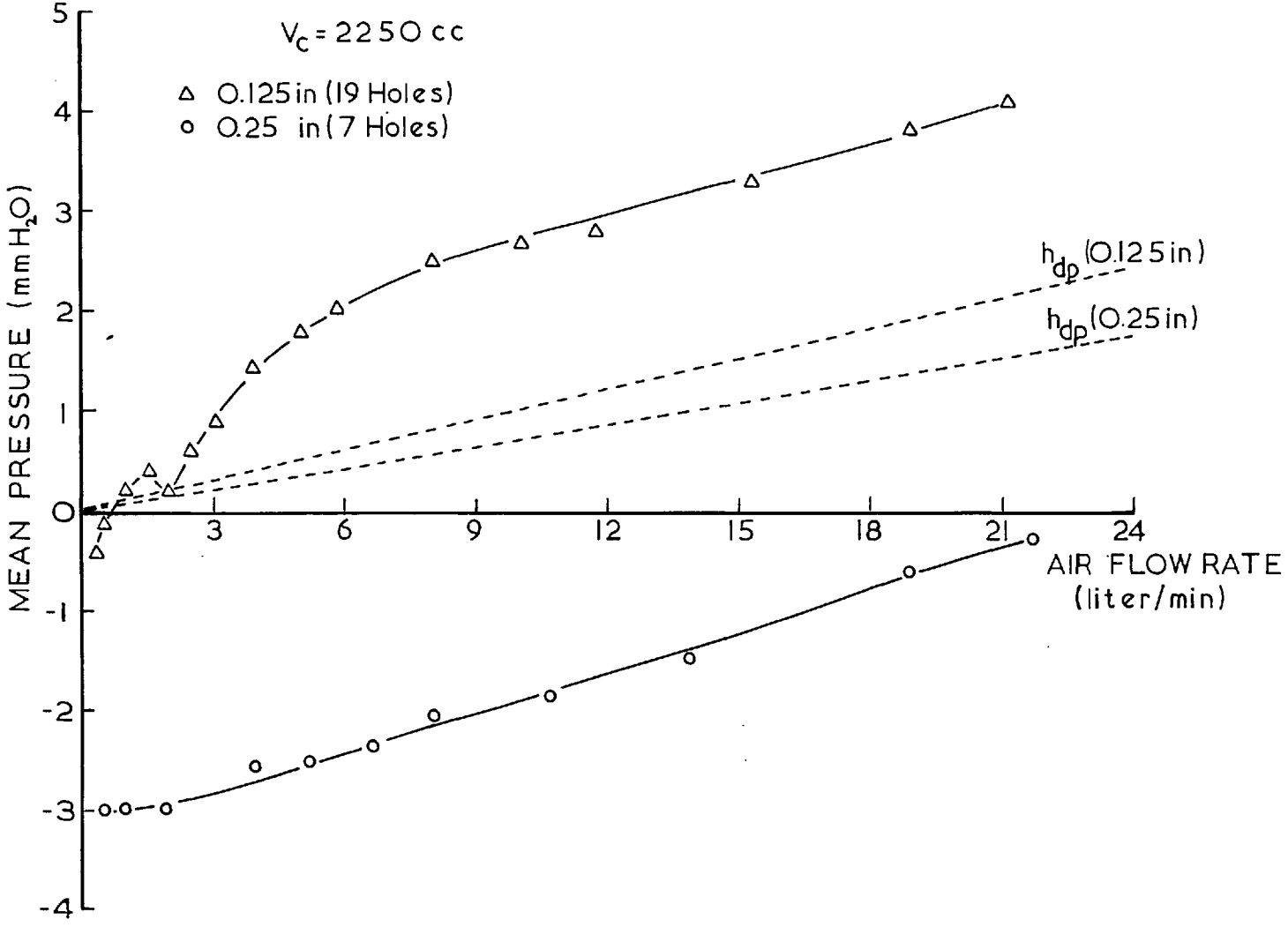

FIG. 5.29.

than the hydrostatic pressure, for low enough gas flow rates. This behaviour might be analysed as follows:

As the bubble starts growing its initial internal pressure is $\frac{2\sigma}{a_o}$ (4. 2. 3). Comparing the different pressure terms affecting the pressure in the bubble (equation 4. 26) it can be seen that $(\frac{2\sigma}{a})$ and $(-\rho_L gs)$ decrease gradually as the bubble expands, whereas $\rho_L \left[a \frac{d^2a}{dt^2} + \frac{3}{2} (\frac{da}{dt})^2 \right]$ usually increases, reaches a maximum and ultimately decreases. This general type of behaviour can be seen in Fig. 5. 20 - 5. 22. Thus, although an overall increase in the pressure in the bubble is expected at the first stages of the growing bubble, an overall decrease in its pressure (compared to the initial conditions) is expected before its detachment. This decrease might be quite sharp, resulting in a value considerably below $\frac{2\sigma}{a_o}$. In case of 1/4 in. orifice this value might be even below zero (i. e. below hydrostatic pressure). Since the pressure in the gas chamber is related to the pressure in the bubble (by equation 4. 22) and since the pressure drop in the orifice is comparatively small at the last stages of bubble growth, the ultimate pressure in the gas chamber might also be quite low, that is below zero (i. e. below hydrostatic pressure) for a 1/4 in. orifice. After the detachment of the bubble, the pressure in the gas chamber increases gradually, according to equation (4. 29). Typical examples of change of pressure in gas chamber for the complete

'bubbling and waiting' cycle can be seen in Figures 5.15 and 5.17. Evaluating the mean pressure in the chamber for such a cycle, it is obvious that its value is much lower than $\frac{2\sigma}{a_o}$ and might be even below zero.

Since h_{dp} is higher than the hydrostatic pressure, the 'residual head' might have negative values, as observed both for a 1/4 in. single orifice and sieve tray, for relative low gas flow rates (Fig. 5.27, 5.29). However the difference between P_{mean} and h_{dp} decreases gradually with the increase in gas flow rate, till the value of h_r becomes positive, corresponding to the observations of other workers for higher gas flow rates. For an 1/8 in. single orifice or sieve tray, h_r has a positive value from very low flow rates (Fig. 5.28, 5.29).

It is clear that the magnitude of the mean pressure is an important variable which must be taken into account in the dumping studies.

CHAPTER 6

MECHANISM OF DUMPING

Since the dumping through performations of a sieve tray is only a stage in the whole process of the tray performance, it is clear that some of the factors which affect bubble formation also affect the dumping, but in quite different ways. Although the pressure effects involved in the system, mainly the pressure in the gas chamber and pressure in the liquid behind a rising bubble, are the main factors responsible for dumping, there are some other factors which may increase the rate of dumping considerably, but are not accounted for the present investigation.

One of those factors which equally apply to dumping through a single orifice or through a sieve tray is the 'Induced Dumping'. In a normal distillation process, the vapour ascending to a higher plate is at a higher temperature than the liquid on the plate. Since the plate temperature is assumed to be equal to that of the liquid on it, some of the vapour might condense and weep back through the perforations (47). Obviously this phenomenon cannot be observed when dealing with an air-water simulating system, operating at room temperature.

Other factors neglected which apply mainly to a sieve tray are

due to the profile of the hydrostatic head across the tray. Oscillations in the liquid on the tray, which change the hydrostatic head in a wavy way, cause a periodic dumping of the liquid in the same side of the tray as the crest of the wave (4, 14).

Even when the oscillations are not large the hydrostatic pressure drop profile on a tray indicates a higher pressure drop near the column wall than at the column centre, resulting in a continuous dumping through some of the perforations near the wall and known as the 'wall effect' (3, 4, 44).

In addition to those assumptions, also all the assumptions which have been described in Chapter 4, still hold for the analysis presented below.

No theoretical attempt has been made in this investigation at explaining the mechanism of dumping through very large orifice diameters, for which a continuous two phase flow is expected in the 'dumping region'.

6.1. Mechanism of Dumping through a Single Orifice

6.1.1. The Idealised Stages for the Dumping Process

The 'Waiting Stage' described in (4.2.1) might be divided into three sub-stages which determine the dumping process (Figure 6.1):

a. 'Drop Formation Stage': (A) is a 'stable bridging' situation

IDEALISED STAGES FOR THE DUMPING PROCESS.

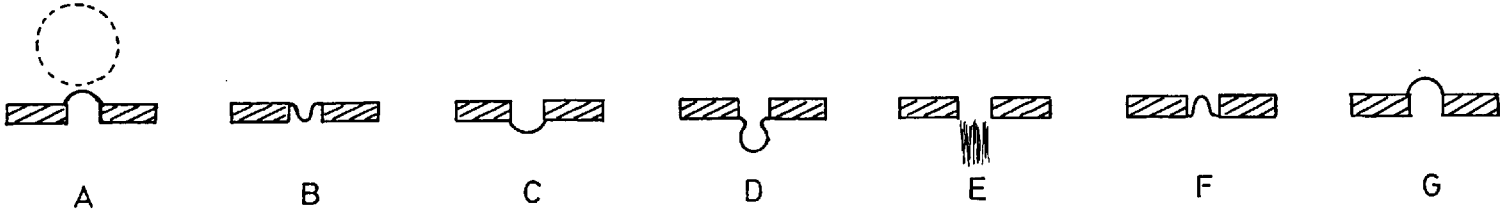

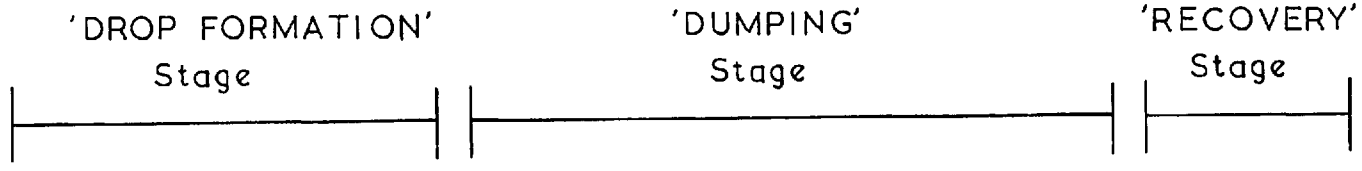

FIG. 6.1.

obtained as the bubble is detached from the orifice. Provided the pressure in the liquid above the orifice exceeds the pressure in the gas chamber, the liquid tends to be pushed through the orifice, forming an 'unstable bridging' condition (B), which might develop in the formation of a pendant drop (C).

b. 'Dumping Stage': The pendant drop (C) increases in size, reaching a condition (D) from which the drop tends to elongate, resulting in a thin stream of liquid dumping through the orifice (E). Once the liquid starts dumping, it continues to do so till the increasing pressure in the gas chamber exceeds the liquid pressure. Another bridging condition is obtained (F).

c. 'Recovery Stage': The pressure in the gas chamber continues to increase till another bubble starts forming (G). Condition (G) is equivalent to the initiation of the 'Growing Stage' as described in (4.2.1).

6.2.1. Criterion for Dumping through an Orifice

It is most convenient to derive a criterion for dumping emerging from a drop formation equation.

The fundamental equation for a pendant drop shape is (Adamson [48], p. 14):

$$\sigma\left(\frac{1}{R_1} + \frac{1}{R_2}\right) = \rho_L g y \qquad (6.1)$$

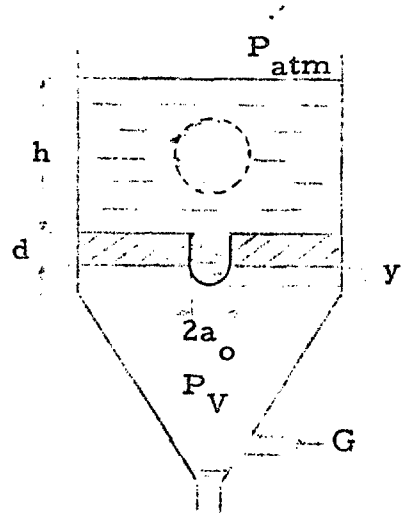

Fig. 6.2: Schematic Model of Drop Formation

where R_1 and R_2 are the principal radii of curvature of the drop.

From a balance of pressures acting on such a drop (Fig. 6.2), it is obvious that it tends to grow provided:

$$(P_{atm} + \rho_L gh) + \rho_L gd + \rho_L gy > P_V + \sigma(\frac{1}{R_1} + \frac{1}{R_2}) \qquad (6.2)$$

For the present situation in which formation of the drop is followed by the detachment of the bubble from the orifice, there is an additional pressure gradient (ΔP) due to the acceleration of the bubble (equation 4.43). The effect of the inertia of the liquid pushed through the orifice is neglected for the present criterion. Following the same treatment as in (4.2.3) that is relating the pressures to $(P_{atm} + \rho_L gh)$, the criterion for a drop formation becomes:

$$\Delta P + \rho_L gd + \rho_L gy > P_V + \sigma(\frac{1}{R_1} + \frac{1}{R_2}) \qquad (6.3)$$

The shape of a drop (i.e. values of R_1, R_2 and y) can be determined by a numerical solution of equation (6.1), assuming that its radius of curvature at the vertex is equal to the radius of the orifice (48). However, Zelfel (49) has shown that for pressure calculations it is much more convenient to assume a hemispherical final shape for the drop (radius equal to that of the orifice), thus the deviation from this shape can be taken into account using a correction factor k which depends on orifice diameter and physical properties of the liquid.

Using the same assumptions the final values for equation (6.3) are:

$$\rho_L g y = k \rho_L g \frac{\frac{2}{3}\pi a_o^3}{\pi a_o^2} = \frac{2}{3} a_o k \rho_L g$$

$$\sigma\left(\frac{1}{R_1} + \frac{1}{R_2}\right) = \frac{2\sigma}{a_o} \qquad (6.4)$$

From equation (6.3) the criterion for dumping through an orifice is:

$$\Delta P + \rho_L g\left(d + \frac{2}{3} a_o k\right) > P_V + \frac{2\sigma}{a_o} \qquad (6.5)$$

6.2. Behaviour of a Single Orifice System-Theoretical Analysis

The parameters investigated in present studies might affect the complex periodic behaviour of any system, in particular the implementation of all or a part of the conditions described in (6.1.1.). An

analysis based on some of the equations derived in Chapter 4 and the criterion derived in (6. 1. 2) is given below.

The initial conditions for such an analysis are the conditions at the termination of the 'Elongating Stage' as derived in Chapter 4, that is the relative magnitude of the gas chamber pressure (P_V) and the liquid pressure behind the bubble (P_L) at the moment of bubble detachment.

I. $P_L > P_V$

The gas-liquid interface tends to be pushed downw through the orifice (B). The gas chamber pressure increases due to nett inflow of gas (equation 4. 29). The liquid pressure at the interface increases due to the both effects of the accelerating bubble (equation 4. 43) and drop formation (equation 6. 2). It is assumed that the 'drop formation' period, that is the time necessary for the interface to move from condition (A) to (C), is equal to t_F.

a. Provided after a time $t = t_F$ the relative pressure changes do not invert the conditions (i. e. $P_L > P_V$), a pendant drop (C) is formed. At this stage there are two possibilities:

1a. If equation (6. 5) can be satisfied, the pendant drop increases in size (D) and the process of dumping continues as described in (6. 1. 1), resulting in a 'liquid stream' dumping. This condition. is represented by Fig. 6. 3 which includes a typical series of photographs

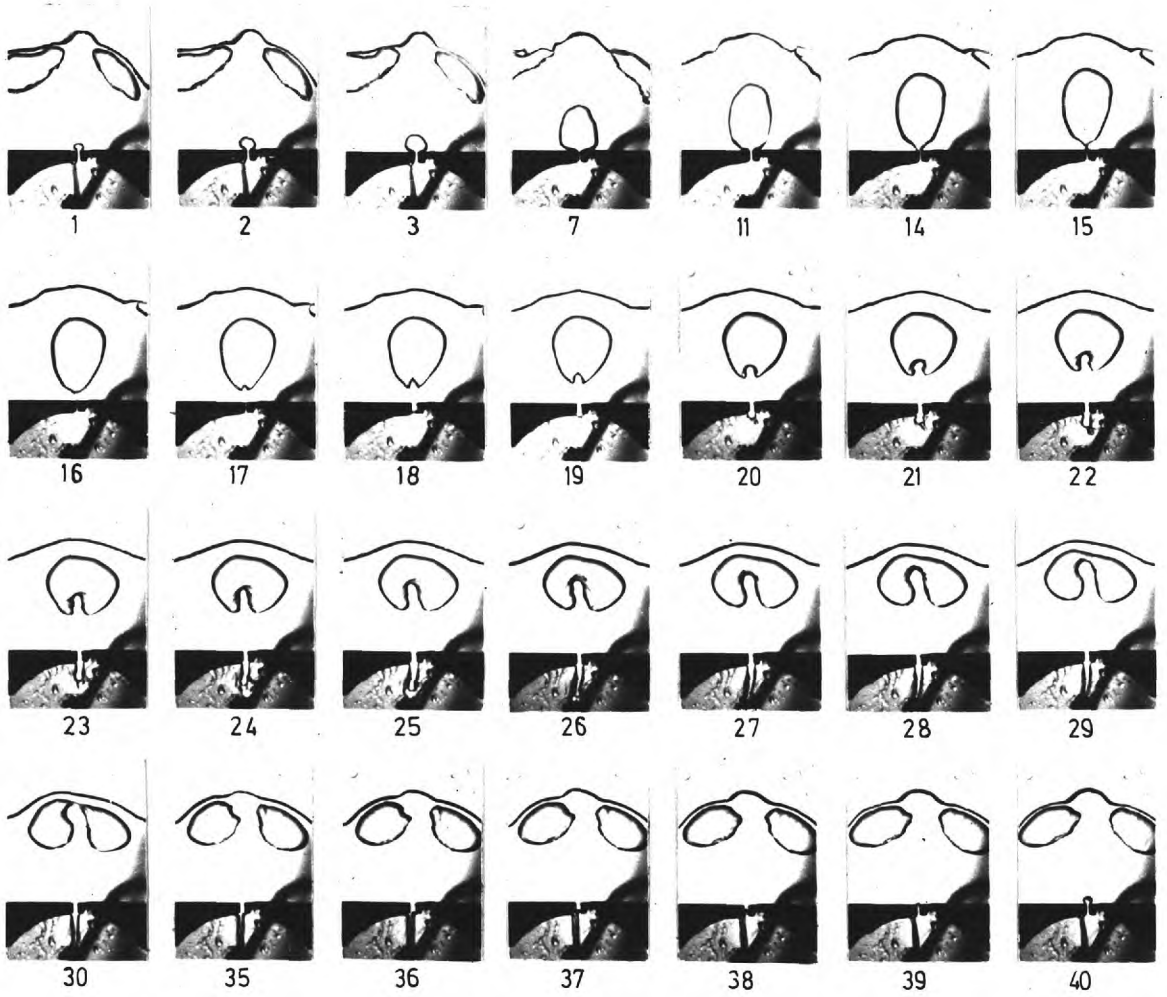

BUBBLING AND 'STREAM' DUMPING IN A 2-DIM. APPARATUS.

(Cine pictures at 200 frames/sec - each picture having its frame number in the cycle.)

A_o = 0.25×0.125 in.^{2} , h = 2 in. , V_c = 200 cc. , G = 42 cc/sec. , L = 178 cc/min.

FIG. 6.3.

BUBBLING AND 'SINGLE DROP' DUMPING IN A 2-DIM. APPARATUS.

(Cine pictures at 200 frames/sec-each picture having its frame number in the cycle.)

A_o = 0.25×0.125 in. , h = 1 in. , V_c = 200 cc. , G = 4.2 cc/sec. , L = 64 cc/min.

FIG. 6.4.

taken from the 'two dimensional' apparatus, showing the different stages involved in a complete 'bubbling + dumping' cycle.

2a. If equation (6. 5) cannot be satisfied, the pendant drop remains somewhere between conditions (C) and (D) till the gas chamber pressure increases to such an extent that the gas-liquid interface is pushed up through the orifice. However, in this period the neck which connects the pendant drop to the orifice collapses (radius of curvature increases to infinity, thus no surface tension effect), resulting in 'single drop' dumping. This conditions is represented by Fig. 6.4 which includes again a typical series of photographs taken from the 'two dimensional' apparatus.

b. Provided after a short enough time the relative pressure changes invert the conditions (i. e. $P_V > P_L$, thus a pendant drop could not have been formed) the gas-liquid interface which has been meanwhile pushed downwards somewhere between (B) and (C) is immediately pushed upwards to a condition similar to (A), resulting in the formation of another bubble, with no dumping through the orifice.

II. $P_V > P_L$

Another bubble starts forming immediately after the detachment of the previous one, as described in (4. 2. 4). Although no theoretical equations have been derived for the estimation of the pressures P_V

and P_L at the moment of detachment of such a bubble, there are again several possibilities, according to their relative magnitude at this stage.

c. Provided still $P_V > P_L$, the process of coalescence might repeat, resulting in a formation of a group of three bubbles, as described in (2.11.d).

d. Provided $P_L > P_V$, the gas-liquid interface tends to be pushed down through the orifice (B). One of the stages described above as a. or b. might occur.

6.3. Application of the Theoretical Analysis - Comparison to Experimental Results

As has been shown in (6.2), for any dumping prediction it is necessary to assess the 'drop formation' time (t_F). This might be regarded as an instability problem, of calcuating the necessary time for the gas-liquid interfac e to move from condition (A) to (C), under various external conditions applied. No attempt has been made at such a treatment in the present investigation. However, some approximate estimations are possible for relative magnitude of the dumping rates under various conditions studied in the present investigation.

6.3.1. Effect of Orifice Diameter

For the present investigation, studying the performance of 1/4 in. and 1/8 in. orifice diameters, drilled in a plate 1.6 mm. thick, and using values of k as given by Zelfel (49), the values of the pressure terms in equation (6.5) for air-water system are:

	k	$\rho_L g(d + \frac{2}{3} a_o k)$ (mm H_2O)	$\frac{2\sigma}{a_o}$ (mm H_2O)
1/8 in. orifice	1.05	2.7	9.2
1/4 in. orifice	1.08	3.9	4.6

From equation (6.5), dumping occurs provided:

1/8 in. orifice: $P_V - \Delta P < -6.5$ (mm H_2O)

1/4 in. orifice: $P_V - \Delta P < -0.7$ (mm H_2O)

For a large gas chamber volume, rate of change in P_V is small, so the time for 'drop formation' affects only the value of ΔP. For a small gas chamber volume, rate of change in P_V is large, so t_F becomes more important in estimating the minimum conditions to assure dumping.

Figure 6.5 shows the change in pressures P_V and ΔP for the beginning of the 'Waiting Stage' (i.e. after bubble detachment) for 1/4 in. and 1/8 in. orifice, under similar operating conditions.

For 1/4 in. orifice $P_V << -0.7$ mm H_2O, thus a large dumping

rate is expected even without considering the ΔP effect. This might be regarded as a condition described as (1a) in (6. 2). Experimentally, it has been found (Fig. 6. 6) : L = 172 cc/min.

For 1/8 in. orifice $P_V > -6.5$ mm H_2O. Adding the ΔP effect it can be seen that $(P_V - \Delta P) < -6.5$ mm H_2O, provided t < 12 m sec. Since the curve for ΔP tends to subside rather more rapidly, as stated in (4. 3), t must be even smaller. Although the value of t_F has not been calculated, it is most likely that the estimated time t is too short for initiation of a 'stream' dumping. It is more likely to regard this case as the condition (2a) described in (6. 2), resulting in 'single drops' dumping. Experimentally it has been found (Fig. 6. 6 : L = 27 cc/min.

Following similar type of analysis it can be observed that a decrease in orifice diameter has a sharp effect in decreasing the dumping rate. In terms of linear gas velocity through the orifice $(\frac{G}{A_o})$ it can be seen (Fig. 6. 6) that for low gas velocities an increase in the diameter of the orifice has a sharp effect of increasing the dumping rate, however this effect tends to become gradually less significant as the gas velocity increases. These observations are in agreement with Pozin et al. (50), who have studied the dumping rate through openings of a grid plate.

FIG. 6.5.

CHANGE IN P_v AND ΔP FOR THE BEGINNING OF THE "WAITING" STAGE FOR VARIOUS ORIFICE DIAMETERS.

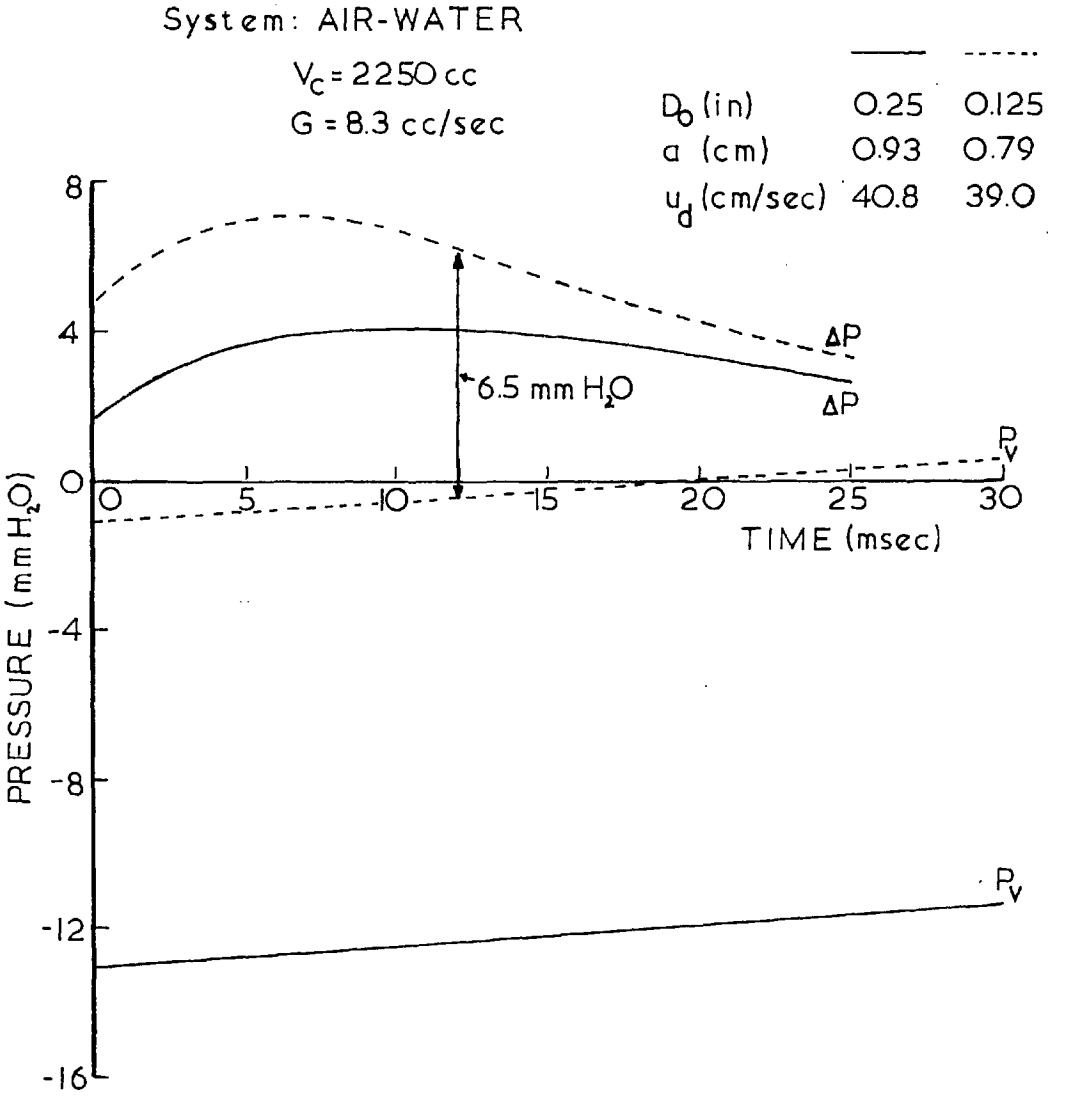

FIG. 6.6.

EFFECT OF GAS FLOW RATE ON DUMPING RATE FOR VARIOUS ORIFICE DIAMETERS. (AIR-WATER SYSTEM).

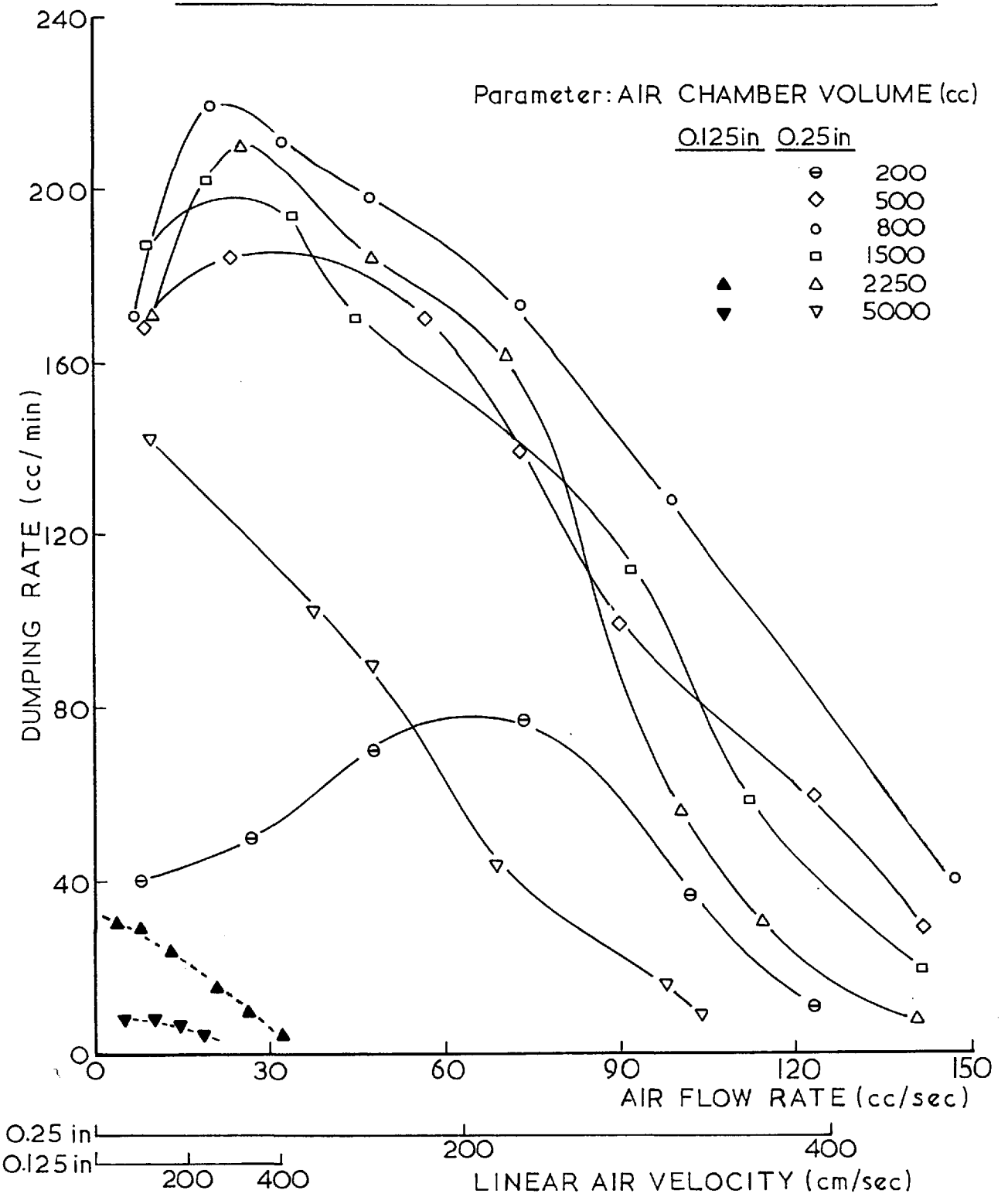

6.3.2. Effects of Gas Flow Rate and Chamber Volume

Although no theoretical equation has been derived in the present investigation for the dumping rate through an orifice, a fair approximation might be to use a similar equation to that for the gas flow rate through an orifice (equation 4.2.1), as suggested also by Prince and Chan (14), thus:

$$\frac{P_L - P_V}{\rho_L} \quad \alpha \quad u_L^2 \tag{6.6}$$

Since the dumping rate is proportional to the liquid velocity through the orifice, the overall amount of dumping for one cycle is roughly proportional to the average square root of the pressure difference $\left| \frac{(P_L - P_V)_{ave}}{\rho_L} \right|^{1/2}$.

Since $\frac{t_D}{T}$ is the partial time allowed for dumping in a cycle, the dumping rate for a unit time is proportional to

$$L \quad \alpha \quad \frac{t_D}{T} \left| \frac{(P_L - P_V)_{ave}}{\rho_L} \right|^{1/2} \tag{6.7}$$

Figure 6.7 shows a comparison between the experimental dumping rate and the equivalent approximate values of $\frac{t_D}{T} \left| \frac{(P_L - P_V)_{ave}}{\rho_L} \right|^{1}$ calculated from the theoretical equations for a 1/4 in. orifice. The approximate values of t_D and $(P_L - P_V)_{ave}$ have been calculated as follows:

FIG. 6.7.

EFFECT OF GAS CHAMBER VOLUME ON DUMPING RATE. (D_o = 0.25 in.)

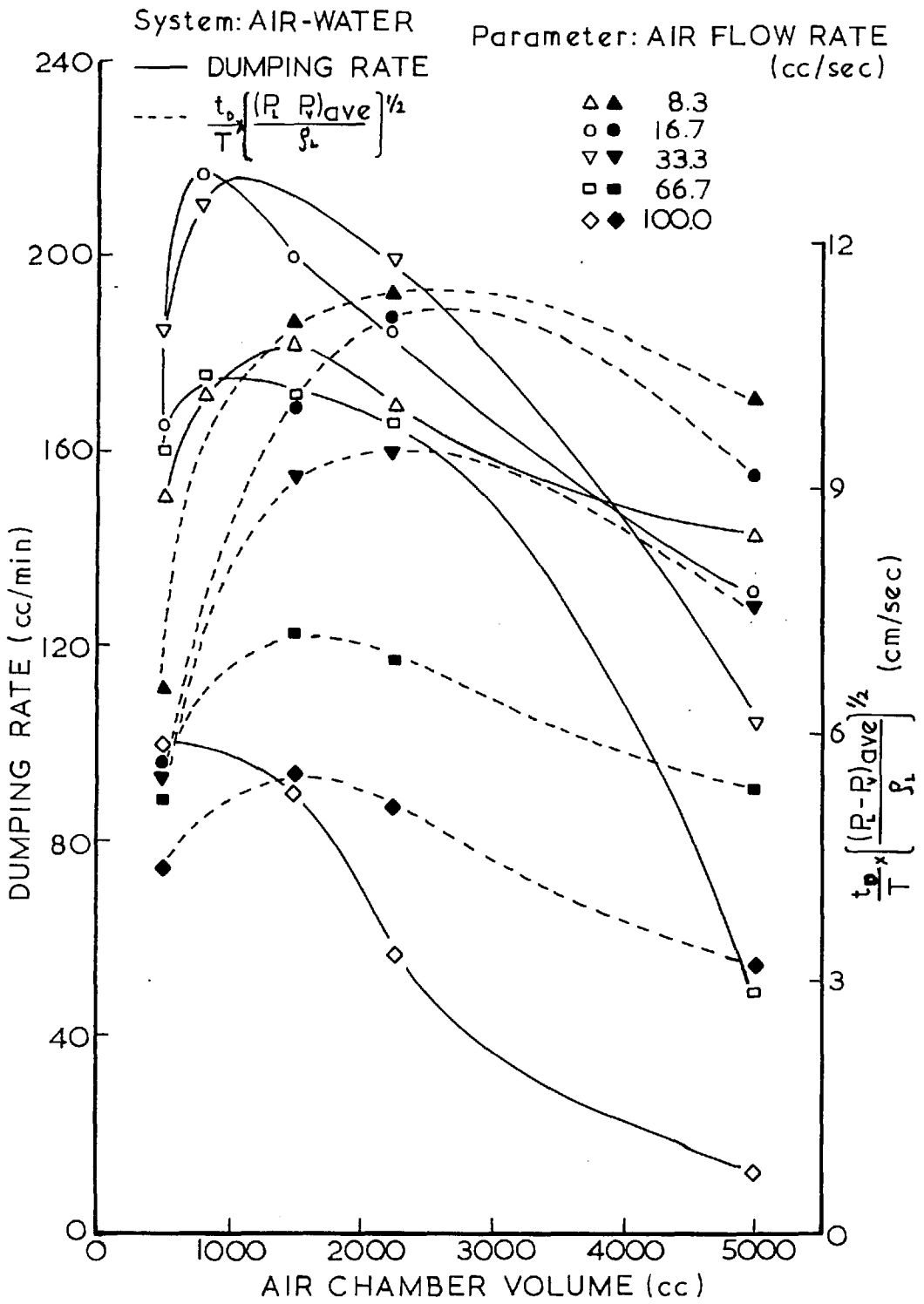

From (4.2.1) and (6.1.1) it is obvious that:

$$t_\omega = T - t_B = t_F + t_D + t_R \qquad (6.8)$$

Since for a 1/4 in. orifice, equation (6.5) is satisfied for almost all conditions investigated and an appreciable amount of dumping has been observed, it is possible to assume that $t_F \ll t_D$, thus the approximate 'dumping' time is:

$$t_D = T - (t_B + t_R) \qquad (6.9)$$

Neglecting the liquid inertia, $(P_L - P_V)_{ave}$ can be assumed to be approximately an average between the values of the pressure in the gas chamber at the beginning and end of the 'dumping' period.

From Figure 6.7 it can be observed that despite all previous aszumptions both types of curves show the same trend of behaviour, that is a maximum in the range of low chamber volumes, and an appreciable decrease in the range of high gas flow rates. Since for high gas flow rates t_D decreases quite appreciably, the error in neglecting t_F increases gradually, resulting in higher values of $\frac{t_D}{T}$ than expected. Thus the theoretical curves subside rather more rapidly compared to the experimental ones.

Considering the experimental results in Figures 6.6 and 6.7, the general behaviour of a 1/4 in. orifice can be summarized as follows:

Effect of Gas Chamber Volume

As has already been shown in (5.2), for a constant gas flow rate, an increase in gas chamber volume (V_c) results in a steady increase in bubble volume (V). Such an increase in gas chamber volume affects all terms in equation (6.8) in a rather complex way. Due to increase in V, an increase in T is expected. Due to increase in V_c an increase in t_B and t_R is expected. Although the overall effects tend to increase the value of t_D, the ratio $\frac{t_D}{T}$ seems to increase gradually in the range of small chamber volumes and remains almost constant in the range of large chamber volume.

Similarly, an increase in gas chamber volume has two opposite effects on change in chamber pressure ($P_{V_o} - P_{Vd}$). Due to increase in V an increase in ($P_{V_o} - P_{Vd}$) is expected, whereas due to increase in V_c a decrease in ($P_{V_o} - P_{Vd}$) is expected. In the range of small chamber volume it seems that the overall change in ($P_{V_o} - P_{Vd}$) is mostly affected by an increase in V, thus overall increase in ($P_{V_o} - P_{Vd}$) is expected, whereas above a certain chamber volume an overall decrease is expected.

Since $(P_L - P_V)_{ave}$ is proportional to $(P_{V_o} - P_{Vd})$, an increase in the product of $\frac{t_D}{T}$ and $\left[\frac{(P_L - P_V)_{ave}}{\rho_L}\right]^{1/2}$ (equation 6.7) is expected with an increase in chamber volume till a 'critical' volume, above

which the product gradually decreases. Thus a maximum dumping rate is expected in this 'critical' region (experimentally, the region is about 800 cc.).

Effect of Gas Flow Rate

A similar analysis to the above is possible for investigating the gas flow rate effect. As has been shown in (5.2), for a constant gas chamber volume, an increase in gas flow rate (G) results in a steady increase in bubble volume (V).

Such an increase in gas flow rate has two opposite effects on $\frac{t_D}{T}$. Due to increase in G, a decrease in T and t_R is expected, whereas t_B is almost constant. Due to increase in V, an increase in T is expected. Nevertheless, a gradual decrease in $\frac{t_D}{T}$ has been observed.

Similarly, an increase in gas flow rate has two opposite effects on $(P_{V_o} - P_{Vd})$. Due to increase in G, a decrease in $(P_{V_o} - P_{Vd})$ is expected, whereas due to increase in V, an increase in $(P_{V_o} - P_{Vd})$ is expected. Nevertheless, it seems that the effect of V is dominant, resulting in an overall increase in $(P_{V_o} - P_{Vd})$, for most of the range of gas flow rates investigated.

Since the increase in gas flow rate has an opposite effect on $\frac{t_D}{T}$ compared to $(P_{V_o} - P_{Vd})$, their product (equation 6.7) might reach a maximum around a 'critical' gas flow rate, which value is most affected by the gas chamber volume. Experimentally, such 'critical' gas flow

rate which is about 65 cc/sec for a 200 cc. chamber volume, is not observed any more for a 5000 cc. chamber volume, resulting in a continuous decrease in dumping rate (Fig. 6. 6).

Comparing values of mean pressure in the gas chamber (Fig. 5.27) the gas flow rate for maximum dumping rate corresponds quite well with that for minimum mean pressure.

6. 3. 3. Effect of Physical Properties of the System

As has been shown in (5. 3) for constant gas flow rate and gas chamber volume, larger bubble volumes (V) are observed for the air-water system. Since for water both surface tension (σ) and density (ρ_L) are higher than for ethanol, the expected effects are as follows:

Due to increase in V, an increase in T is expected. Due to increase in σ, an increase in t_R is expected. Since t_B is almost constant, an increase in t_D is expected. However, the ratio $\frac{t_D}{T}$ seems to increase for small chamber volumes, whereas the ratio decreases for large chamber volumes.

Due to increase in V, an increase in $(P_{V_o} - P_{Vd})$ is expected, however, due to increase in ρ_L, a decrease in $\frac{(P_L - P_V)_{ave}}{\rho_L}$ is expected. Nevertheless, comparing the two systems the overall effect results in higher values for the air-water system.

Thus, it seems that for the air-water system the product of $\frac{t_D}{T}$ and $\left[\frac{(P_L - P_V)_{ave}}{\rho_L}\right]^{1/2}$ is higher for small chamber volumes, and is lower for large chamber volumes (for low gas flow rates only), resulting in larger dumping rate for small volumes (500 cc.) and lower dumping rate for large volumes (5000 cc.). (Fig. 6.8).

6.3.4. Effect of Hydrostatic Head

As has been shown in (4.2.2), the theory derived in the present investigation neglects the effects of a limited depth of liquid on bubble formation. However, from visual observations it has been found that bubbles vary in size with an increase in liquid depth (from 0 to 15 cm), having a maximum size in the region of 5 - 10 cm, depending on gas flow rate and chamber volume.

For a constant gas flow rate and chamber volume, due to an increase in V, an increase in T is expected. Since t_B might also increase, the ratio $\frac{t_D}{T}$ might be slightly affected.

However, it seems that for small chamber volumes the important factor is $(P_V - P_{Vd})$ which may increase quite significantly, resulting in a larger dumping rate.

Thus having a maximum bubble diameter, a maximum dumping rate is expected. However for large enough chamber volumes this maximum is assumed to disappear.

FIG. 6.8.

EFFECT OF GAS FLOW RATE ON DUMPING RATE FOR VARIOUS SYSTEMS (D_o=0.25 in).

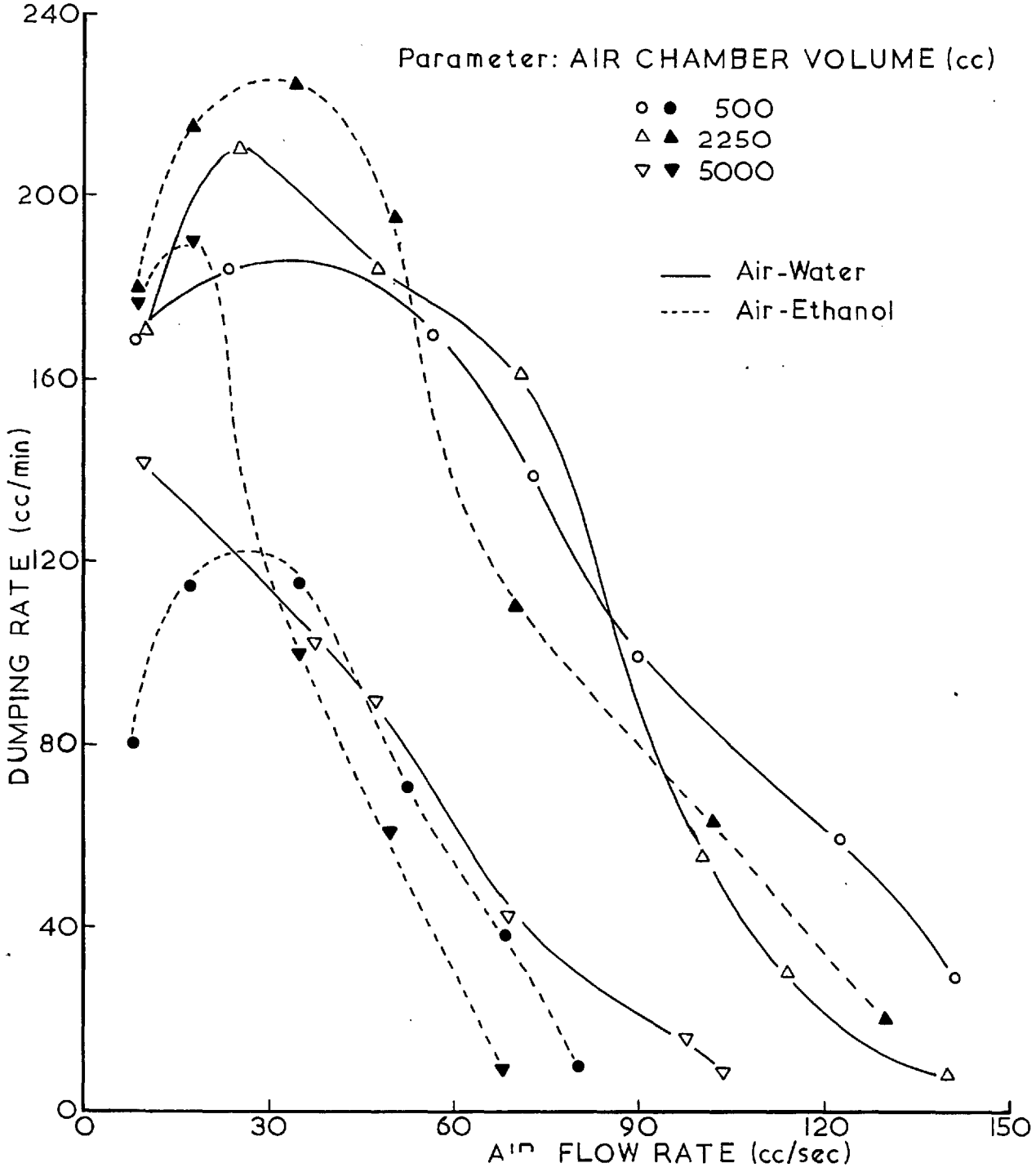

FIG. 6.9.

EFFECT OF LIQUID DEPTH ON DUMPING RATE.
(AIR-WATER SYSTEM)

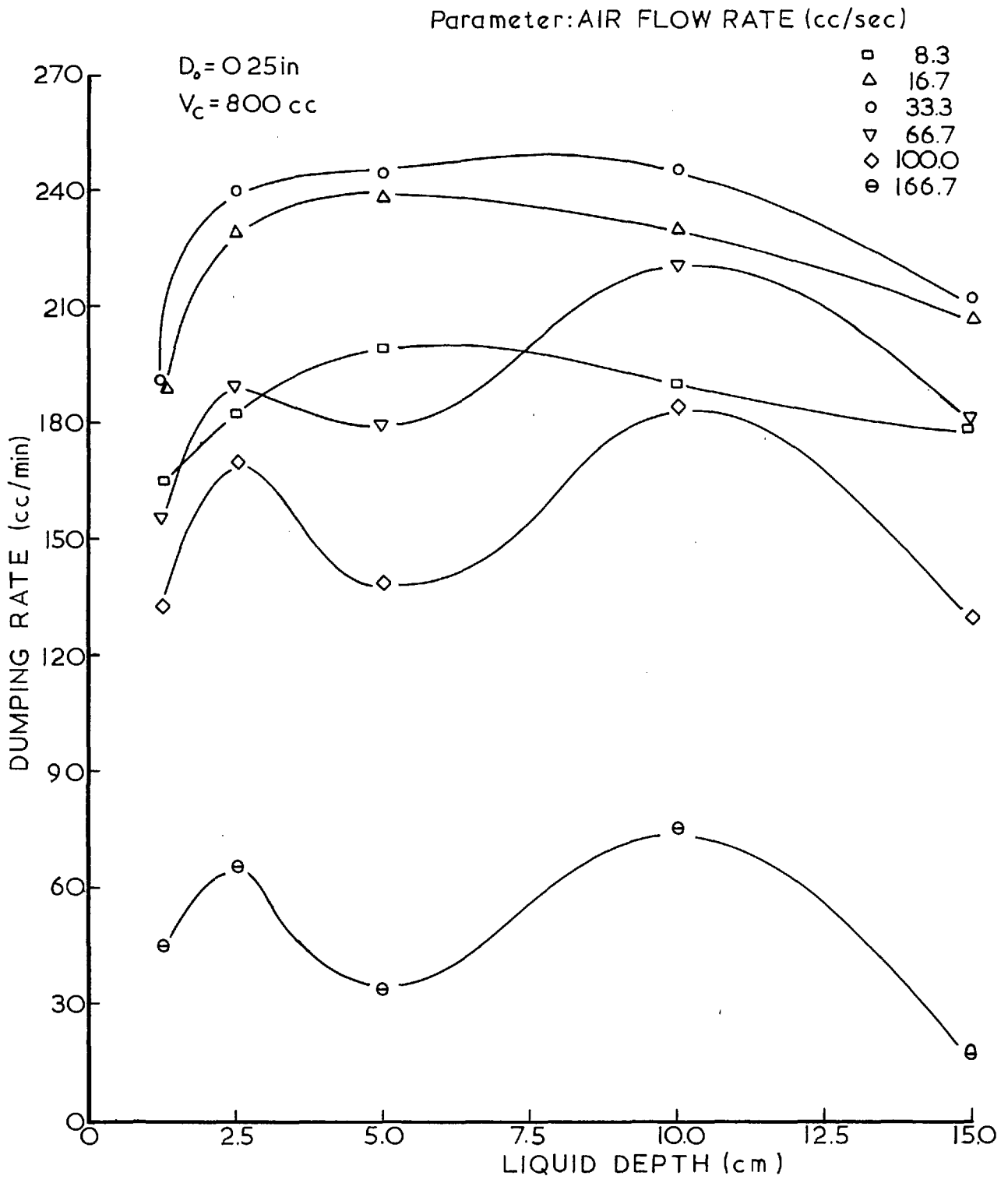

Figure 6. 9 shows the experimental results for an 800 cc. chamber volumes.

More experiments on hydrostatic head effects have been carried out with the 'Two Dimensional' Apparatus (6. 4).

Pozin et al. (50) have also observed a similar maximum dumping rate (at about 20 cm. foam height for a grid plate).

6. 4. Dumping in the 'Two Dimensional' Apparatus - Experimental Results

A large number of experiments have been carried out for measurements of rate of dumping under various conditions, for an air-water system in the 'Two Dimensional' Apparatus, but since no theory has been derived, only the main conclusions are described below.

Although the absolute magnitude of the dumping rate might vary compared to a 'Three Dimensional' Apparatus operating under similar conditions (also different size of bubbles are formed), a general similar trend of behaviour is expected.

Most of the experiments have been carried out for a gas chamber volume of 200 cc. only, and a limited number of experiments have been carried out for a 5000 cc. volume. Thus the importance of these experiments is mainly in a qualitative explanation of the effect of various parameters on the dumping rate, especially those parameters

EFFECT OF GAS FLOW RATE ON DUMPING RATE FOR VARIOUS GAS CHAMBER VOLUMES.

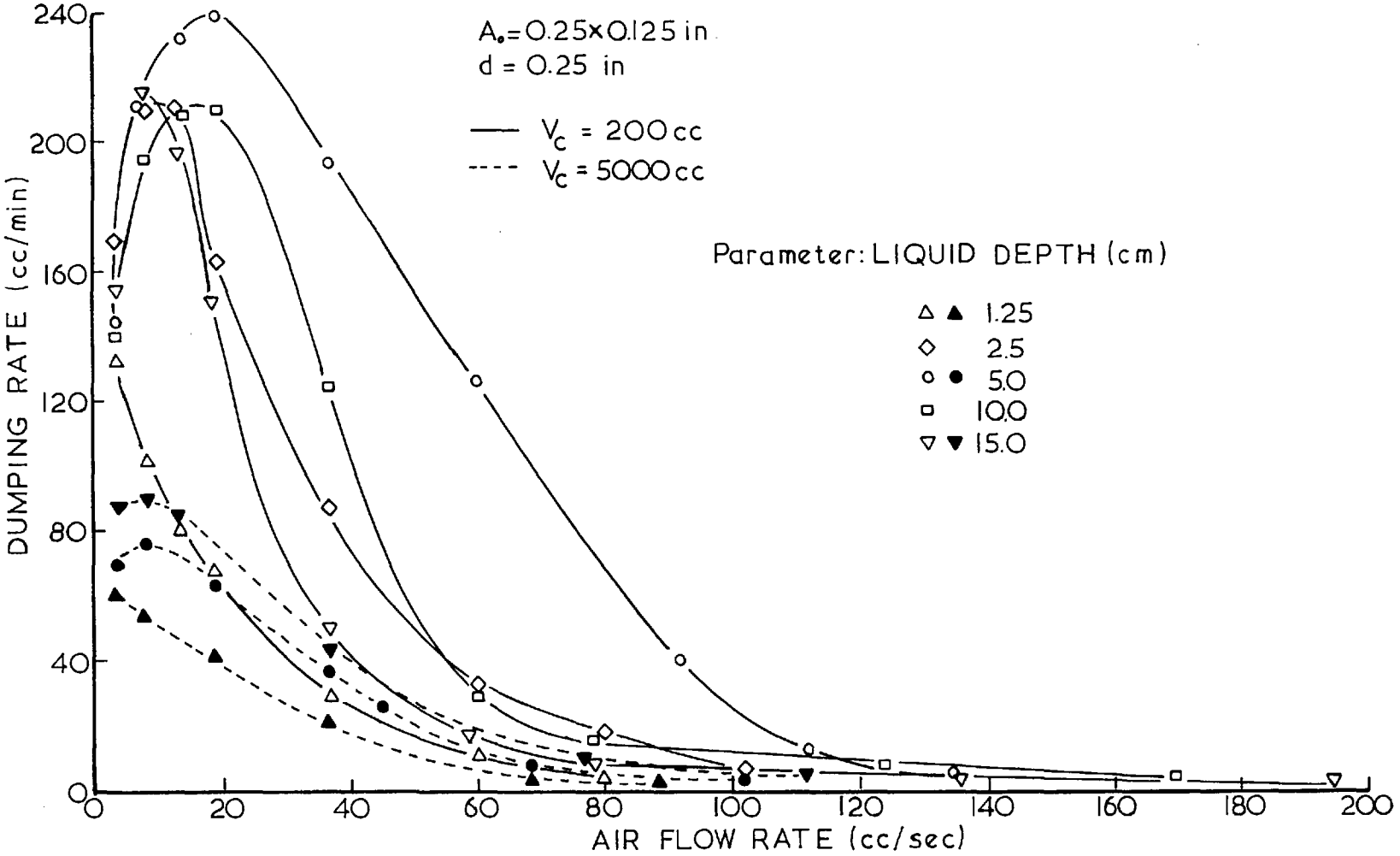

FIG. 6.10.

FIG. 6.11.

EFFECT OF HYDROSTATIC HEAD ON DUMPING RATE FOR VARIOUS ORIFICE CROSS SECTIONS.

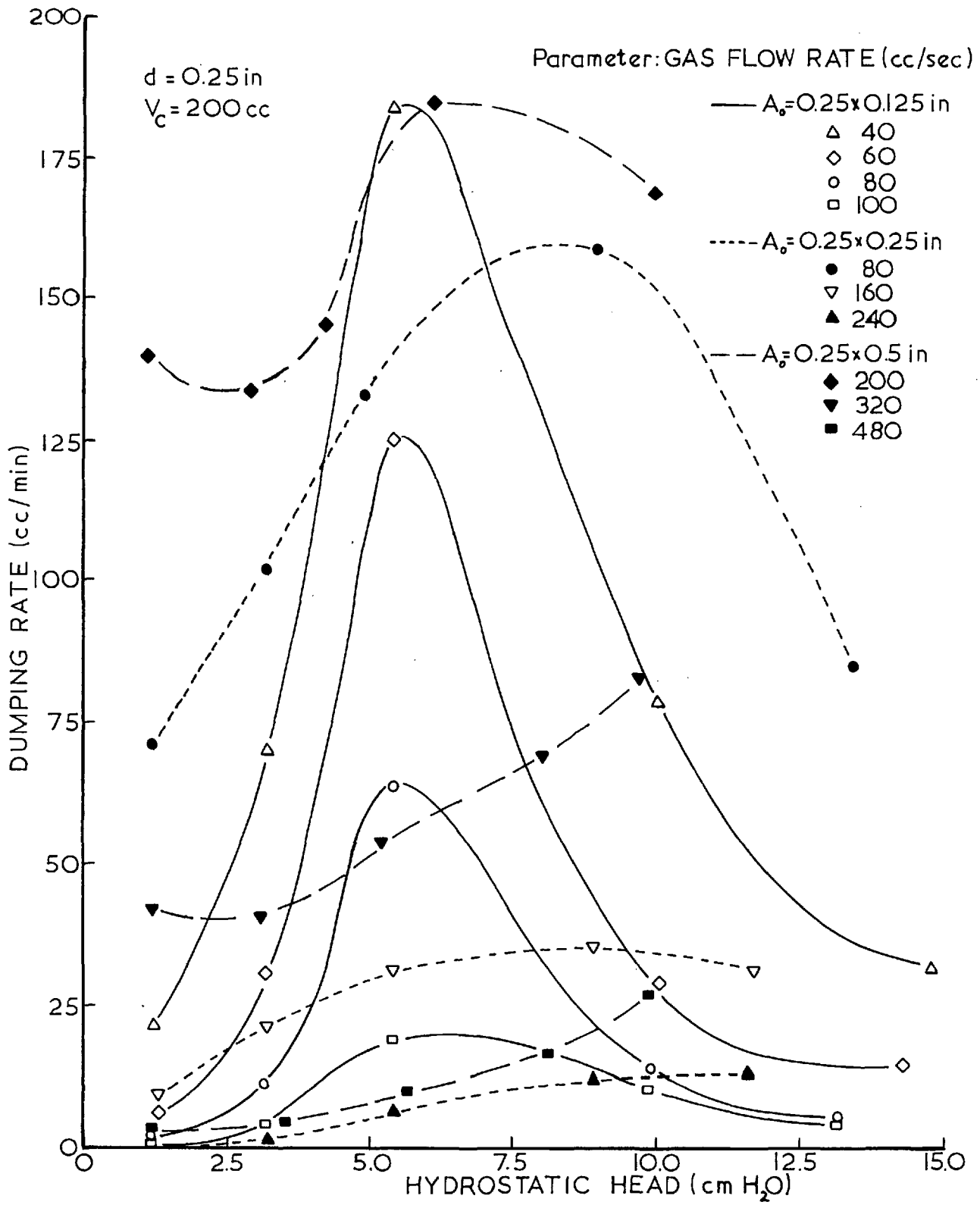

EFFECT OF GAS FLOW RATE ON DUMPING RATE FOR VARIOUS PLATE THICKNESS AND ORIFICE CROSS SECTIONS.

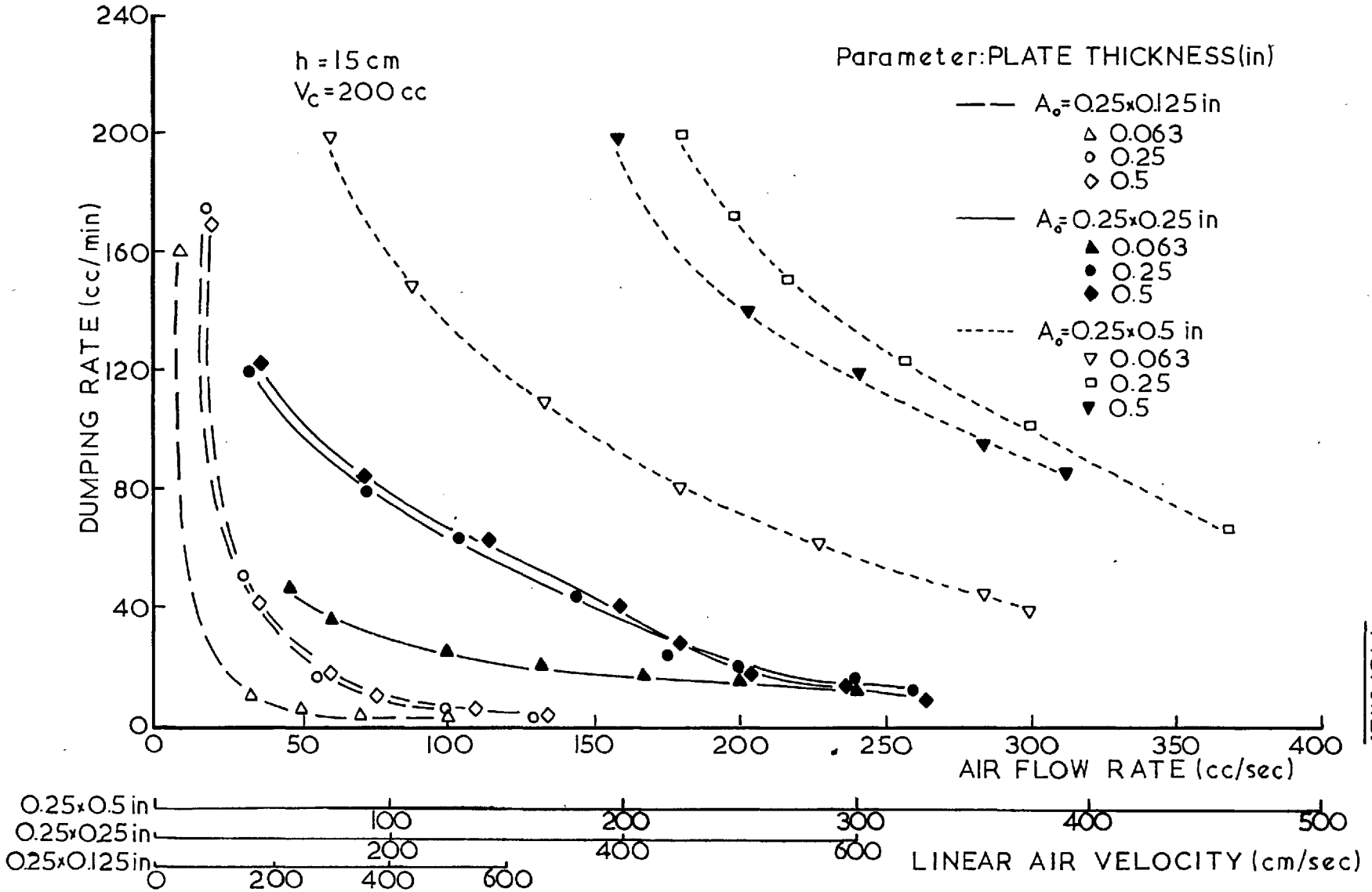

FIG. 6.12.

EFFECT OF GAS FLOW RATE ON DUMPING RATE FOR VARIOUS PLATE THICKNESS AND ORIFICE CROSS SECTIONS.

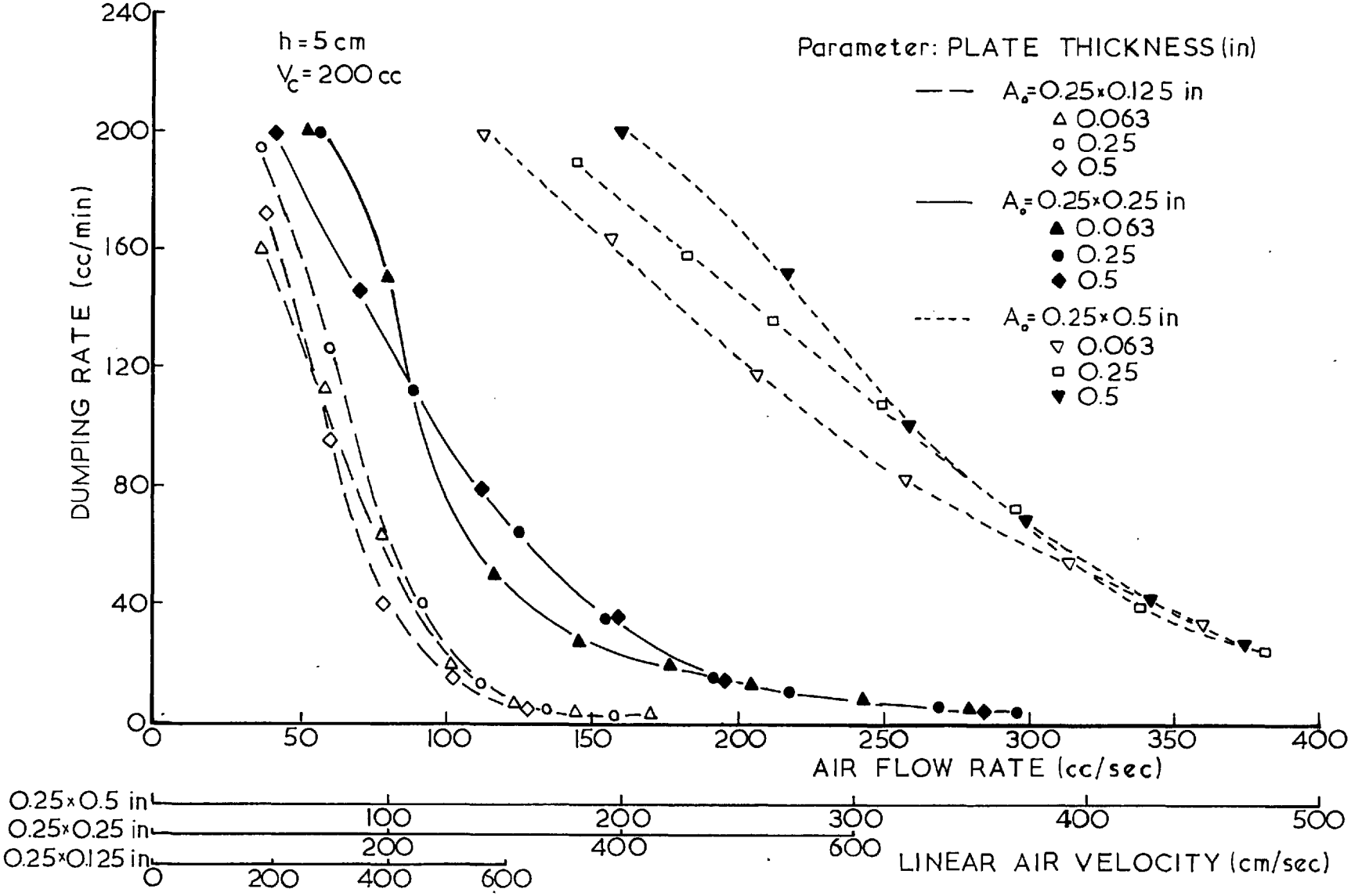

FIG. 6.13.

which have not been investigated with the 'Three Dimensional' Apparatus.

Effect of Gas Flow Rate (Fig. 6.10 - 6.13)

A similar trend of behaviour has been observed compared to the 'Three Dimensicnal' Apparatus (6.3.2), that is a sharp increase in the dumping rate with the decrease in gas flow rate, and a possibility of a maximum in the range of the low flow rates, which depends on gas chamber volume, orifice size and hydrostatic head.

Effect of Gas Chamber Volume (Fig. 6.10)

Since only two chamber volumes have been investigated, no 'critical' volume has been detected, compared to the 'Three Dimensional' Apparatus (6.3.2). However the effect of large chamber volumes is similar, that is, a decrease in dumping rate with an increase in chamber volume.

Effect of Hydrostatic Head (Fig. 6.10 - 6.11)

For very low gas chamber volume (200 cc) and small orifice size (0.25 x 0.125 in), there is a sharp increase in the dumping rate for an increase in liquid depth till about 5 cm, above which there is a sharp decrease in the dumping rate with further increase in liquid depth. However this maximum tends to become less significant with the increase of orifice size, resulting in almost a steady increase

in dumping rate with the increase in liquid depth for large orifice size (0.25 x 0.5 in). (Fig. 6.11).

For large gas chamber volume (5000 cc), there is only a slight steady increase in dumping rate with the increase in liquid depth.

Effect of Orifice Size (Fig. 6.11 - 6.13)

An increase in the dumping rate has been observed for an increase in the orifice size, that is, in agreement with the observations for the 'Three Dimensional' Apparatus (6.3.1).

In terms of linear gas velocity, provided the liquid depth is large enough (15 cm), there is a steady increase in dumping rate with the increase of orifice size for the same gas velocity (Fig. 6.12), the effect becoming less significant as the gas velocity increases. However, for a smaller liquid depth (5 cm), since this is the region of the 'critical' depth, mainly for 0.125 in. and 0.25 in. orifices, no reasonable difference has been observed between these two; nevertheless the effect becomes more significant in comparison to the larger orifice (0.5 in.) (Fig. 6.13).

Effect of Orifice Thickness (Fig. 6.12 - 6.13)

Since this parameter has not been investigated with the 'Three Dimensional' Apparatus, a similar type of analysis as described in (6.3) might be applied for this parameter.

According to Hughes et al. (20) and Hayes et al. (18) the orifice thickness has no effect on bubble size, provided the ratio $\frac{\text{orifice thickness}}{\text{orifice diameter}} = \frac{d}{D_o} < 100$. Thus no effect on $\frac{t_D}{T}$ is expected.

An increase in the orifice thickness increases the term $\rho_L g d$ in equation (6.5); thus, provided a drop forms, it facilitates the initiation of dumping, resulting in an increase in dumping rate. This effect of orifice thickness is shown in Fig. 6.12. However, for the larger orifice (0.25 x 0.5 in) a maximum of the dumping rate has been observed for the 0.25 in. thickness. Comparing the effect of the orifice thickness for a lower liquid depth (5 cm), the effect is less significant, and no specific trend is observed. (Fig. 6.13).

Posin et al. (50) have found a maximum dumping rate for $0.6 < \frac{d}{D_o} < 1.5$.

6.5. Mechanism of Dumping in a Sieve Tray

A simplified criterion for dumping in a sieve tray may be derived using the same assumptions as those for a single orifice (6.1.2). For the normal operation of a sieve tray in the 'dumping region' it is assumed that for a certain instant a part of the holes is bubbling, another part is dumping and the rest is bridging. As has already been stated for these conditions the pressure in gas chamber fluctuates periodically, the amplitude tends to decrease with the increase

in number of holes and gas flow rate.

It is most convenient to define a minimum instantaneous pressure in the gas chamber ($P_{V_{min}}$) necessary to ensure stable operating conditions for this 'dumping region'. Thus in order to prevent 'raining' (that is an instantaneous 'stream' dumping throughout all of the holes) the necessary condition:

$$P_{V_{min}} \geq \frac{-2\sigma}{a_o} \tag{6.10}$$

For a certain hole the formation of a drop, and consequently 'single drop' dumping, might occur provided:

$$-\sigma\left(\frac{1}{R_1}+\frac{1}{R_2}\right)+\rho_L g\,(d+y) > P_{V_{min}} > \frac{-2\sigma}{a_o} \tag{6.11}$$

To ensure stable bridging condition for a hole:

$$P_{V_{min}} > -\sigma\left(\frac{1}{R_1}+\frac{1}{R_2}\right)+\rho_L g(d+y) \tag{6.12}$$

Suppose that a bubble has been detached from a certain hole leaving a pressure gradient ΔP in the liquid. Under these conditions such a hole starts dumping, provided:

$$\Delta P - \frac{2\sigma}{a_o}+\rho_L g\left(d+\frac{2}{3}a_o k\right) > P_{V_{min}} > -\frac{2\sigma}{a_o}+\rho_L g\left(d+\frac{2}{3}a_o k\right) \tag{6.13}$$

Thus comparing this criterion to that for a single orifice (equation

6.5), it seems that the criterion for dumping from a hole in a sieve tray is mainly affected by the pressure change in the liquid above the particular hole (ΔP), whereas for a single orifice the pressure in the gas chamber (P_V) is often the dominating factor [As has been seen mainly for a 1/4 in. orifice in (6.3.1)] .

Since it is much more convenient for practical purposes to derive a criterion similar to equation (6.13) as a function of the mean pressure in the gas chamber (P_{mean}), and since for a fluctuating pressure $P_{mean} > P_{Vmin}$, the r.h.s. of the inequality (6.13) still holds by substituting P_{mean} instead of P_{Vmin}. However the l.h.s. of the inequality might be violated, thus an approximate limit for P_{mean} might be derived above which dumping is impossible:

$$P_{mean} > \Delta P - \sigma\left(\frac{1}{R_1} + \frac{1}{R_2}\right) + \rho_L g(d+y) \qquad (6.14)$$

Since ΔP, R_1, R_2 and y are all functions of time, it is understood that an accurate analysis of dumping in a sieve tray is rather complicated, and more investigation is necessary in this field. However, as stated in (5.5.2) the main difficulty is in a theoretical prediction of mean pressure in the system.

Nevertheless, limited experimental results obtained for the rate of dumping for the two sieve trays investigated are given in figure (6.14). Comparing to Figure 5.29 it is quite clear that the mean

FIG. 6.14.

EFFECT OF GAS FLOW RATE ON DUMPING RATE FOR A SIEVE TRAY (V_c=2250 cc).

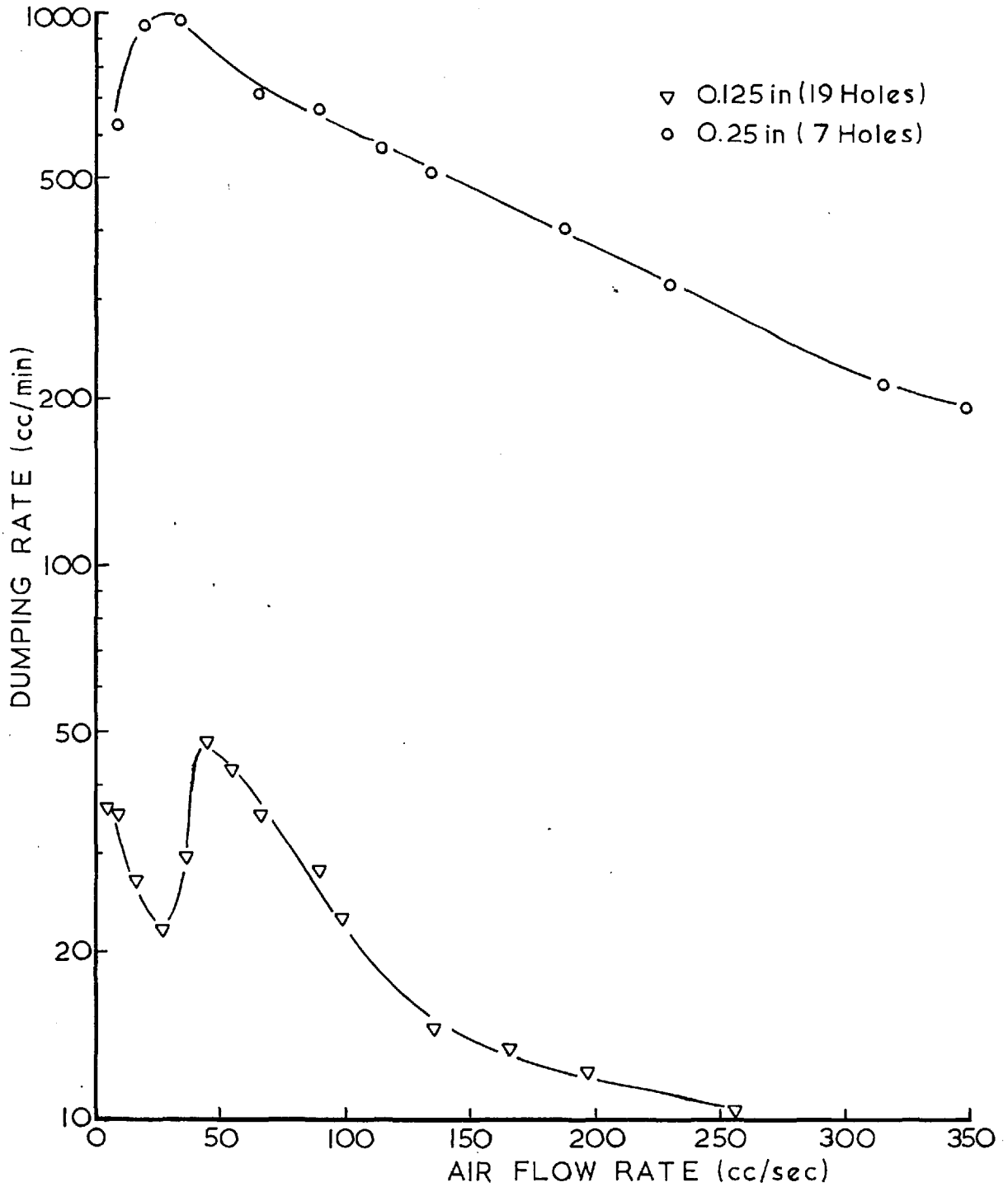

pressure is an important factor in determining the dumping rate, having an increase in the dumping rate for a decrease in the mean pressure.

The effect of gas flow rate on the dumping rate seems to be similar to a single orifice, that is a maximum in the range of low gas flow rates and a sharp decrease for higher flow rates. Such a sharp decrease has been observed also by Hunt et al. (3).

CHAPTER 7

GENERAL CONCLUSIONS

The present investigation can be considered as a step forward in the studies of the complex behaviour of a sieve tray in the 'dumping region'. Since bubble size and frequency are two of the main factors which determine the occurrence of dumping and since no general theoretical equations for growing bubbles were available so far, the equations derived in this investigation, despite their limitations, might be regarded as a basis for further studies in this field. Although a large part of the research has been devoted to these studies, which nevertheless have ultimately enabled a fair qualitative explanation of the dumping phenomenon, it has also been shown that the liquid pressure behind a rising bubble in the vicinity of the plate and the mean gas pressure in the chamber below the plate are important factors in the dumping studies.

1. The model which has been used and the equations which have been derived for the radial expansion of a growing bubble above an orifice are strictly applicable to spherical bubbles formed individually in an inviscid irrotational liquid. A simplified criterion for the limit of single bubble formation, that is the initiation of coalescence, has been established.

Since the bubbles formed under the conditions investigated in the present studies were not completely spherical, a discrepancy between experimental results and the theory is expected, which is mainly affected by the size of the bubble. (Increase in bubble size under the conditions investigated increases the distortion of the bubble). Provided a bubble is not spherical, the nett effect of surface tension force is no longer zero, and it must be taken into consideration in the balance of forces acting on a bubble. Walters and Davidson (27) have calculated the shape of a distorted bubble assuming that the pressure inside the bubble is invariant across its surface, although practically there might be some differences in pressure magnitudes. In addition a resistance of the interface to any change in its shape due to application of a pressure gradient must be taken into account in an accurate theoretical investigation. Thus any theoretical equations which take into consideration the true bubble shape are expected to be far too complicated.

Another limitation of the theory is in the case of a high bubble frequency, for which the assumption that the liquid in the vicinity of the orifice is at rest when the bubble starts forming becomes invalid. The bubble formation is bound to be affected by an additional liquid inertia effect.

2. Despite some discrepancies compared to the experimental results, the general trend of the theoretical results agrees quite well with most of the previous work which has been done in similar regions of 'Slowly increasing bubble volume' or 'Constant bubble frequency'.

An important contribution of the theory derived is the possibility of estimating the relative magnitudes of different pressure components involved in the system and their effect on bubble size under various conditions investigated.

3. An attempt at evaluating bubbles size formed above a sieve tray has been described. However any basic theory in this field must be followed by a theoretical prediction of the frequency of pressure fluctuations under such a tray, which needs much more study.

4. An approximate magnitude of the pressure in the bubble wake, which has an appreciable effectin dumping studies, has been calculated. Since there is a gradual decrease in the acceleration of the bubble while it rises through the liquid, changing its shape to a stable spherical cap shape and attaining a terminal constant velocity, this pressure field tends to diminish quicker than predicted by the theory.

5. The mean pressure in the gas chamber has been investigated, and it has been shown that its magnitude is also important in dumping studies. However a main contribution of these studies is in the explanation and evaluation of the 'residual head', which many other

workers have so far only estimated experimentally.

Another important conclusion is that a 1/4 in. single orifice or sieve tray may operate in the 'dumping region' while the mean pressure in the gas chamber is lower than the hydrostatic pressure on the plate.

6. A simple criterion for initiation of dumping has been established. Although this criterion is based on many assumptions, its applicability has been shown together with the theory of bubble formation, thereby obtaining a fair qualitative analysis of the various possibilities of the behaviour of a system, that is: formation of single or group bubbles, followed by 'stream' dumping, 'single drop' dumping or no dumping at all.

No theoretical equation for calculating the dumping rate has been derived so far, but the relative magnitude of this value under different conditions investigated has been estimated qualitatively. An accurate theoretical prediction of the dumping rate seems rather complicated and much more preliminary work is necessary, mainly for the region in which the meniscus of liquid starts forming below the orifice, prior to the dumping itself.

APPENDIX A: Application of 'Method of Images' for the Plate Effect on a Growing Sphere

A-1. 'Method of Images'

It is most convenient to regard the motion of the liquid as being initiated from points or singularities in the field of flow. If the motion of a liquid consists of symmetrical radial flow in all directions proceeding from a point, the point is called a source. Similarly, if the radial flow is inward towards a point, the point is called a sink. The strength of a source (or a sink) is regarded as the volume of the liquid emitted in unit time. A dipole is regarded as a combination of a source and a sink of equal strength.

Thus, considering the flow of liquid around a translating sphere (equation 4. 8), the flow can be described by a dipole of strength $\frac{1}{2} a^3 u$, whose axis passes through the centre of the sphere. Similarly, considering the flow of liquid arcund a pulsating sphere (equation 4. 9), the flow can be described by a source of strength $a^2 \frac{da}{dt}$, at the centre of the sphere.

The usefulness of those concepts lies in the fact that restrictions on the flow of fluid imposed by geometrical boundaries can be satisfied by superimposing the flow from suitable combinations of these sources placed at points inaccessible to the fluid. Such a combination of

sources on both sides of the boundary can be regarded as a system of images. The presence of a rigid boundary in the vicinity of the sphere violates the two boundary conditions which are imposed for solving the Laplace's Equation. By introducing successive images of a suitable combination of sources with decreasing strengths, a remedy for the boundary condition is obtained.

A-2. Effect of a Plate on the Velocity Potential for a Translating Sphere

The 'method of images' used for estimating the effect of a plate on the velocity potential for the flow around a translating sphere is described in detail. by Lamb (40), p. 130.

Figure A-1 shows the schematic diagram for this method.

A_1, A_2 are the successive images of point A (which is the centre of the real sphere)

B_1, B_2 are the successive images of point B (which is the centre of the imaginary sphere).

For any arbitrary point P, it has been shown (Lamb [40] , p. 115) that the velocity potential due to a dipole of unit strength which axis passes through the centre of the sphere, at a distance f from the centre is:

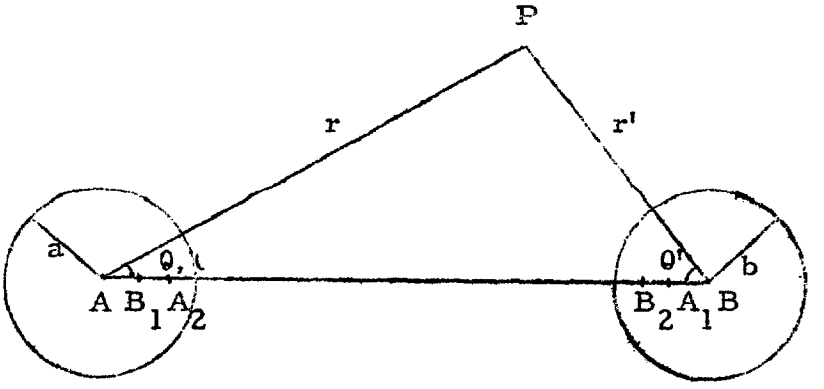

Fig. A-1: Schematic Diagram for the 'Method of Images'

$$\text{For } r < f: \quad \phi = -\left[\frac{1}{f^2} + 2P_1\frac{r}{f^3} + 3P_2\frac{r^2}{f^4} + \ldots\right]$$

$$\text{For } r > f: \quad \phi = P_1\frac{1}{r^2} + 2P_2\frac{f}{r^3} + \ldots$$

Where P_n are Legendre's coefficients. (Zonal Harmonics)

Since the flow of the liquid around the translating sphere is described by a dipole whose axis passes through the centre of the sphere A, the image of such a dipole of unit strength is another dipole of strength $\frac{-b^3}{(AB)^3}$ at the inverse point A_1 along the axis which passes through the centre of the imaginary sphere. Similarly, the image of the dipole at A_1 is another dipole of strength $\left[\frac{-b^3}{(AB)^3}\right]\left[\frac{-a^3}{(AA_1)^3}\right]$ at the inverse point A_2, along the axis which passes through the centre of the real sphere.

It can be seen that the velocity potential includes an infinite series of zonal harmonics of ascending orders. However, any two zonal harmonics of different orders which are finite over a unit sphere are orthogonal, thus in virtue of the orthogonal property these harmonics will disappear after being included in a surface integration. Since the subsequent calculations (equation 4.18) include in fact a surface integration for determining the nett upward force on the bubble, all the zonal harmonics which will disappear might be omitted.

Using this property and calculating a series of successive images, it has been shown that the velocity potential near the surface of the sphere A, when sphere A moves with unit velocity towards B while sphere B is at rest, is given by:

$$\phi = (\mu_o + \mu_2 + \mu_4 + \dots)\frac{\cos\theta}{r^2} - 2\left(\frac{\mu_1}{f_1^3} + \frac{\mu_3}{f_3^3} + \dots\right) r\cos\theta$$

where μ_n are the strengths of the successive images and f_n their distances from A.

Similarly, the velocity potential near the surface of the sphere A, when sphere B moves with unit velocity towards A while sphere A is at rest, is given by

$$\phi' = (\mu_1' + \mu_3' + \mu_5' + \dots)\frac{\cos\theta}{r^2} - 2\left(\frac{\mu_o'}{c^3} + \frac{\mu_2'}{(c-f_2')^3} + \frac{\mu_4'}{(c-f_4')^3} + \dots\right) r\cos\theta$$

where μ'_n are the strengths of the successive images and $c - f'_n$ their distances from A.

Evaluation of ϕ and ϕ', neglecting powers of c^{-1} higher than the sixth, gives:

$$\phi = \left(\frac{a^3}{2r^2} + \frac{a^6 b^3}{2r^2 c^6} + \frac{a^3 b^3 r}{c^6}\right) \cos\theta$$

$$\phi' = \left(\frac{b^3 r}{c^3} + \frac{a^3 b^3}{2c^3 r^2}\right) \cos\theta$$

Since the overall velocity potential is given by:

$$\phi_T = \phi u + \phi' u'$$

where u is the velocity of A towards B and u' that of B towards A, and since u = u', and a = b:

$$\phi_T = u\left[\frac{a^3}{2r^2} + \frac{a^3 r}{c^3} + \frac{a^6}{2c^3 r^2} + \frac{a^6 r}{c^6} + \frac{a^9}{2r^2 c^6}\right] \cos\theta \qquad (4.11)$$

A-3. Effect of a Plate on the Velocity Potential for a Pulsating Sphere

The method used is similar to that for the translating sphere, based on Lamb (40), p. 130.

For any arbitrary point P (Fig. A-1) it has been shown (Lamb, [40], p. 115) that the velocity potential due to a source of unit strength, at a distance f from the centre of a sphere, is:

For $r < f$: $\phi = \frac{1}{f} + P_1 \frac{r}{f^2} + P_2 \frac{r^2}{f^3} + \ldots$

For $r > f$: $\phi = \frac{1}{r} + P_1 \frac{f}{r^2} + P_2 \frac{f^2}{r^3} + \ldots$

where P_n are Legendre's coefficients.

Since the flow of the liquid around the pulsating sphere is described by a source situated at the centre A, the image of such a source of unit strength is another source of strength $\frac{b}{AB}$ situated at A_1 and a line sink of strength $-\frac{1}{b}$ per unit length from B to A_1, as shown by Basset (41), p. 249, or Ramsey (42), p. 48. Following their analysis, the image of this combination of source and line sink is another source of strength $\frac{b}{AB} \cdot \frac{a}{AA_1}$ situated at A_2 and a line sink of strength $(-\frac{1}{b})(-\frac{a}{A_2B_1})$ per unit length from A_2 to B_1.

Using successive images and applying the properties of zonal harmonics as described in (A-2), it can be shown that the velocity potential near the surface of the sphere A, when sphere A pulsates, while sphere B is at rest, is given by:

$$\phi = \frac{\mu_o}{r} + \frac{1}{2}\left[\mu_2 (f_2 - f_2^{\varkappa}) + \mu_4 (f_4 - f_4^{\varkappa}) + \mu_6 (f_6 - f_6^{\varkappa}) + \ldots\right] \frac{\cos\theta}{r^2}$$

$$+ \left[\mu_1 \left(\frac{1}{f_1^2} - \frac{1}{f_1 f_1^{\varkappa}}\right) + \mu_3 \left(\frac{1}{f_3^2} - \frac{1}{f_3 f_3^{\varkappa}}\right) + \mu_5 \left(\frac{1}{f_5^2} - \frac{1}{f_5 f_5^{\varkappa}}\right) + \ldots\right] r\cos\theta$$

where μ_n are the strengths of the successive images.

f_n and $f_n^{\varkappa}$ are the distances of the two extremities of the line sink images, from A.

f_n, $f_n^{\varkappa}$ and μ_o are given by:

$$f_1^{\varkappa} = c \qquad f_2^{\varkappa} = \frac{a^2}{f_1^{\varkappa}} \qquad f_3^{\varkappa} = c - \frac{b^2}{c - f_2^{\varkappa}} \qquad f_4^{\varkappa} = \frac{a^2}{f_3^{\varkappa}}$$

$$f_1 = c - \frac{b^2}{c} \qquad f_2 = \frac{a^2}{f_1} \qquad f_3 = c - \frac{b^2}{c - f_2} \qquad f_4 = \frac{a^2}{f_3}$$

$$\mu_o = a^2 \frac{da}{dt} \qquad \frac{\mu_2}{\mu_o} = \frac{b}{c}$$

$$\frac{\mu_2}{\mu_1} = \frac{a}{f_1} \qquad \frac{\mu_3}{\mu_2} = \frac{b}{c - f_2}$$

$$\frac{\mu_4}{\mu_3} = \frac{a}{f_3} \qquad \frac{\mu_5}{\mu_4} = \frac{b}{c - f_4}$$

Similarly, the velocity potential near the surface of the sphere A_1 when sphere B pulsates, while sphere A is at rest, is given by:

$$\phi' = \frac{1}{2}\left[\mu_1' f_2^{\varkappa} + \mu_3'(f_4^{\varkappa} - f_2) + \mu_5'(f_6^{\varkappa} - f_4) + \ldots\right] \frac{\cos\theta}{r^2}$$

$$+ \left[\mu_o' \frac{1}{f_1^{\varkappa_2}} + \mu_2'\left(\frac{1}{f_3^{\varkappa_2}} - \frac{1}{f_3^{\varkappa} f_1}\right) + \mu_4'\left(\frac{1}{f_5^{\varkappa_2}} - \frac{1}{f_5^{\varkappa} f_3}\right) + \ldots\right] r\cos\theta$$

where: μ_n' are the strengths of the successive images.

f_n and $f_n^{\varkappa}$ are the distances of the two extremities of the line sink images, from A.

f_n and $f_n^{\star}$ are the same as above, while μ_n' are given by:

$$\mu_o' = b^2 \frac{db}{dt} \qquad \frac{\mu_1'}{\mu_o'} = \frac{a}{f_1^{\star}}$$

$$\frac{\mu_2'}{\mu_1'} = \frac{b}{c - f_2^{\star}} \qquad \frac{\mu_3'}{\mu_2'} = \frac{a}{f_3^{\star}}$$

$$\frac{\mu_4'}{\mu_3'} = \frac{b}{c - f_n^{\star}} \qquad \frac{\mu_5'}{\mu_4'} = \frac{a}{f_5^{\star}}$$

Evaluation of ϕ and ϕ', neglecting powers of c^{-1} higher than the sixth, gives:

$$\phi = a^2 \frac{da}{dt} \left[\frac{1}{r} + \left(\frac{b^3 r}{c^5} + \frac{a^3 b^3}{2c^5 r^2} \right) \cos\theta \right]$$

$$\phi' = b^2 \frac{db}{dt} \left[\frac{r}{c^2} + \frac{a3}{2c^2 r^2} \right] \cos\theta$$

Since the overall velocity potential is given by:

$$\phi_P = \phi + \phi'$$

And since $a = b$ and $\frac{da}{dt} = \frac{db}{dt}$:

$$\phi_P = \frac{da}{dt} \left[\frac{a^2}{r} + \left(\frac{a^2 r}{c^2} + \frac{a^5}{2c^2 r^2} + \frac{a^5 r}{c^5} + \frac{a^8}{2c^5 r^2} \right) \cos\theta \right] \qquad (4.11)$$

APPENDIX B: Solution of the Dynamic Equations for the Bubbling System

B-1. Method of Solution

The dynamic equations have been solved on the computer type IBM 7090, which uses FORTRAN IV language.

The numerical method applied for solving the equations has been the Modified Euler Method, using iterative approximations.

Any second order differential equation $\frac{d^2y}{dx^2} = f(x, y)$ can be reduced to a set of two first order equations: $\frac{dy}{dx} = z$

$$\frac{dz}{dx} = f(x, y)$$

If the values z_n, y_n at the beginning of an interval of length Δx are known, the values at the end of the interval, for a first approximation can be found as follows:

Evaluate $\left(\frac{dz}{dx}\right)_n$

$$Z^{(1)}_{ave} = Z_n + \left(\frac{dz}{dx}\right)_n \frac{\Delta x}{2}$$

$$Z^{(1)}_{n+1} = Z_n + \left(\frac{dz}{dx}\right)_n \Delta x$$

$$y^{(1)}_{n+1} = y_n + Z^{(1)}_{ave} \Delta x$$

For a second approximation:

Evaluate $\left(\frac{dz}{dx}\right)_{n+1}$

$$\left(\frac{dz}{dx}\right)_{ave} = \frac{1}{2}\left[\left(\frac{dz}{dx}\right)_n + \left(\frac{dz}{dx}\right)_{n+1}\right]$$

$$Z^{(2)}_{ave} = Z_n + \left(\frac{dz}{dx}\right)_{ave} \frac{\Delta x}{2}$$

$$Z^{(2)}_{n+1} = Z_n + \left(\frac{dz}{dx}\right)_{ave} \Delta x$$

$$y^{(2)}_{n+1} = y_n + Z^{(2)}_{ave} \Delta x$$

Further approximations with the same procedure.

In the case for which two second order differential equations need to be solved simultaneously, the procedure is similar, by simultaneous iterative calculations for both equations.

Usually this Modified Euler Method requires comparatively small intervals and many iterative approximations to improve the accuracy of the solution, which results in a longer running time on the computer.

For the interval chosen (0. 001 sec), it has been found that there is almost no difference between the results using a second approximation. A very short computing time also results using this method, mainly because of the comparative simplicity of the equations, so it has been decided to use this method all along the investigation.

B-2. General Properties of the System Investigated

Calculations have been carried out for two systems: air-water and air-ethanol. A constant temperature of 20°C has been assumed for

all the physical properties used.

a. Physical properties of the air (1 atm):

Density = 0.0012 $\frac{gr}{cm^3}$

Velocity of sound = 3.4×10^4 cm/sec

b. Physical properties of the liquid

	Water	Ethanol
Density ($\frac{gr}{cm^3}$)	1.0	0.79
Surface Tension ($\frac{dyne}{cm}$)	72.8	22.5

c. Orifice constant (K)

The relation between the orifice constant K (equation 4.21) and the orifice discharge coefficient c_d is given by:

$$K = \frac{1}{2c_d^2}$$

Because c_d depends slightly on the system properties for $Re < 10^4$ it is more convenient to determine the value of K experimentally, by measuring the dry pressure drop across the orifice for the range of flow rates investigated. Although the flow of gas through the orifice for a bubbling system is pulsating, the difference in the value of K for an average pulsating flow compared with a continuous flow can be neglected, as shown also by Davies and Porter (44).

The average values of K which have been obtained:

Orifice diameter 1/4 in. : K = 1.20

Orifice diameter 1/8 in. : K = 1.13

B-3. Computing Program Example

A written computing program example is given below.

```
C CALCULATION FOR SYSTEM AIR-WATER (TEMP=20CT)
C
      INTEGER   C,Z,W
      DIMENSION T(200),RD(200),D(200),E(200),RDRD(200),RDS(200),RDRDS
     1(200),V(200),DD(200),DAVE(5),A(20),VC(20),G(20),S(200),Y(200),
     2X(200),SS(200),XX(200),RS(200),XAVE(200),PH(200),OK(5),
     3          FI(200),FB(200),PV(200),PB(200),PVL(200),POR(200),
     4PST(200),PIN(200),PT(200),AS(10),PL(200)
      READ (5,1001) (A(K),K=1,1)
      READ (5,1002) (VC(L),L=1,8)
      READ (5,1003) (G(M),M=1,6)
 1001 FORMAT (5X,F5.3)
 1002 FORMAT (4(4X,F7.1)/4(4X,F7.1))
 1003 FORMAT (6(5X,F5.1))
C NOTATION D=DRD/DT,E=DD/DT,H=DT,X=DS/DT,Y=DX/DT
      DO 50 K=1,1
      DO 50 L=1,8
      DO 50 M=1,6
      T(1) = 0.
      RD(1) = A(K)
      RDS(1) = A(K)*A(K)
      D(1) = 0.
      V(1) = 4.19*A(K)**3.
      PV(1) = 0.147/A(K)
      PB(1) = 0.147/A(K)
      PST(1) = 0.147/A(K)
      PVL(1) = 0.
      POR(1) = 0.
      PIN(1) = 0.
      PT(1) = 0.
      OK(1) = 1.20
      H = 0.001
      J = 1
      AR = 3.14*A(K)*A(K)
      ARS = AR*AR
      VOL = 4.19*A(K)**3.
      WRITE (6,1110) A(K),VC(L),G(M)
      WRITE (6,1101)
C
C CALCULATION FOR GROWING STAGE
      DO 30 I=1,199
C CALCULATION OF RADIUS OF THE BUBBLE (RD)
C FIRST APPROXIMATION
      RDS(I) = RD(I)*RD(I)
      E(I) =   145.6*(RD(I)-A(K))/(RDS(I)*A(K))-(0.19*OK(1)*RD(I)**3./
     1ARS+1.5/RD(I))*D(I)*D(I) - 5.93E6*(RDS(I)-A(K)**3./RD(I))/VC(L)
     2+ 1.415E6*G(M)*T(I)/(VC(L)*RD(I)) + 981.
      DAVE(1) = D(I) + H*E(I)/2.
      DD(I+1) = D(I) + H*E(I)
      RDRD(I+1) = RD(I) + H*DAVE(1)
C SECOND APPROXIMATION
      RDRDS(I+1) = RDRD(I+1)*RDRD(I+1)
      T(I+1) = T(I) + H
      E(I+1) =      145.6*(RDRD(I+1)-A(K))/(RDRDS(I+1)*A(K))-(0.19*OK(1)*
     1RDRD(I+1)**3./ARS+1.5/RDRD(I+1))*DD(I+1)*DD(I+1) - 5.93E6*(RDRDS
```

```
     2(I+1)-A(K)**3./RDRD(I+1))/VC(L) + 1.415E6*G(M)*T(I+1)/(VC(L)*RDRD
     3(I+1)) + 981.
      EAVE = (E(I)+E(I+1))/2.
      DAVE(2) = D(I) + H*EAVE/2.
      D(I+1) = D(I) + H*EAVE
      RD(I+1) = RD(I) + H*DAVE(2)
      RDS(I+1) = RD(I+1)*RD(I+1)
      V(I+1) = 4.19*RD(I+1)**3.
C CALCULATION OF PRESSURE IN THE VESSEL (PV)
      PVL(I+1) =                1445.*(V(I+1)-VOL-G(M)*T(I+1))/VC(L)
      PV(I+1) = PV(1) - PVL(I+1)
C CALCULATION OF PRESSURE IN THE BUBBLE (PB)
      POR(I+1)= 1.94E-4*OK(1)*D(I+1)*D(I+1)*RDS(I+1)*RDS(I+1)/ARS
      PST(I+1) = 0.147/RD(I+1)
      PIN(I+1) = 1.02E-3*(RD(I+1)*E(I+1)+1.5*D(I+1)*D(I+1))
      PH(I+1) = RD(I+1)
      PB(I+1) = PV(I+1) - POR(I+1)
C CALCULATION OF MEAN INTEGRATED PRESSURE
      PAVE = (PV(I)+PV(I+1))/2.
      PT(I+1) = PT(I) + PAVE*H
C CALCULATION OF INERTIA FORCE (FI) AND BUOYANCY FORCE (FB)
      FB(I+1) = 981.*RD(I+1)
      FI(I+1) = 1.13*RD(I+1)*E(I+1) + 2.13*D(I+1)*D(I+1)
C WRITE EACH FIFTH ITERATION
      IF ((I+1) - J) 20,10,10
   10 CONTINUE
C IN THIS PART FI AND FB APPEAR INSTEAD OF X AND Y
      WRITE (6,1112) T(J),RD(J),RDRD(J),D(J),FI(J),E(J),FB(J),V(J),
     1PV(J),PB(J),POR(J),PVL(J),PIN(J),PST(J),PH(J)
      J = J + 5
   20 CONTINUE
      IF (FB(I+1).GE.FI(I+1)) GO TO 40
   30 CONTINUE
   40 CONTINUE
      C = I + 1
      WRITE (6,1112) T(C),RD(C),RDRD(C),D(C),FI(C),E(C),FB(C),V(C),
     1PV(C),PB(C),POR(C),PVL(C),PIN(C),PST(C),PH(C)
C
C CALCULATIONS FOR ELONGATING STAGE
      S(C) = RD(C)
      X(C) = D(C)
      W = C
      DO 80 N=C,199
C CALCULATION OF RADIUS OF THE BUBBLE (RD)
C FIRST APPROXIMATION
      RDS(N) = RD(N)*RD(N)
      AS(1) = RD(N)/S(N)
      AS(2) = (RD(N)/S(N))**2.
      AS(3) = (RD(N)/S(N))**3.
      AS(4) = (RD(N)/S(N))**4.
      AS(5) = (RD(N)/S(N))**5.
      AS(6) = (RD(N)/S(N))**6.
      AS(7) = (RD(N)/S(N))**7.
      Y(N)    = (981. - (0.375*AS(2)+0.047*AS(5))*E(N) - (1.125*AS(2)+
```

```
     10.282*AS(5))* D(N)  * D(N)  /  RD(N)   + (0.563*AS(4)+0.141*AS(7))
     2* X(N)  * X(N)  /  RD(N)   - (1.5-0.070*AS(6))* D(N)  * X(N)  /
     3  RD(N)  )/ (0.5+0.188*AS(3)+0.023*AS(6))
      XAVE(1) = X(N) + H*Y(N)/2.
      XX(N+1) = X(N) + H*Y(N)
      SS(N+1) = S(N) + H*XAVE(1)
      E(N) =   145.6*(RD(N)-A(K))/(RDS(N)*A(K))-(0.19*OK(1)*RD(N)**3./
     1ARS+1.5/RD(N))*D(N)*D(N) - 5.93E6*(RDS(N)-A(K)**3./RD(N))/VC(L)
     2+ 1.415E6*G(M)*T(N)/(VC(L)*RD(N)) + 981.*S(N)/RD(N)
      DAVE(1) = D(N) + H*E(N)/2.
      DD(N+1) = D(N) + H*E(N)
      RDRD(N+1) = RD(N) + H*DAVE(1)
C SECOND APPROXIMATION
      RDRDS(N+1) = RDRD(N+1)*RDRD(N+1)
      AS(1) = RDRD(N+1)/SS(N+1)
      AS(2) = (RDRD(N+1)/SS(N+1))**2.
      AS(3) = (RDRD(N+1)/SS(N+1))**3.
      AS(4) = (RDRD(N+1)/SS(N+1))**4.
      AS(5) = (RDRD(N+1)/SS(N+1))**5.
      AS(6) = (RDRD(N+1)/SS(N+1))**6.
      AS(7) = (RDRD(N+1)/SS(N+1))**7.
      Y(N+1) = (981. - (0.375*AS(2)+0.047*AS(5))*E(N) - (1.125*AS(2)+
     10.282*AS(5))*DD(N+1)*DD(N+1)/RDRD(N+1) + (0.563*AS(4)+0.141*AS(7))
     2*XX(N+1)*XX(N+1)/RDRD(N+1) - (1.5-0.070*AS(6))*DD(N+1)*XX(N+1)/
     3RDRD(N+1))/ (0.5+0.188*AS(3)+0.023*AS(6))
      YAVE = (Y(N)+Y(N+1))/2.
      XAVE(2) = X(N) + H*YAVE/2.
      X(N+1) = X(N) + H*YAVE
      S(N+1) = S(N) + H*XAVE(2)
      T(N+1) = T(N) + H
      E(N+1) =      145.6*(RDRD(N+1)-A(K))/(RDRDS(N+1)*A(K))-(0.19*OK(1)*
     1RDRD(N+1)**3./ARS+1.5/RDRD(N+1))*DD(N+1)*DD(N+1) - 5.93E6*(RDRDS
     2(N+1)-A(K)**3./RDRD(N+1))/VC(L) + 1.415E6*G(M)*T(N+1)/(VC(L)*RDRD
     3(N+1)) + 981.*S(N+1)/RDRD(N+1)
      EAVE = (E(N)+E(N+1))/2.
      DAVE(2) = D(N) + H*EAVE/2.
      D(N+1) = D(N) + H*EAVE
      RD(N+1) = RD(N) + H*DAVE(2)
      RDS(N+1) = RD(N+1)*RD(N+1)
      V(N+1) = 4.19*RD(N+1)**3.
C CALCULATION OF PRESSURE IN THE VESSEL (PV)
      PVL(N+1) =                1445.*(V(N+1)-VOL-G(M)*T(N+1))/VC(L)
      PV(N+1) = PV(1) - PVL(N+1)
C CALCULATION OF PRESSURE IN THE BUBBLE (PB)
      POR(N+1)= 1.94E-4*OK(1)*D(N+1)*D(N+1)*RDS(N+1)*RDS(N+1)/ARS
      PST(N+1) = 0.147/RD(N+1)
      PIN(N+1) = 1.02E-3*(RD(N+1)*E(N+1)+1.5*D(N+1)*D(N+1))
      PH(N+1) = S(N+1)
      PB(N+1) = PV(N+1) - POR(N+1)
C CALCULATION OF MEAN INTEGRATED PRESSURE
      PAVE = (PV(N)+PV(N+1))/2.
      PT(N+1) = PT(N) + PAVE*H
C CALCULATION OF DIFFERENCE BETWEEN SUM OF RADIUS AND DISTANCE (RS)
      RS(N+1) = A(K) + RD(N+1) - S(N+1)
```

```
C WRITE EACH FIFTH ITERATION
      IF ((N+1) - W) 70,60,60
   60 CONTINUE
      WRITE (6,1102) T(W),RD(W),RDRD(W),S(W),D(W),X(W),E(W),Y(W),V(W),
     1PV(W),PB(W),POR(W),PVL(W),PIN(W),PST(W),PH(W)
      W = W + 5
   70 CONTINUE
      IF (RS(N+1).LE.0.) GO TO 90
   80 CONTINUE
   90 CONTINUE
      Z = N+1
      WRITE (6,1102) T(Z),RD(Z),RDRD(Z),S(Z),D(Z),X(Z),E(Z),Y(Z),V(Z),
     1PV(Z),PB(Z),POR(Z),PVL(Z),PIN(Z),PST(Z),PH(Z)
C
C CALCULATION OF PRESSURE IN LIQUID AT DETACHMENT
      PL(Z) = ((1.-0.375*AS(2)-0.047*AS(5))*RD(Z)*E(Z) - (0.5+0.188*
     1AS(3)+0.023*AS(6))*RD(Z)*Y(Z) + (1.5-1.125*AS(2)-0.282*AS(5))*D(Z)
     2*D(Z) + (0.5+0.563*AS(4)+0.141*AS(7))*X(Z)*X(Z) - (1.5-0.070*AS(6)
     3)*D(Z)*X(Z))/981. - S(Z) + RD(Z)
C
C CALCULATION OF WAITING TIME
      TW = (PV(1)-PV(Z))*VC(L)/(1445.*G(M))
C CALCULATION OF MEAN INTEGRATED PRESSURE FOR WAITING STAGE
      PTW = (PV(1)+PV(Z))*TW/2.
C CALCULATION OF PERIOD TIME
      TP = T(Z) + TW
C CALCULATION OF MEAN PRESSURE
      PMEAN = (PT(Z)+PTW)/TP
      WRITE (6,1120) TP,TW,PMEAN,PL(Z)
   50 CONTINUE
C
 1110 FORMAT(/20X,3HA =,F6.3,4H(CM),5X,4HVC =,F7.1,4H(CC),5X,3HG =,F6.2,
     18H(CC/SEC)/)
 1101 FORMAT (1X,6HT(SEC),1X,6HRD(CM),1X,4HRDRD     ,1X,  5HS(CM),1X,
     19HD(CM/SEC),1X,9HX(CM/SEC),1X,13HE(CM/SEC/SEC),1X,13HY(CM/SEC/SEC)
     2,1X,5HV(CC),1X,12HPV(GR/CM/CM),1X,2HPB,4X,3HPOR,4X,3HPVL,4X,3HPIN,
     34X,3HPST,3X,2HPH)
 1112 FORMAT (1X,F5.3,2X,F5.3,1X,F5.3, 8X,       F7.2,3X,F7.2,4X,F8.2,
     16X,F8.2,3X,F6.3,3X,F7.3,2X,F7.3,F6.3,F7.3,F7.3,F6.3,F6.3)
 1102 FORMAT (1X,F5.3,2X,F5.3,1X,F5.3,1X,F5.3,2X,F7.2,3X,F7.2,4X,F8.2,
     16X,F8.2,3X,F6.3,3X,F7.3,2X,F7.3,F6.3,F7.3,F7.3,F6.3,F6.3)
 1120 FORMAT (/1X,4HTP =,F6.3,5H(SEC),5X,4HTW =,F6.3,5H(SEC),5X,
     17HPMEAN =,F7.3,10H(GR/CM/CM),5X,4HPL =,F7.3,10H(GR/CM/CM)//)
      STOP
      END
$DATA
      .318
      200.       500.       800.       1500.
     2250.      3000.      5000.      10000.
       8.3       16.7       33.3       66.7      100.       133.3
$EOF
```

NOMENCLATURE

A_o	Crifice cross section area
a	Radius of bubble ($\hat{a}$ = dimensionless radius)
a_o	Radius of orifice ($\hat{a}_o$ = dimensionless radius)
a_x	Major axis of a spheroid
b	Radius of imaginary sphere
b_x	Minor axis of a spheroid
c	Distance between centres of two spheres moving in their line of centres
c_o	Velocity of sound
c_D	Drag coefficient
c_d	Crifice discharge coefficient
D_B	Diameter of bubble
$\bar{D}_B$	Average diameter of bubble
D_o	Diameter of orifice
d	Thickness of plate
F	Force
F_B	Buoyancy force
F_I	Inertia force
F(t)	External force
$\hat{Fr}$	Froude number (equation 4.33)
f	Frequency

f_n Distance of successive images from centre of a sphere

G Gas flow rate ($\acute{G}$ = dimensionless flow rate)

g Acceleration of gravity

h_4 Hydrostatic head

h_{dp} Dry plate pressure drop

h_l Pressure drop due to liquid on a plate

h_r 'Residual' head (equation 5.4)

h_T Total plate pressure drop

h_v Pressure drop due to passage of vapour through a plate

K, k Experimental constants

L Dumping rate

M Constant (equation 4.6)

N_c 'Capacitance Number' (equation 2.7)

n Number of bubbles

P Pressure ($\hat{P}$ = dimensionless pressure)

P_{atm} Surrounding atmospheric pressure

P_B Pressure in bubble

P_{LD} Pressure in liquid behind a bubble at detachment

P_V Pressure in gas chamber

P_{Vd} Pressure in gas chamber at detachment of a bubble

P_{Vmin} Minimum pressure in gas chamber

P_{mean} Mean pressure in gas chamber

P_∞ Pressure at a rest point in absence of motion

ΔP Pressure change at a rest point due to motion

P_n Legendre coefficients

q Velocity in space

R Radius of a drop

Re Reynolds Number based on gas properties $(\frac{D_o u_o \rho_G}{\mu_G})$

Re_L Reynolds Number based on liquid properties $(\frac{2au\rho_L}{\mu_L})$

r Distance of centre of a moving sphere from a point fixed in space

s Vertical distance of centre of a bubble from the plate ($\hat{s}$, $\tilde{s}$ = dimensionless distances)

T Time of a cycle

t Time ($\hat{t}$ = dimensionless time)

t_B 'Bubbling' time

t_D 'Dumping' time

t_F 'Drop Formation' time

t_R 'Recovery' time

t_ω 'Waiting' time

u Vertical velocity of the bubble

u_d Velocity of bubble at detachment

u_L Velocity of liquid through orifice

u_o Velocity of gas through orifice

V Volume of bubble

V_c Volume of gas chamber

We Weber Number $(\frac{2a\rho_L u^2}{\sigma})$

$\hat{We}$ Weber Number (equation 4. 33)

y Vertical coordinate

Z_F Foam height

β Ratio between frequency of bubbles and pressure fluctuations in a sieve tray

γ Ratio of heat capacities

θ Angle

μ_G Gas viscosity

μ_L Liquid viscosity

μ_n Strengths of successive images

ν Kinematic viscosity

ρ_G Gas density

ρ_L Liquid density

ρ_F Foam density

σ Surface tension

ϕ Velocity potential

ϕ_P Velocity potential for flow around a pulsating sphere

ϕ_T Velocity potential for flow around a translating sphere

χ Ratio of cross axis to parallel axis for an oblate spheroid

BIBLIOGRAPHY

1. Mayfield, F.D., Church, W.L., Green, A.C., Lee , D.C. and Rasmussen, R.W., Ind. Eng. Chem., 44, p. 2238 (1952)

2. Arnold, D.S., Plank, C.A. and Schoenborn, E.M., Chem. Eng. Prog., 48, p. 633 (1952)

3. Hunt, C.A., Hanson, D.N. and Wilke, C.R., A.I.Ch.E. Journal, 1, (4), p. 441 (1955)

4. McAllister, R.A., McGinnis, P.H. and Plank, C.A., Chem. Eng. Sci., 9, p. 25 (1958)

5. Hughmark, G.A. and O'Connell, H.E., Chem. Eng. Prog., 53, p. 127M (1957)

6. Eduljee, H.E., Brit. Chem. Eng., 3 (1), p. 14 (1958)

7. Norman, W.S., 'Absorption, Distillation and Cooling Towers', Longmans, Green and Co. Ltd., London (1961)

8. Hengstebeck, R.J., 'Distillation: Principles and Design Procedures', Reinhold Publishing Corp, New York (1961)

9. Valentin, F.H.H., 'Absorption in Gas-Liquid Dispersions', E. and F.N. Spon Ltd., London (1967)

10. Harris, I.J., Brit. Chem. Eng., 10, p. 377 (1965)

11. Prince, R.G.H., International Symposium on Distillation, p. 177, Brighton, England (1960)

12. Leibson, I., Holcomb, E. G., Cacoso, A. G. and Jacmic, J. J., A. I. Ch. E. Journal, 2, p. 296 (1956)

13. Lockhart, F. J. and Legget, C. W., 'Advances in Petroleum Refining and Chemistry', Vol. 1, Interscience Publishers Inc. (1958)

14. Prince, R. G. H. and Chan, B. K. C., Trans. Inst. Chem. Engrs., 43, p. 49 (1965)

15. Chan, B. K. C., and Prince, R. G. H., A. I. Ch. E. Journal, 12 (2), p. 232 (1966)

16. Davidson, J. F. and Schuler, B. O. G., Trans. Inst. Chem. Engrs., 38, p. 144 (1960)

17. Davidson, J. F. and Schüler, B. O. G., Trans. Inst. Chem. Engrs., 38, p. 335 (1960)

18. Hayes, W. B., Hardy, B. W. and Holland, C. D., A. I. Ch. E. Journal, 5, p. 319 (1959)

19. Davidson L. and Amick, E. H , A. I. Ch. E. Journal, 2, p. 337 (1956)

20. Hughes, R. R., Handlos, A. E., Evans, H. D. and Maycock, R. L. Chem. Eng. Prog., 51, p. 557 (1955)

21. Helsby, F. W., Ph. D. Thesis, University of London (1958)

22. van Krevelen, D. W. and Hoftijzer, P. J., Chem. Eng. Prog., 46, p. 29 (1950)

23. Sideman, S., Hortacsu, O. and Fulton, J. W., Ind. Eng. Chem., 58, p. 32 (1966)

24. Calderbank, P. H., Brit. Chem. Eng., 1, p. 267 (1956)

25. Davidson, J. F. and Harrison, D., 'Fluidised Particles', Cambridge University Press (1963)

26. Walters, J. K. and Davidson, J. F., J. Fluid Mech., 12, p. 408 (1962)

27. Walters, J. K. and Davidson, J. F., J. Fluid Mech., 17, p. 321 (1963)

28. Danckwerts, P. V., Sawistowski, H. and Smith, W., International Symposium on Distillation, p. 7, Brighton, England (1960)

29. Yoshitome, H., Bull. Tokyo Inst. Technol., 64, p. 51 (1965)

30. Quigley, C. J., Johnson, A. I. and Harris, B. L., Chem. Eng. Prog. Symposium Series, 16, p. 31 (1955)

31. Calderbank, P. H., Trans. Inst. Chem. Engrs., 37, p. 173 (1959)

32. Bridge, A. G., Lapidus, L. and Elgin, J. C., A. I. Ch. E. Journal, 10, p. 819 (1964)

33. Calderbank, P. H., Chem. Engr., 45, p. CE 209 (1967)

34. Rennie, J. and Smith, W., A. I. Ch. E. - I. Ch. E. Joint Meeting, No. 6 (Transport Phenomena), p. 62, London (1965)

35. Moore, D. W., J. Fluid Mech., 6, p. 113 (1959)

36. Moore, D. W., J. Fluid Mech., 16, p. 161 (1963)

37. Moore, D. W., J. Fluid Mech., 23, p. 749 (1965)

38. Batchelor, G. K. 'An Introduction to Fluid Dynamics', Cambridge University Press (1967)

39. Krishnamurthi, S., Kumar, R. and Kuloor, N. R., Chem. and Proc. Eng., 49 (1), p. 91 (1968)

40. Lamb, H., 'Hydrodynamics', Cambridge University Press (1932)

41. Basset, A. B., 'A Treatise on Hydrodynamics', Vol. 1, Dover Publications Inc., New York (1961)

42. Ramsey, A. S., 'A Treatise on Hydromechanics', Part II, G. Bell and Sons Ltd., London (1960)

43. Jameson, G. J. and Kupferberg, A., Chem. Eng. Sci., 22, p. 1053 (1967)

44. Davies, B. T. and Porter, K. E., Proceedings of the Symposium on Two Phase Flow, Vol. 2, p. F301, University of Exeter (1965)

45. 'Underwater Explosion Research', Vol. 2: The Gas Globe, Office of Naval Research, Department of U. S. Navy (1950)

46. Bernard, J. D. T., Ph. D. Thesis, University of London (1967)

47. Standard, G., Chem. Eng. Sci., 20, p. 611 (1965)

48. Adamson, A. W., 'Physical Chemistry of Surfaces', Interscience Publishers (1964).

49. Zelfel, E., Chemie Ingenieur Technik, 39 (7), p. 433 (1967)

50. Pozin, M. E., Tarat, E. Ya, and Mrnyak, L., Khim. i. Khim. Tekhnol., 6, p. 310 (1963)

Chemical Engineering Science, 1967, Vol. 22, pp. 1053–1055. Pergamon Press Ltd., Oxford. Printed in Great Britain.

Shorter Communications

Pressure behind a bubble accelerating from rest: Simple theory and applications

(*Received* 2 *December* 1966; *in revised form* 21 *January* 1967)

WHEN A gas bubble is formed at a point in a relatively inviscid liquid, its initial motion is determined by the balance between buoyancy and inertia. The bubble breaks off when its base reaches the gas supply point and accelerates away from the source.

In this note, it is shown that in its wake, the bubble leaves a distinct pressure field. It is suggested that this pressure, whose approximate magnitude can be calculated by potential flow theory, is responsible for the phenomenon of dumping or weeping on sieve trays. It may also have important effects in other situations involving accelerating bubbles such as in fluidized beds and in nucleate boiling.

THEORY

It is assumed that the bubble starts from rest after having been formed at a single orifice in a flat plate. The depth of liquid on the plate is large compared with the bubble diameter. The effect of viscosity on the motion of the bubble is assumed negligible. This is reasonable, for since the bubble begins from rest, the motion is initially irrotational. Actually the bubble does have a small initial velocity, because its centre is moving upward while it is being formed. But it may be easily shown (following the work of DAVIDSON and SCHÜLER [6]) that this initial velocity is very small compared with the velocities reached after the bubble leaves the orifice.

The effect of the flat orifice plate on the motion of the bubble is ignored in this simple theory. Thus the problem is reduced to investigating the pressure field around a spherical bubble moving from rest under the action of the buoyancy force in a liquid of infinite extent.

We describe the motion with the velocity potential function

$$\phi=\frac{Ua^3}{2r^2}\cos\theta \tag{1}$$

where (r, θ) are polar coordinates fixed at the centre of the moving bubble, U is the upward velocity and a is the radius of the bubble. The pressure around the bubble is given by Bernoulli's equation (LAMB [1], p.124)

$$\frac{p}{\rho}=\frac{\partial\phi}{\partial t}-\tfrac{1}{2}q^2-g(s+r\cos\theta)+\frac{P_\infty}{\rho} \tag{2}$$

where

$$s=a+\int_0^t U\,dt$$

is the distance between the centre of the bubble and the original rest point, i.e. the point (a, π) at $t=0$. The density of the liquid is ρ and P_∞ is the pressure at the rest point in the absence of motion. The absolute velocity is given by

$$q^2=\left(\frac{\partial\phi}{\partial r}\right)^2+\left(\frac{1}{r}\frac{\partial\phi}{\partial\theta}\right)^2 \tag{3}$$

Substituting into (2) and remembering that (r, θ) are time-dependent since the origin is in motion, we obtain:

$$\frac{p}{\rho}=\frac{dU}{dt}\left[\frac{a^3}{2r^2}\cos\theta\right]+\frac{U^2a^3}{r^3}\left[1-\frac{3}{2}\sin^2\theta-\frac{a^3}{2r^3}\cos^2\theta-\frac{a^3}{8r^3}\sin^2\theta\right]-g(s+r\cos\theta)+\frac{P_\infty}{\rho} \tag{4}$$

The nett upward force on the bubble is found by integrating the vertical component of p over its surface (i.e. at $r=a$)

$$F=\int_0^\pi (2\pi r^2 p\sin\theta\cos\theta)_{r=a}d\theta \tag{5}$$

and if we ignore the mass of the bubble, the equation of motion is obtained by putting $F=0$. In this way we find

$$\tfrac{1}{2}\rho V\frac{dU}{dt}=\rho Vg \tag{6}$$

where V is the volume of the bubble. Solving (6),

$$\frac{dU}{dt}=2g \tag{7}$$

The validity of this expression for spherical bubbles accelerating from rest has been shown by WALTERS and DAVIDSON [3].

For present purposes we are interested in the pressure behind the bubble along the line of motion, i.e. along the vertical path followed by the centre of the bubble. Thus, in (4), we put $\theta=\pi$, $dU/dt=2g$ and $U=2gt$ and $r=s$, giving

$$\frac{\Delta p}{\rho g a}=-\frac{a^2}{s^2}+\frac{4gt^2}{a}\left(\frac{a^3}{s^3}-\frac{a^6}{2s^6}\right) \tag{8}$$

where $\Delta p=p-P_\infty$ and is the pressure change at the rest point due to the motion.

A dimensionless distance $\tilde{s}$ may be defined:

$$\tilde{s}=\frac{s}{a}=1+\frac{gt^2}{a} \tag{9}$$

Substituting in (8)

$$\frac{\Delta p}{\rho g a} = \frac{3}{\tilde{s}^2} - \frac{4}{\tilde{s}^3} - \frac{2}{\tilde{s}^5} + \frac{2}{\tilde{s}^6} \qquad (10)$$

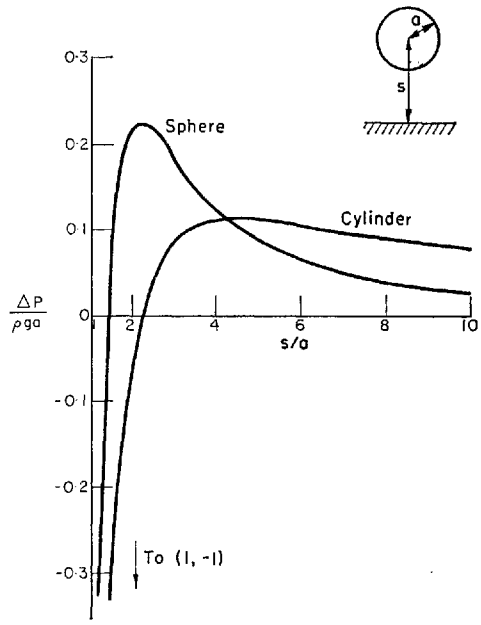

FIG. 1. Pressure at the rest point behind a sphere or cylinder accelerating from rest.

This equation is plotted in Fig. 1. It is seen that initially the pressure behind the bubble is *less* than the ambient, but that after it has moved a short distance, Δp becomes positive. This indicates that the point from which the bubble departed (the rest point) is acted upon by a short pressure decrement and then by a much longer excess, compared with the pressure at a distance from the bubble. The maximum pressure excess occurs at $\tilde{s} = 2{\cdot}15$.

When is the expression for Δp likely to be correct? There are two main sources of error. First, viscosity will begin to be important as U increases so the bubble will tend to stop accelerating. Secondly, the bubble will deform from the spherical shape, so that the assumed form of ϕ will be in error. Now, WALTERS and DAVIDSON [3] investigated the motion of spherical bubbles accelerating from rest and found that Eq. (7) was valid up to $\tilde{s} = 1{\cdot}65$ approx. They also found (theoretically) that a tongue of liquid began to penetrate the rear of the bubble at $\tilde{s} = 1{\cdot}36$, although their photographs showed that the bubble was still approximately spherical for a slightly greater distance than this.

Thus it appears likely that in the region of $\tilde{s} = 1{\cdot}65$ the assumptions made in this work begin to break down. Nevertheless, by the time this value is reached, Δp has almost reached its maximum. The shape of the curve beyond $\tilde{s} = 1{\cdot}65$ is in doubt, but $\Delta p/\rho g a$ probably subsides to zero rather more rapidly than shown in Fig. 1.

By an identical process, the pressure behind a cylindrical bubble may be calculated. The result is:

$$\frac{\Delta p}{\rho g a} = \frac{1}{\tilde{s}} - \frac{2}{\tilde{s}^2} - \frac{1}{\tilde{s}^3} + \frac{1}{\tilde{s}^4} \qquad (11)$$

This equation is also plotted in Fig. 1.

In passing, it is interesting to note that the pressure surge behind an accelerating body can easily be seen in a large vessel of water. If one holds one's hand horizontal and just beneath the surface of the water and then accelerates it rapidly downward, a large symmetrical bulge occurs on the surface behind the hand which can reach a height of 2 or 3 in.

APPLICATIONS

1. *Leakage of liquid from sieve trays*

This investigation was originally begun to try to explain why leakage of liquid occurs in sieve tray distillation columns. This liquid leakage, variously known as "weeping" or "dumping", occurs most seriously at low gas flow rates when the gas flow is apparently unable to stop liquid from draining through the holes.

An apparatus was constructed in which two-dimensional (i.e. cylindrical) bubbles could be formed in liquids of varying depths. Air was blown into a water layer through the gap between two pieces of brass held between two large flat Perspex sheets 0·25 in. apart. The gap between the brass plates was variable up to 0·5 in. so that the orifice could be varied up to $0{\cdot}25 \times 0{\cdot}5$ in. The thickness of the brass plate near the orifice was 0·25 in. A cine camera was used to take photographs of bubble formation at 64 frames/sec.

It was soon found that in the region where dumping occurred, large discrete bubbles were formed in the liquid. (Indeed, it has been shown that bubbles are formed at single orifice even at extremely high gas rates [3]). Photographs of bubble growth and departure are shown in Fig. 2. In these the gap width was $\frac{1}{8}$ in., air rate 42 cm³/sec, liquid depth 2 in. It is seen that the bubble's shape is roughly cylindrical, although as it moves further from the the plate it rapidly deforms in the way described by WALTERS and DAVIDSON [2].

But the most interesting part of these figures is the behaviour of the region near the orifice, in particular the gas–liquid interface. For just after the bubble detaches from the plate it is seen that the interface is pushed down the hole and eventually leads to weeping in the form of a thin stream of liquid as shown in Fig. 2(d).

The general outline of this behaviour can be explained with reference to the above theory. Just as the liquid begins to lift away from the orifice, but is still connected to the gas source by a small tube or tail [Fig. 2(b)], the theory predicts that there is a strong deficit in the liquid surrounding the tail. Since the pressure in the gas inside the small tube is approximately the same as that at the bottom of the liquid on the sieve plate some distance from the hole, it will therefore be greater than the pressure in the surrounding liquid and hence the tail will tend to stay open. This is of course an unstable situation and the tail will collapse under the action of surface tension in the same way as a liquid jet breaks up into droplets. Once the tail has severed, the bubble accelerates rapidly away from the plate and it is obvious from the photographs that there is a pressure gradient tending to push liquid down the orifice. Such a pressure is predicted by the theory as shown in Fig. 1. There appears to be some discrepancy between this prediction and the

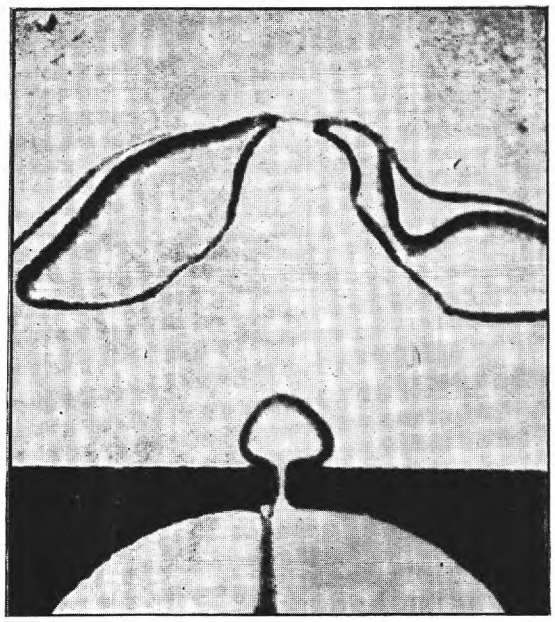

(a) Frame 1.

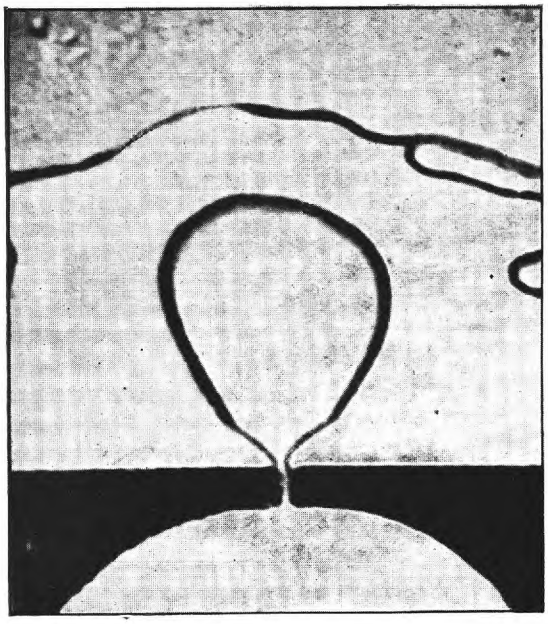

(b) Frame 4.

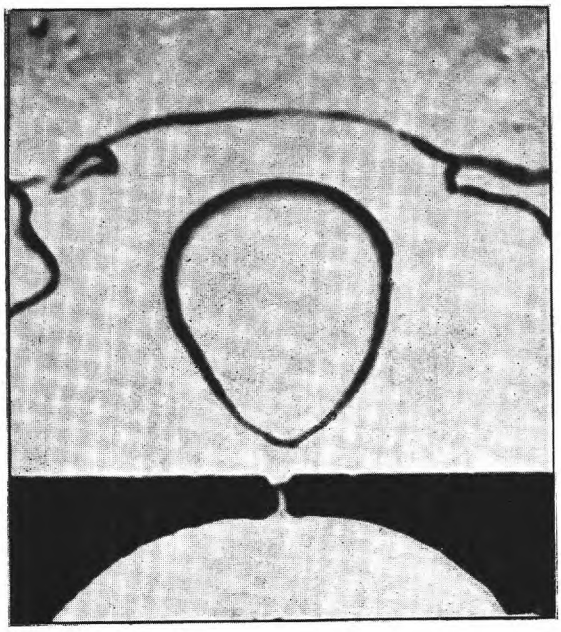

(c) Frame 5.

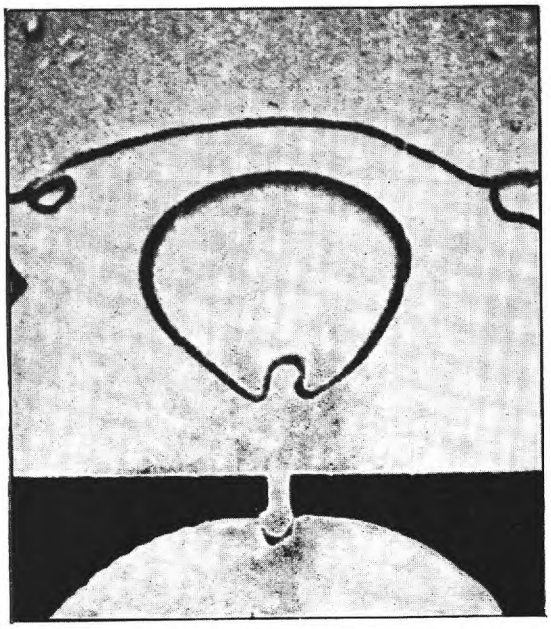

(d) Frame 6.

FIG. 2. (a–d) A cylindrical bubble forming at an orifice. Toward the top of each frame can be seen the surface of the liquid layer and the remains of the previous bubble. From a cine film at 64 frames/sec.

Facing page 1054

actual behaviour, for Fig. 2(d) shows that flow of liquid down the hole is well under way at $\bar{s} = 2$ approx., while the theory predicts that Δp is negative up to $\bar{s} = 2{\cdot}25$. However, it is likely that the curves in Fig. 1, calculated for a bubble in an infinite body of fluid, are affected by the presence of the flat plate. Initial calculations have been done for the sphere, using the method of images (LAMB [1], p.131) and there is a significant difference from the theory for the infinite liquid, at least for small values of $\bar{s}$. The minimum value of $\Delta p/\rho ga$ is $-1{\cdot}406$, but the pressure rises rather more rapidly, being zero at $\bar{s} = 1{\cdot}35$ (compared with 1·45 for the infinite case) and reaches a maximum of $0{\cdot}306\ \rho ga$ at $\bar{s} = 2{\cdot}04$ (compared with a maximum of $0{\cdot}224\ \rho ga$ at $\bar{s} = 2{\cdot}15$). Thus it is possible that the curve for the cylinder is affected in a similar way, being shifted generally to the left. Another factor as yet unexamined is the effect of the distortion of the bubble.

This seems a plausible way of explaining how pressure variations are caused in the liquid near a bubbling orifice. However, it must not be overlooked that the volume of the gas space beneath the hole could also play an important role [6, 7]. This aspect of the dynamics of the system is being investigated further.

2. *Other applications*

There are several fields involving accelerating bubbles in which the pressure behaviour in the wake may be important. The well-known analogy between the fluidized bed and inviscid fluids may lead to an explanation of particle dumping at the support plate. Thus when a bubble forms and rises from a hole in a gas distributor in a fluidized bed, it may lead to pressure gradients which force particles downward through the hole in the same way as liquid weeps, Fig. 2. However, the pressure gradients in unsteady flow in a fluidized bed are not well understood and it is possible that effects other than Bernoulli-equation pressures may predominate.

In nucleate boiling, a phenomenon known as hysterisis exists, in which the heat flux from a heated flat plate is dependent on whether the flux is increasing or decreasing [4]. Thus when a pool of liquid is heated on a flat plate, there is initially a relation between heat flux and temperature difference such as one would find for normal free convection without boiling. When the liquid is considerably superheated, it suddenly starts boiling vigorously and the same boiling rate (or heat flux) can be maintained even with much reduced temperature difference. Thus existing bubbles may assist more bubbles to form. This phenomenon can perhaps be explained with reference to Fig. 1, in that just as a bubble lifts off the flat plate, the pressure deficit may increase the pressure drop across the interface enclosing the nucleation cavity, making it easier for another bubble to begin to grow. This effect may also be connected with the instability observed in boiling liquid metals [5].

CONCLUSION

The simple theory presented here is strictly applicable only to rigid spheres (or cylinders) accelerating from rest in an inviscid fluid of infinite extent. It predicts that at the point at which the sphere was originally resting the pressure suffers a sharp decrease below the ambient. But after a short time the pressure becomes an excess over the ambient and remains so until the object has moved to infinity.

Clearly this analysis must be modified for specific applications. With bubbles the constant pressure condition in the gas will lead to departure from the spherical shape assumed. With very small bubbles, viscosity and surface tension must be taken into account. And of course geometrical aspects (e.g. motion near a flat plate) will have to be considered.

Nevertheless, it is likely that the pressure behaviour described above does exist in practice and may be important in the study of sieve tray dynamics, in nucleate boiling phenomena, in bubbling fluidized beds and wherever accelerating bubbles occur.

G. J. JAMESON
A. KUPFERBERG
Department of Chemical Engineering and Chemical Technology
Imperial College
London S.W.7

REFERENCES

[1] LAMB Sir H., *Hydrodynamics*, Cambridge University Press 1932.
[2] WALTERS J. K. and DAVIDSON J. F., *J. Fluid Mech.* 1962 **12** 408.
[3] WALTERS J. K. and DAVIDSON J. F., *J. Fluid Mech.* 1963 **17** 321.
[4] CORTY C. and FOUST A. S., *Chem. Engng Prog. Symp. Ser.* 1955 **51** 1.
[5] MARTO P. J. and ROHSENOW W. M., *J. Heat Transfer* 1966 **88** 183.
[6] DAVIDSON J. F. and SCHÜLER B. O. G., *Trans. Instn Chem. Engrs* 1960 **38** 335.
[7] CHAN B. K. C. and PRINCE R. G. H., *A.I.Ch.E.Jl* 1966 **12** 232.

Chemical Engineering Science, 1967, Vol. 22, pp. 1056–1057. Pergamon Press Ltd., Oxford. Printed in Great Britain.

Some observations on pulsed flow past a cylinder

(*Received* 15 *January* 1967)

MANY previous workers have found that vibration or pulsation has a favourable effect on heat and mass transfer rates [1]. For example, if a cylinder is rapidly vibrated transversely in a stagnant fluid, an oscillating boundary layer is formed and a steady circulation (acoustic streaming) occurs. JAMESON [2] has obtained a theoretical expression for heat and mass transfer in these circumstances and the theory has been confirmed experimentally [2, 3]. However, the theory [2] is confined to laminar flow conditions and amplitudes much smaller than the cylinder radius. A different model can be used for vibration or pulsation at extremely low frequencies when the flow pattern is assumed to be fully developed at any instant with respect to the velocity at that instant. Thus the average heat or mass transfer coefficient may be found simply by integrating the steady-state relation between transfer coefficient and velocity. This quasi-steady-state model has been used to predict heat transfer in pulsed flow in a tube [4–6]. It is necessary to know the flow conditions in any given situation before deciding whether the quasi-steady-state model or the boundary-layer model is more suitable. Such information is available for oscillations of liquid in a U-tube as a result of observations of decrement rates [7–9]. The important parameter affecting the transition from quasi-steady to unsteady behaviour is given by:

$$\alpha = R^2\omega/\nu \qquad (1)$$

In laminar conditions, Poiseuille flow is found at values of α below 20, while if α exceeds 70 the bulk of the liquid oscillates in plug flow, with a boundary layer near the tube wall. STOKES [10] has shown that the oscillating laminar boundary-layer thickness is of the order of $(\nu/\omega)^{\frac{1}{2}}$, so the parameter α represents the square of the ratio of tube radius to boundary-layer thickness. The transition from laminar to turbulent conditions in an oscillating liquid occurs at Reynolds numbers well above the steady-state value of 2000 if α exceeds 20 [9].

The present investigation is intended to provide some qualitative information on flow conditions around a rigid cylinder fixed in a liquid which oscillates transversely with respect to the cylinder axis. Relatively low frequencies and high amplitudes have been used as these are typical of the pulsators which are available for large scale industrial application. Brass cylinders of $\frac{1}{2}$ in. and 1 in. dia. were used; each cylinder was $\frac{1}{4}$ in. long and was mounted in a perspex test section 4 in. wide and $\frac{1}{2}$ in. thick internally. The liquids used were water (ν=0·010 Stokes) and mixtures of toluene and liquid paraffin (ν=0·081 and 0·54 Stokes). Liquid pulsations were generated by an air-driven pulsator [11] which gave frequencies within the range 1–2·5 c/s and amplitudes up to 4 cm. In this work, amplitude is defined as one-half of the distance between the extreme positions of the liquid. The flow patterns were observed using fine aluminium powder as a tracer, with back-illumination of the test section.

The oscillations were characterized by the value of α and by the maximum Reynolds number with respect to the cylinder. Although the wave-form produced by the pulsator [11] was not strictly sinusoidal, the maximum velocity of oscillation was taken for simplicity to be ωA. Therefore in the absence of a net flow past the cylinder, the maximum Reynolds number during the cycle was given by:

$$Re = 2R\omega A/\nu \qquad (2)$$

At very low Reynolds numbers, the liquid was seen to oscillate in a laminar fashion about the cylinder, with the tracer particles traversing the same path during successive cycles. No streaming motion could be detected by eye. At higher Reynolds numbers, separation occurred for part of the cycle and vortex pairs were seen to detach from either side of the cylinder in the direction of the oscillations. Simultaneously, fresh liquid was drawn in towards the cylinder at right-angles to the direction of the oscillations. This process is shown in Fig. 1(a) in which a vortex pair is being formed at the top of the cylinder, while the remains of the pair shed in the previous cycle can be seen about three diameters above the cylinder. Figure 1(b) shows that at very high Reynolds numbers the vortex shedding becomes asymmetrical and turbulence extends for a considerable distance around the cylinder.

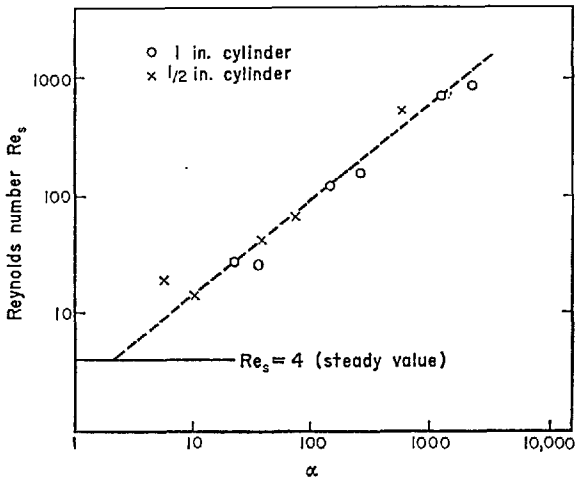

FIG. 2. Effect of α upon separation Reynolds number.